

1980

DEVELOPING REGION OF LAMINAR JETS.

GARY W. RANKIN

University of Windsor

Follow this and additional works at: <http://scholar.uwindsor.ca/etd>

Recommended Citation

RANKIN, GARY W., "DEVELOPING REGION OF LAMINAR JETS." (1980). *Electronic Theses and Dissertations*. Paper 1693.

This online database contains the full-text of PhD dissertations and Masters' theses of University of Windsor students from 1954 forward. These documents are made available for personal study and research purposes only, in accordance with the Canadian Copyright Act and the Creative Commons license—CC BY-NC-ND (Attribution, Non-Commercial, No Derivative Works). Under this license, works must always be attributed to the copyright holder (original author), cannot be used for any commercial purposes, and may not be altered. Any other use would require the permission of the copyright holder. Students may inquire about withdrawing their dissertation and/or thesis from this database. For additional inquiries, please contact the repository administrator via email (scholarship@uwindsor.ca) or by telephone at 519-253-3000ext. 3208.



NOTICE

The quality of this microfiche is heavily dependent upon the quality of the original thesis submitted for microfilming. Every effort has been made to ensure the highest quality of reproduction possible.

If pages are missing, contact the university which granted the degree.

Some pages may have indistinct print especially if the original pages were typed with a poor typewriter ribbon or if the university sent us a poor photocopy.

Previously copyrighted materials (journal articles, published tests, etc.) are not filmed.

Reproduction in full or in part of this film is governed by the Canadian Copyright Act, R.S.C. 1970, c. C-30. Please read the authorization forms which accompany this thesis.

THIS DISSERTATION
HAS BEEN MICROFILMED.
EXACTLY AS RECEIVED

AVIS

La qualité de cette microfiche dépend grandement de la qualité de la thèse soumise au microfilmage. Nous avons tout fait pour assurer une qualité supérieure de reproduction.

S'il manque des pages, veuillez communiquer avec l'université qui a conféré le grade.

La qualité d'impression de certaines pages peut laisser à désirer, surtout si les pages originales ont été dactylographiées à l'aide d'un ruban usé ou si l'université nous a fait parvenir une photocopie de mauvaise qualité.

Les documents qui font déjà l'objet d'un droit d'auteur (articles de revue, examens publiés, etc.) ne sont pas microfilmés.

La reproduction, même partielle, de ce microfilm est soumise à la Loi canadienne sur le droit d'auteur, SRC 1970, c. C-30. Veuillez prendre connaissance des formules d'autorisation qui accompagnent cette thèse.

LA THÈSE A ÉTÉ
MICROFILMÉE TELLE QUE
NOUS L'AVONS REÇUE

DEVELOPING REGION OF LAMINAR JETS

A Dissertation
Submitted to the Faculty of Graduate Studies through the
Department of Mechanical Engineering in Partial Fulfillment
of the Requirements for the Degree of
Doctor of Philosophy at the
University of Windsor

by



Gary W. Rankin

Windsor, Ontario, Canada
1980

© Gary W. Rankin

747976

S


9

For

my son Bryce,

my wife Janice,

and my parents, Myrtle and Lloyd.



ABSTRACT

The development region of axisymmetric laminar jets with uniform and parabolic exit velocity profiles are considered analytically using separate mathematical modelling assumptions. Both solutions employ integral techniques and are shown to be relatively simple, and also in reasonable agreement with existing experimental and theoretical results. The results of an experimental investigation of the parabolic exit velocity case is also reported. A Laser Doppler Anemometer was used to measure velocity profiles without disturbing the flow. Flow visualization was also employed to ensure that measurements were taken only in the laminar region. As well as providing additional verification of the present analytical method, certain observations were made concerning the axial variation of momentum, location of the virtual origin and development length. The proper nondimensional coordinate was also verified to be $x/d Re_c$ as obtained from a dimensional analysis of the pertinent equations of motion.

ACKNOWLEDGEMENTS

The author is grateful to Dr. T.W. McDonald, Head of the Mechanical Engineering Department, for his interest and continuous support as well as participation as a committee member.

The author wishes to express his sincere gratitude to Dr. K. Sridhar for his excellent supervision, generous aid and encouragement throughout the course of this study. He has always been available and willing to discuss problems as they arise.

Thanks are also extended to Dr. W.T. Kierkus, Dr. H.J. Tucker, Dr. A.C. Smith, Dr. A. Raouf and Dr. G.F. Marsters for their efforts in helping the author to better understand the problem considered and report it effectively.

The technical help and expert advice given by Mr. Robert Tattersal in the construction of the experimental facility is gratefully acknowledged. Thanks are also due to Mrs. Marion Campeau for her patience in typing the entire manuscript.

The author wishes to express his deep appreciation to his family for their support, understanding and the sacrifices made throughout the duration of this work.

The work was financially supported through a Shell Canada Post-graduate Fellowship and Natural Science and Engineering Research Council Canada grant number A-2190.

TABLE OF CONTENTS

	Page
ABSTRACT	i
ACKNOWLEDGEMENTS	ii
TABLE OF CONTENTS	iii
LIST OF FIGURES	v
LIST OF TABLES	vii
NOMENCLATURE	viii
CHAPTER I INTRODUCTION	1
1.1 Subject of Investigation	1
1.2 Significance	2
1.3 Aims	3
1.4 Method of Presentation	4
CHAPTER II LITERATURE SURVEY	5
2.1 Introduction	5
2.2 Theoretical Studies	5
2.2.1 Point Source Models and Matching	5
2.2.2 Integral Methods	8
2.2.3 Numerical Methods	11
2.3 Experimental Studies	12
2.3.1 Uniform Exit Velocity Profile	13
2.3.2 Parabolic Exit Velocity Profile	14
2.4 Related Studies	18
CHAPTER III ANALYSIS FOR UNIFORM EXIT CONDITION	21
3.1 Introduction	21
3.2 Theoretical Analysis	21
3.3 Comparison with External Experimental and Theoretical Results	26
3.4 Simplified Theory	31
3.5 Conclusions	33

	Page
CHAPTER IV ANALYSIS FOR PARABOLIC EXIT CONDITION	34
4.1 Introduction	34
4.2 Theoretical Analysis	34
4.3 Comparison with External Experimental and Theoretical Results	37
4.4 Conclusions	40
CHAPTER V EXPERIMENTAL INVESTIGATION	42
5.1 Objectives	42
5.2 Experimental Equipment	43
5.2.1 General Test Facility	43
5.2.2 Jet Chamber	44
5.2.3 Supply Tube	45
5.2.4 Settling Chamber	45
5.2.5 Traverse Mechanism	46
5.2.6 Laser Doppler Anemometer Arrangement	46
5.3 Experimental Procedure	48
5.3.1 Initial Setup, Adjustments and Calibration	48
5.3.2 Velocity Profiles	49
5.4 Results and Discussion	50
5.4.1 Velocity-Frequency-Voltage Relationship	50
5.4.2 Measuring Volume Dimensions	52
5.4.3 Verification of Laminar Jet	53
5.4.4 Centre Line Velocity	53
5.4.5 Jet Half-Radius	54
5.4.6 Velocity Profiles	55
5.4.7 Jet Momentum Flux and Virtual Origin	56
5.5 Conclusions	63
CHAPTER VI SUMMARY OF CONCLUSIONS AND RECOMMENDATIONS	64
6.1 Summary of Conclusions	64
6.2 Recommendations	65
REFERENCES	67
FIGURES	71
TABLES	110
APPENDICES	
A Equipment Table	112
B Rotameter Calibration Curve	113
C Experimental Data	114
D Uncertainty Analysis	135
E Details of Uniform Exit Condition Analysis	144
F Details of Parabolic Exit Condition Analysis	152
VITA AUCTORIS	158

LIST OF FIGURES

Figure	Title	Page
1.1	Characteristic Jet Lengths	71
3.1	Definition of the Flow Model	72
3.2	Nondimensional Velocity Profile ($Re_C=1000$, $x/d=1.250$)	73
3.3	Nondimensional Velocity Profile ($Re_C=200$, $x/d=1.250$)	74
3.4	Nondimensional Velocity Profile ($Re_C=50$, $x/d=1.250$)	75
3.5	Modified Velocity Profile Plot	76
3.6	Variation of W_z with Z for Different Values of W_z	77
3.7	Variation of Potential Core Radius along the Jet	78
3.8	Spread Parameter Variation along the Jet	79
3.9	Plot of X_{cv} vs. X_C	80
3.10	Centre Line Velocity Decay	81
3.11	Jet Half-Radius Variation along the Jet	82
4.1	Jet Flow Regions	83
4.2	Variation of Profile Parameters along the Jet	84
4.3	Centre Line Velocity Decay	85
4.4	Jet Growth	86
4.5	Nondimensional Velocity Profile ($X_C=0.00085$)	87
4.6	Nondimensional Velocity Profile ($X_C=0.00427$)	88
4.7	Nondimensional Velocity Profile ($X_C=0.00692$)	89
4.8	Nondimensional Velocity Profile (Fully Developed)	90
5.1	Flow Test Facility	91
5.2	Overall View of Test Facility	92
5.3	Jet Chamber	93
5.4	Settling Chamber	94
5.5	Laser Doppler Anemometer Arrangement	95
5.6	Laser and Transmitting Optics	96

List of Figures Continued ...

Figure	Title	Page
5.7	Receiving Optics	96
5.8	Signal Processor and Oscilloscope	97
5.9	Flow Visualization of Laminar Jet	97
5.10	Details of Measuring Volume	98
5.11	Verification of Laminar Jet	99
5.12	Centre Line Velocity Variation with Axial Distance	100
5.13	Centre Line Velocity Variation with X^*	101
5.14	Half-Radius Variation with Axial Distance	102
5.15	Nondimensional Velocity Profile ($X_c=0.001$)	103
5.16	Nondimensional Velocity Profile ($X_c=0.005$)	104
5.17	Nondimensional Velocity Profile ($X_c=0.010$)	105
5.18	Nondimensional Velocity Profile (Fully Developed)	106
5.19	Variation of Momentum Ratio with Axial Distance	107
5.20	Variation of Momentum Flux Coefficient with Axial Distance	108
5.21	Determination of K/K_0 and X_{cv} using Centre Line Velocity	109

LIST OF TABLES

Table	Title	Page
4.1	Values of f_m in Equation 4.7	110
4.2	Values of g_m in Equation 4.8	111

NOMENCLATURE

A	area; constant in equations 5.26 and 5.28
b	radial distance to edge of potential core
B	b/d; constant in equations 5.26 and 5.28
d	diameter of tube
d_e^{-2}	diameter of laser beam at the focal point
dm	diameter (minor axis) of ellipsoidal measuring volume
D_e^{-2}	diameter of laser beam at the source
e	2.71828
E	voltage output of tracker; entrainment constant in equation 2.7
E_s	voltage output of tracker due to frequency shift
f_d	doppler frequency
f_s	shift frequency
f_i	indicated frequency
f_n	coefficients in equation 4.7
F	pressure force $\int \frac{pdA}{A}$
F_n	coefficients in equation 4.6
g_m	coefficients in equation 4.8
G_n	coefficients in equation 4.6
I	integral defined as $\int_0^{r_\infty} u^2 d(r^2)$
J	momentum flux
K	kinematic momentum flux = J/ρ

l_f	focal length
l_m	length (major axis) of ellipsoidal measuring volume
l_{nl}	natural laminar length
m	mass of a quantity of fluid
m_c	mass of a container
\dot{m}	mass flowrate
p	pressure
r	radial distance
R	r/d
Re	Reynolds Number based on average velocity at the nozzle exit, $\frac{Vd}{\nu}$
Re_c	Reynolds Number, based on the centre line velocity at the nozzle exit, $\frac{u_{mo} d}{\nu}$
S	range switch setting on the frequency tracker
t	time
T	temperature
u	$u(x,r)$ = axial velocity component
u_m	$u(x,0)$
u_{mo}	$u(0,0)$
u_r	radial velocity component in spherical coordinates
u_θ	azimuthal velocity component in spherical coordinates
U	u/u_m
U_0	u/u_{mo}
U_m	u_m/u_{mo}

- v radial component of velocity
- V average velocity at nozzle exit
- W_n uncertainty in an arbitrary quantity n
- x axial distance measured from nozzle exit plane
- x_v axial distance from point source to the nozzle exit
- x_d axial distance from nozzle exit to the end of the development region
- x_s axial distance measured from the point source
- X $\frac{x}{d Re}$
- x^* $\frac{x}{d \sqrt{Re}}$
- X_{cd} $\frac{x_d}{d Re_c}$
- X_c $\frac{x}{d Re_c}$
- X_{cv} $\frac{x_v}{d Re_c}$
- y radial distance measured from edge of core $y=r-b$; in Chapter V it is a cartesian coordinate defined in Figure 5.3
- z cartesian coordinate
- Z variable defined as $(U^{-3/2} - 1)^{+1/2}$
- α half angle of jet spread = $\cot^{-1}(\gamma/2)$; a constant in equations 2.8 and 2.22
- β momentum flux coefficient, $\int_0^{\infty} U^2(\eta) d\eta^2$; a constant in equations 2.8 and 2.22

- γ Schlichting's jet spread parameter; a constant in equations 2.8 and 2.22
- δ Δ/d
- Δ radial location of $U = 0$
- ϵ $e^{-1/\lambda}$
- ζ a variable defined as $B/(\gamma/Re)$
- η $r/r_{m/2}$
- θ spherical coordinate
- κ half of included angle between intersecting laser beams
- λ unknown function of x ; wavelength of laser light
- μ dynamic viscosity
- ν kinematic viscosity
- ξ similarity variable defined in equation 2.3
- ρ density
- σ a constant in equations 2.8 and 2.22
- ψ r/Δ

Subscripts

- d condition at end of developing region
- m/2 condition where $U = 0.5$
- o condition at $x = 0$
- pc condition at end of potential core
- RMS root mean square

CHAPTER I
INTRODUCTION

1.1. Subject of Investigation

This study deals with a jet of fluid exiting from a round tube or nozzle into a space filled with the same fluid. Such a jet is called an axisymmetric submerged jet and can be either laminar or turbulent at the tube exit. The present study is restricted to jets which are laminar. The velocity profile at the exit of the tube depends upon the length of the tube. If the tube length is very short and there is a smooth entrance, the velocity profile is very nearly uniform across the exit plane since the boundary layer is still negligible in size. If the tube is long, however, a wall layer builds up on the inside tube surface. For long tubes, the wall layer converges at the tube axis. Downstream of this point, no further changes occur regardless of the tube length. In such a case the flow is fully developed and the velocity profile may be shown to be parabolic.

In either of the two velocity profile cases mentioned above the flow in the jet remains laminar for some distance downstream of the tube exit. This distance is referred to as the natural laminar length and is primarily a function of the Reynolds number of the flow. This thesis is devoted only to this laminar region. As the flow proceeds downstream from the tube exit the velocity profile shape changes from that at the tube exit. Beyond a certain distance from the tube exit

the velocity profiles assume a similarity form. This distance is referred to as the development length. Figure 1.1 is provided to make the distinction between development length and transition length. One of these will be shorter than the other. If the transition length is shorter, the question of a laminar development length becomes irrelevant. Similar developed and development regions exist in the turbulent portion of the jet, however, they are of no concern here.

In this study only the laminar jet is considered and special emphasis is given to the developing laminar region.

1.2 Significance

Traditionally, the laminar jet has been studied in connection with gas jet flames and their sensitivity to sound [B3]. Extensive research has been directed at studying the unstable nature of such flows and this effort is still continuing today.

The laminar jet has received increased attention recently due to new and potential applications. The advent of space travel has made necessary the flight and free fall of obstacles at high altitudes. Under such fluid property conditions, laminar flow becomes important. The axisymmetric laminar jet has been considered for use as a wind tunnel to simulate such conditions [G2,G3,G4]. In this case it was especially important to make the exit velocity profile as uniform as possible so that a large potential core existed. The core region was to be used as the test section.

The laminar jet with parabolic or partly parabolic exit profile has found use in the relatively new field of fluidics. The Turbulence Amplifier is a fluidic device which depends upon a laminar jet for its operation. Geometric conditions in this case are such that the development region of the jet is most important. The present work is also important to other fluidic free jet sensing devices.

1.3 Aims

The overall aims of the present work include the following:

(1) to present relatively simple theoretical solutions to describe the velocity field in the developing regions of laminar jets with uniform and parabolic exit velocity profiles.

(2) to evaluate the above mentioned solutions by comparing them with other theoretical and experimental information that is available in the literature.

(3) to investigate, experimentally, the particular case of the parabolic exit velocity profile for the purpose of obtaining information concerning:

- (a) the conservation of momentum
- (b) the proper nondimensional scaling coordinates
- (c) the virtual origin
- (d) the development length

1.4 Method of Presentation

The information to be presented in this investigation is conveniently divided into sections according to a certain rationale. The information available in the literature is considered first and discussed in Chapter II. Analytical investigations are considered next. The uniform and parabolic exit velocity profile solutions are given in Chapters III and IV respectively and compared with the investigations existing in the literature. Chapter V includes the details of the present experimental investigation of the parabolic exit velocity case. A summary of the major conclusions and recommendations is given in Chapter VI.

CHAPTER II

LITERATURE SURVEY

2.1 Introduction

The citations included in this Chapter are, for the most part, restricted to those which deal with newtonian, axisymmetric, isothermal, incompressible jets issuing into an infinite expanse of still fluid. They are further restricted to those which are concerned with the velocity field. Those papers that consider instability, laminar to turbulent transition, "creeping jets" and sensitivity to sound are not, in general, covered. Some exceptions are considered in Section 2.4, entitled 'Related Work'.

2.2 Theoretical Work

2.2.1 Point Source Models

Schlichting [S3] was the first investigator to obtain a solution for the incompressible axisymmetric laminar jet. He found an exact solution for the boundary layer equations assuming that the static pressure is a constant and hence the axial momentum is conserved. The resulting jet may be thought to exit from an infinitesimal orifice with infinite velocity. The axial and radial velocity components are found to be

$$u = \frac{3J}{8\pi\mu} \frac{1}{x_s} \frac{1}{[1 + \xi^2]^2} \quad (2.1)$$

and

$$v = \sqrt{\frac{3J}{4\pi\rho}} \frac{1}{x_s} \frac{\xi - \xi^3}{[1 + \xi^2]^2} \quad (2.2)$$

where

$$\xi = \frac{1}{8v} \left[\frac{3J}{\pi\rho} \right]^{\frac{1}{2}} \frac{r}{x_s} \quad (2.3)$$

Landau [L1, L2] was apparently the first author to obtain a solution, in closed form, for the Navier-Stokes equations applied to the circular, laminar jet, issuing from a point source. The expressions for the flow quantities that result from this method are considerably more difficult to apply than those of Schlichting. Landau also shows that his expression for axial velocity reduces to that of Schlichting for small distances away from the jet centre line.

Squire [S4] independently obtained the same solution as Landau a short time later. As in the case of Landau, the solution is expressed in spherical coordinates. The radial and azimuthal velocity components are given by:

$$u_r = \frac{2v}{r} \left[\frac{2(c+1 - \cos \theta) \cos \theta - \sin^2 \theta}{(c+1 - \cos \theta)^2} \right] \quad (2.4)$$

and

$$u_\theta = \frac{v}{r} \left[\frac{-2 \sin \theta}{c+1 - \cos \theta} \right] \quad (2.5)$$

where

$$\frac{J}{\rho v^2} = 2\pi \frac{32(c+1)}{3c(c+2)} + 8(1+c) - 4(1+c)^2 \ln \left[\frac{(c+2)}{c} \right] \quad (2.6)$$

Morton [M3] derived an analytical solution for the axisymmetric, laminar jet issuing from a point source using an entrainment model. The solution is inferior to Schlichting's but demonstrates the way in which a viscous entrainment model can be constructed.

The velocity profile is included here for completeness.

$$u = \frac{J}{\pi \rho v E x} \exp \left[\frac{-J r^2}{2 \pi \rho v^2 E^2 x^2} \right] \quad (2.7)$$

where E is the entrainment constant.

In reality, jets issue from finite size nozzles and hence the preceding results, if applicable at all, will only be reasonable at points in the flow at great distances from the nozzle exit (Fully Developed Region).

Andrade and Tsien [A3] suggested the concept of a "virtual origin" in order to reduce the differences between their experimental data and Schlichting's model. The virtual origin is a point located inside of the supply tube where the theoretical jet may be assumed to originate. The point is located such that some characteristic in the real flow is matched to that of the theory. As well as determining an experimental value they suggested an analytical method of determination. This consisted of matching the kinetic energy of the flow exiting the nozzle to that in the jet. Other investigators have suggested different flow quantities for matching. These include the centre line velocity and mass flowrate at the nozzle exit and are summarized by Bell [B1].

Although it is possible to reasonably describe conditions in the fully developed region using the virtual origin concept, the predicted velocity profiles in the developing region are unrealistic.

Rumer [R1] considered this problem and found an approximate solution which includes two terms. The first term is the solution of Landau and the other, a second order approximation, important for small distances from the exit. The difficulty with this solution is that a large number of higher order terms would be required to accurately predict velocity conditions. The extreme difficulty in obtaining the second approximation precludes this method. The integral methods of the next section provide a better approximation in this regard.

2.2.2 Integral Methods

Okabe [O1] was the earliest investigator to use an integral method to attempt a solution for the velocity profiles immediately downstream of the nozzle exit. He assumed an equation for the velocity profile which involved the integral of unknown functions of the axial coordinate. The boundary conditions were such that this profile reduced to that of a uniform profile at the nozzle exit. In order to determine the unknown functions he solved the integral momentum equation and the differential momentum equation, subject to the boundary layer assumptions, along the jet centre line and at the jet edge. This solution involved extensive numerical computation which led Okabe to a second approximate solution [O2]. In this case he assumed an

equation of the following form.

$$U_0 = \frac{u}{u_{m0}} = (1 - e^{-\frac{\psi-1}{\lambda}})^3 + \alpha\psi + \beta\psi^2 + \gamma\psi^3 + \sigma\psi^4$$

and

$$\text{for } 0 < \psi < 1$$

$$U_0 = 0$$

$$\text{for } 1 < \psi < \infty$$

(2.8)

where $\psi = r/\Delta$ and Δ is the radial distance to where the velocity is zero. α , β , γ and σ are determined from boundary conditions while λ and Δ are functions of x . These values are determined using a numerical procedure similar to that previously used, however, it was much easier in this case.

Hatta and Nozaki [H1] also considered the uniform exit velocity case. The main body of their paper consisted of an extensive theoretical and experimental study of turbulent jets. In the appendix, however, they extended their theoretical method to the laminar case. An approximate solution for the velocity profiles far downstream was obtained by using the integral form of the momentum and energy equations. The equation form is as given below.

$$U = \frac{u}{u_m} = (1 - \psi)^4(1 + 4\psi) \quad (2.9)$$

where ψ is the same as that previously mentioned for Okabe. In the developing region the flow model consisted of a potential core of radius b and in the free shear layer they used the profile given in equation

2.9 with a modified value of ψ ; that is $\psi = (r-b)/(\Delta-b)$. Using this velocity profile model, along with the momentum and energy equation previously mentioned resulted in a first order, nonlinear, differential equation. This equation, expressed in terms of the present notation, is given as follows

$$\frac{dB}{dX} = \frac{-6188(49) G(21G + 2B)}{9 \sqrt{(7G - 46B)(27027 + 12124GB - 51168B^2)}} \quad (2.10)$$

where $B = b/d$ and $G = (99/7 - 656B^2/49)^{3/2}$. It should be noted that the 49 in brackets in equation 2.10 is missing in Hatta and Nozaki's paper. This equation was solved numerically and the jet boundary, $\delta = \Delta/d$ found from

$$2\delta = \sqrt{G} - 32 B/7 \quad (2.11)$$

In the fully developed region the following equations are given for the centre-line velocity and jet width.

$$\frac{u_m}{u_{m0}} = \left[\frac{247520}{21087} (X - X_{pc}) + 1 \right]^{-1} \quad (2.12)$$

and

$$2\delta = \frac{35360 \sqrt{77}}{7029} (X - X_{pc}) + \frac{3 \sqrt{77}}{7} \quad (2.13)$$

The value X_{pc} is the nondimensional potential core length and is found to be approximately 0.023 from Fig. 24 of Hatta and Nozaki's paper.

It should be stressed that all of the methods in this section apply only to jets with initially uniform velocity profiles. Such a treatment is not available for the laminar, axisymmetric jet with a parabolic exit velocity profile. An analytical investigation of the plane laminar jet with parabolic exit velocity is, however, discussed in Section 2.4, entitled 'Related Work'.

2.2.3 Numerical Methods

Pai and Hsieh [P1] presented finite difference solutions of the boundary layer equations for the cases of two dimensional, axisymmetrical and general three dimensional laminar jets with and without a moving free stream. The axisymmetrical case without free stream is of particular importance here. Results are given in nondimensional terms for the centre line velocity decay and the half-width as functions of distance away from the nozzle exit. The use of the nondimensional distance, X_c , is particularly notable. Uniform and parabolic velocity profiles were assumed at the nozzle exit and the results compared with Schlichting's solution. Also, Schlichting's solution altered by using a virtual origin was also compared. The values of the virtual origin used were those suggested by Andrade and Tsien, obtained by matching the kinetic energy of the exit velocity profile to that of Schlichting's. These values were $X_{cv} = 0.025$ and 0.05625 for the parabolic and uniform cases respectively. They concluded that the value for the parabolic profile agreed reasonably with their analytical result, however, in the uniform case they

obtained a value of 0.075 instead of 0.05625. It should be noted, however, that Pai and Hsieh's interpretation of Andrade and Tsien's X_{cv} values as being experimentally determined is unacceptable.

Fox et al. [F2] presented a numerical finite difference method which can be used for both jet and wake problems. This method is quite general in that it includes heterogeneous mixing of dissimilar gases at different temperatures. Only a few example solutions were presented. Although the present case was not one of those given, this paper is discussed here due to the fact that Greene and Brink [G3] use this method as described later.

du Plessis et al. [D2] and Tsang [T2] used an explicit numerical method to solve the boundary layer equations for the case of the laminar jet. They compared this solution with their own experimental results and with Schlichting's solution. It was found that if the virtual origin was given by $X_{cv} = 0.0275$, Schlichting's profile agreed with their solution in the range $X_c > 0.015$. It should be mentioned that x/d was used in the discussion of results rather than X_c . Only the parabolic exit velocity case was considered.

2.3 Experimental Work

Although there is evidence [B2] of experimental work being conducted in this area near the turn of the century it will not be considered here. This omission is due to the difficulty in obtaining the information and improvements made in measurement methods since that time.

2.3.1 Uniform Exit Velocity Profile

Andrade and Tsien [A3] experimentally studied the case of a liquid, axisymmetric jet issuing into a tank containing the same liquid. They used a suspended particle method to determine the velocity profiles within the jet at large values of x/d . They did not determine profiles in the developing region near the exit of the tube. However, using experimental velocity profiles downstream they inferred that the exit velocity profile was uniform. The profiles that they measured downstream agreed quite well with Schlichting's solution if the theoretical jet was assumed to issue from a virtual origin inside of the tube. An equation relating the position of the virtual origin to geometrical and flow properties was found to be $X_{cv} = 0.04$, using experimental data and a curve fitting technique.

Hrycak et al. [H2] performed experiments with jets that impinged onto a flat plate at ninety degrees. Although the majority of their work concerned turbulent and wall jet flows, a limited number of their experiments can be classified as being laminar. The construction of the nozzle and comparison of the centre line and average velocities ($V/u_{mo} = 0.96$) indicate that the exit velocity profile was almost uniform. It should be noted that only centre line velocity information was presented for the case of interest here.

Greene and Brink [G2, G3 and G4] demonstrated a method of producing a low Reynolds number axisymmetric jet with an initially uniform profile using a porous plate nozzle. They experimentally obtained a

number of velocity profiles in the developing flow region. Plots of u/u_m versus r/r_0 and $r_{m/2}/r_0$ versus x/r_0 were compared with a numerical solution obtained using the finite difference solution of Fox et al. [F2]. The Reynolds number, Re , range covered was from 50 to 1000.

2.3.2 Parabolic Exit Velocity Profile

Vaz [V1], in a study of the response times of Turbulence Amplifiers, used a hot-wire anemometer to measure velocities in a laminar air jet with parabolic exit velocity profile. Both mean velocity and turbulence intensity measurements were made. The jet issued from a 6.35 mm diameter tube into still air. Two values of Reynolds number, Re , were used, namely, 2342 and 3050. These relatively high Reynolds numbers coupled with axial distances which are small yield small values of X_c . As a result, all of the data falls within the first one quarter of the developing region. It was also concluded that no discernible potential core existed.

Symons and Labus [S5] experimentally investigated a helium into helium laminar free jet with a parabolic velocity distribution at the supply tube exit. A total pressure probe was used to obtain velocity profiles for Reynolds numbers, Re , of 437 and 1839 at, 0, 3, 6, 10, 15 and 25 diameters from the nozzle exit. Jet centre line velocity decay and jet spread were also obtained over a range of Reynolds numbers, Re , from 255 to 1839. They also noticed that there was no definable potential core and that centre line velocity decay was larger for lower values

of jet Reynolds number.

The relative size of the total pressure probe and the nozzle diameter, 0.015 and 0.25 cm respectively, gave velocity readings which were significantly in error for measurements taken in regions of high velocity gradient. Also, no steps were taken to ensure that the observed readings were taken only from the laminar portion of the jet.

Chang [C1] experimentally studied the flow development region of the laminar jet and determined the following empirical equation in the range of $0 \leq x/d \leq 10$ for jets with $Re_c = 860$ and 1200 .

$$U = \frac{u}{u_m} = \frac{1 + ab\xi^2 \left[\frac{1 - c\xi^2 - \xi^4}{1 + b\xi^6} \right]}{(1 + \xi^2)^2} \quad (2.14)$$

where $a = 1 - 0.1 x/d$

$b = 1.1026$

$c = 1.2150$.

The numerator in equation 2.14 is a modifying term for the Schlichting profile which gives an almost parabolic profile at $x/d = 0$. This profile is similar to that used by Sato [S2] to study the plane jet. The above empirical equation seems reasonable except that it does not account for the dependence of the development length on Reynolds number. Chang also claims that the value of X_{cv} , determined by matching the centre line velocity of the Schlichting profile to the parabolic, is a reasonable one to use. This gives X_{cv} equal to

0.03125. It should also be mentioned that the experimental data was taken using a hot-film probe. The data was plotted in such a nondimensional fashion that recovery of the dimensional data was impossible.

Tsang [T2] reported the results of his experiments on oil into oil laminar jets. The tube diameter was 9.53 mm and a hot-film probe was used to measure the velocity profiles. Reynolds numbers, Re , of 168 and 290 were used and axial distances such that X_c varied from approximately 0.0025 to 0.035.

Abramovich and Solan [A1, A2] obtained an experimental correlation for the centre line velocity decay as follows.

$$U_m = \frac{1}{aX^*+b} \quad \text{for } X^* > 0.2 \quad (2.15)$$

where $X^* = \frac{x}{d \sqrt{Re}}$

and $a = 1.13$ with $b = 0.89$.

The use of X^* as the axial coordinate is contrary to that obtained by nondimensionalizing the boundary layer equations applied to this case and hence, is questionable.

By comparing their correlations to Schlichtings solution, they concluded that the jet momentum is not conserved as is commonly assumed. In view of the fact that hot wire measurements were taken only along the jet axis, as opposed to velocity profiles, there is no check to determine whether any portion of the jet, namely, the edge of the free shear layer had become

turbulent. It is felt that such a condition could drastically reduce the velocity in the laminar portion of the jet at the centre.

Dmitriev and Kulesova [D1] used the results of a finite difference solution to modify Schlichting's similarity result for use in the developing region of the jet. Further downstream Schlichting's solution is used with a virtual origin that matched kinetic energies as suggested by Andrade and Tsien. The flow model can be summarized mathematically in a convenient form for this investigation as

$$U_0 = \frac{u}{u_{m0}} = \frac{u_m/u_{m0}}{(1 + BR^2)^2} = \frac{U_m}{(1 + BR^2)^2} \quad (2.16)$$

where

$$U_m = 1 - 16X_c \quad \text{for } 0 \leq X_c \leq 0.0188 \quad (2.17)$$

and

$$U_m = \frac{1}{32(X_c + X_{cv})} \quad \text{for } 0.0188 \leq X_c \leq \infty \quad (2.18)$$

also

$$X_c = \frac{x}{d \left(\frac{u_{m0} d}{\nu} \right)} = \frac{x}{d Re_c} \quad (2.19)$$

$$B = 4 U_m^2 \quad (2.20)$$

and

$$X_{cv} = \frac{x_v}{d Re_c} \quad (2.21)$$

They also provided an extremely limited amount of experimental data which was obtained using a miniature total pressure probe.

2.4 Related Work

This section includes a description of a few investigations which do not strictly fall under any of the previous headings and yet are of importance in this study.

Thomas [T1], using an integral method, obtained a solution which gives the concentration and velocity profiles in a planar laminar jet which took into account the occurrence of a parabolic velocity profile at the nozzle exit. Although his solution technique is somewhat different, the method is based upon an assumed form for the velocity profile which is a modification of that used by Okabe [02] for the case of a uniform velocity profile at the nozzle exit. The assumed profile is:

$$U_0 = \frac{u}{u_{m0}} = (1 - \psi^2)(1 - \epsilon e^{\psi/\lambda})^3 + \alpha\psi + \beta\psi^2 + \gamma\psi^3 + \sigma\psi^4$$

$$\text{for } 0 < \psi < 1$$

and

$$U_0 = 0$$

$$\text{for } 1 < \psi < \infty$$

(2.22)

where $\epsilon = e^{-1/\lambda}$, other quantities are the same as for Okabe's.

Samuels and Wetzel [S1] measured velocity profiles in the region close to the exit of a submerged laminar jet issuing from a square nozzle. A Laser Doppler Velocimeter was used to take readings just

upstream and downstream of the exit plane for Reynolds numbers, Re , between 0.25 and 320. Of particular interest to this study is the examination of the flow in the region upstream of the tube exit. They were interested in determining whether any flow adjustment took place within this region.

They conclude that for Reynolds numbers above 40 the fluid is not aware of the exit until the exit is actually reached. It appears, however, from their centre line velocity plot that perhaps a Reynolds number of approximately 300 is a more conservative lower value in this regard.

In any investigation of laminar jets it is important to know the laminar length. Of the information available concerning this topic only two are selected and discussed below.

McNaughton and Sinclair [M2] studied the laminar to turbulent transition of a liquid into liquid jet that was exiting into a variety of short cylindrical vessels. The vessel diameters ranged from 76 to 600 mm and length to diameter ratios were from 1 to 3. The supply tube diameters ranged from 6.35 to 25.4 mm while Reynolds numbers, Re , were in the range of 100 to 28,000. The following empirical relationship was found for the natural laminar to turbulent transition length, l_{nl} .

$$\frac{l_{nl}}{d} = 9.97 \times 10^7 Re^{-2.46} \left(\frac{a}{d}\right)^{-0.48} \left(\frac{b}{d}\right)^{0.74} \quad (2.23)$$

where a and b are the diameter and length of the cylindrical

containing vessel respectively.

Marsters [M1] performed a similar experiment except that the jets were gaseous and exited into free space rather than a containment vessel. Tube sizes from 0.09 to 0.22 cm were used and Reynolds numbers, Re , from 1000 to 2800. The equation that is suggested for obtaining the extent of the laminar region is:

$$\frac{\lambda_{nl}}{d} = 2.25 \times 10^8 Re^{-2.3} \quad (2.24)$$

CHAPTER III.

ANALYSIS FOR UNIFORM EXIT CONDITION

3.1 Introduction

In this Chapter the integral form of the momentum and energy equations, subject to the boundary layer simplifications, are used to obtain an approximate solution for an axisymmetric laminar jet with a uniform profile at the nozzle exit. The solution is expressed in a closed form. The jet flow field is divided into a developing and developed region. In the developing region a potential core is assumed to exist, bounded by an annular free shear layer. Schlichting's velocity profile for an axisymmetric laminar jet is assumed in the free shear layer. The present solution is compared with existing experimental and analytical results.

Also a graphical method for determining the potential core radius and the parameters of the assumed Schlichting profile is given.

3.2 Theoretical Analysis

The following theoretical analysis is similar to that of Hatta and Nozaki [H1]. Their solution, however, only approximately satisfies the boundary layer equations beyond the potential core region. Schlichting's exact solution to the boundary layer equations has been experimentally verified at large distances from the exit of the tube [A3]. Therefore, it seems reasonable to assume Schlichting's form in the free shear

layer surrounding the potential core. At the end of the potential core the solution reduces to Schlichting's.

The flow model and coordinate system are shown in Fig. 3.1. The jet issues from the nozzle with a uniform velocity profile. In the flow development region the potential core extends to a radial distance b . Beyond this is the free shear layer. The axial distance corresponding to $b=0$ defines the end of the flow development region.

The assumed velocity profile in the flow development region may be written nondimensionally as:

$$U_0 = 1 \quad \text{for } 0 \leq R \leq B \quad (3.1)$$

and

$$U_0 = \frac{2(\gamma/Re_c)^2}{(X_c + X_{cv})} \left[1 + \frac{(\gamma/Re_c)^2(R - B)^2}{4(X_c + X_{cv})^2} \right]^{-2} \quad \text{for } B \leq R \leq \infty. \quad (3.2)$$

Equation 3.2 is Schlichting's velocity profile expressed in a convenient form for this study. The centre line of the Schlichting jet has been shifted to the edge of the potential core. It should be noted that continuity of $\frac{\partial u}{\partial r}$ at $R=B$ is automatically attained by this shift. In order to ensure velocity continuity at $R=B$

$$\frac{2(\gamma/Re_c)^2}{(X_c + X_{cv})} = 1 \quad (3.3)$$

or

$$X_c + X_{cv} = 2(\gamma/Re_c)^2 \quad (3.4)$$

Substituting equation 3.4 into equation 3.2 yields

$$U_0 = \left[1 + \frac{(R-B)^2}{16(\gamma/Re_c)^2} \right]^{-2} \quad \text{for } B \leq R \leq \infty \quad (3.5)$$

From the basic conservation equations for mass and momentum of flow, in a constant pressure region without contacting solid surfaces and subject to the boundary layer approximations, the integral momentum and energy equations can be found as:

$$\frac{d}{dx} \int_0^{\infty} ru^2 dr = 0 \quad (3.6)$$

and

$$\frac{1}{2} \frac{d}{dx} \int_0^{\infty} ru^3 dr = -\nu \int_0^{\infty} r \left(\frac{\partial u}{\partial r} \right)^2 dr \quad (3.7)$$

in a manner similar to that given in reference S3.

Using the nondimensional quantities of this study these equations become:

$$\frac{d}{dX_c} \int_0^{\infty} RU_0^2 dR = 0 \quad (3.8)$$

and

$$\frac{1}{2} \frac{d}{dX_c} \int_0^{\infty} RU_0^3 dR = - \int_0^{\infty} R \left(\frac{\partial U_0}{\partial R} \right)^2 dR \quad (3.9)$$

Substituting the velocity profiles (equations 3.1 and 3.5) into the fundamental integral equations (equations 3.8 and 3.9)

and performing the integration we obtain the following two ordinary differential equations:

$$\frac{d}{dX_c} \left[\frac{8}{3} (\gamma/Re_c)^2 + \frac{5\pi}{8} (\gamma/Re_c)B + \frac{B^2}{2} \right] = 0 \quad (3.10)$$

and

$$\begin{aligned} \frac{d}{dX_c} \left[\frac{8}{5} (\gamma/Re_c)^2 + \frac{63\pi}{128} (\gamma/Re_c)B + \frac{B^2}{2} \right] \\ = - \left[\frac{4}{5} + \frac{7\pi}{64} \frac{B}{(\gamma/Re_c)} \right] \end{aligned} \quad (3.11)$$

subject to the boundary conditions

$$\text{at } X_c = 0, B = \frac{1}{2} \text{ and } \gamma = 0.$$

Physically these conditions mean that at the exit of the nozzle the potential core fills the nozzle and the spread rate is zero indicating parallel flow. Integrating equation 3.10 and applying the boundary condition at $X_c = 0$ we get:

$$\frac{8}{3} (\gamma/Re_c)^2 + \frac{5\pi}{8} (\gamma/Re_c)B + \frac{B^2}{2} = \frac{1}{8} \quad (3.12)$$

Introducing a new variable $\zeta = B/(\gamma/Re_c)$ and rearranging equations 3.11 and 3.12 we get:

$$(\gamma/Re_c)^2 = \frac{1}{8(8/3 + \frac{5\pi}{8} \zeta + \frac{\zeta^2}{2})} \quad (3.13)$$

and

$$\frac{d}{dX_c} \left[(\gamma/Re_c)^2 \left(\frac{8}{5} + \frac{63\pi}{128} \zeta + \frac{\zeta^2}{2} \right) \right] = - \left[\frac{4}{5} + \frac{7\pi}{64} \zeta \right] \quad (3.14)$$

Elimination of $(\gamma/Re_c)^2$ between equations 3.13 and 3.14, differentiations inside the brackets and an extensive rearrangement yields:

$$\frac{(3060\pi \zeta^2 + 49152 \zeta + 14400\pi)}{(12 \zeta^2 + 15\pi \zeta + 64)^2 (512 + 70\pi \zeta)} d\zeta = -dX_c \quad (3.15)$$

The method of partial fractions is used to integrate equation 3.15 with the result:

$$\begin{aligned} \bar{A} \ln \left[\frac{12 \zeta^2 + 15\pi \zeta + 64}{(512 + 70\pi \zeta)^2} \right] + \bar{B} \tan^{-1} \left[\frac{24 \zeta + 15\pi}{\sqrt{3072 - 225\pi^2}} \right] \\ + \frac{\bar{C} \zeta - \bar{D}}{(12 \zeta^2 + 15\pi \zeta + 64)} + \bar{E} = X_c \end{aligned} \quad (3.16)$$

where $\bar{A} = -0.1039533$

$$\bar{B} = 0.0269929$$

$$\bar{C} = -0.5161301$$

$$\bar{D} = 2.8176776$$

$$\bar{E} = -0.9053732$$

The above equation is solved by choosing a value of ζ and finding X_c from equation 3.16. The value of $(\gamma/Re_c)^2$ is obtained from equation 3.13 and B from the definition of ζ . The value of X_{cv} may be calculated using equation 3.4. Details of the above solution can be found in Appendix E.

The velocity profile in the free shear layer of the development region can be found by substituting γ/Re_c , X_{cv} and B into equation 3.2. In the developed flow region $B = 0$, also γ/Re_c and X_{cv} are constant corresponding to the Schlichting jet. The values of γ/Re_c and X_{cv} are taken as those at the end of the potential core.

3.3 Comparison with External Experimental and Theoretical Results

In this section, and similar ones to follow, every effort is made to include comparisons with available experimental and theoretical results. In some cases information is available for comparison in one manner but not in another. For example, centre line velocity information is not given by Greene [G4], however, jet spread information is. This fact is mentioned in order to avoid any confusion.

Figures 3.2 to 3.4 show typical velocity profile plots for various values of X_c . These values were chosen because they represent X_c positions near the beginning, the middle and end of the potential core region respectively. The experimental points are those obtained by Greene [G4]. To the author's knowledge these are the only experimental velocity profiles available which accurately represent the development region of an axisymmetric laminar jet with an initially uniform velocity profile. The points denoted as Fox et al. are taken from Greene's thesis [G4]. They are based on the finite difference method given by Fox et al. [F2]. Greene found it necessary to assume that the free stream velocity at a large radial distance was 5% of the centre line

velocity in order to keep computer times down to a reasonable value. This fact indicates that the plotted values may not truly represent the solution by Fox et al., especially near the outer edge of the free shear layer.

Hatta and Nozakji's points were found by solving numerically the differential equation given in their paper [H1], using a modified Euler's method, and following the procedure given therein. The generation of Okabe's curve [O1] involved two stages of numerical integration (functions of modified Bessel functions of the first kind, of orders 0 and 1). This was necessary due to the fact that the tables presented by him do not cover the range of X_c required for this paper.

The present solution can be found either using equation 3.16 and the procedure thereafter described or by using the simplified equations presented in section 3.4. Either method yields essentially the same curve considering the accuracy to which Figs. 3.2 to 3.4 are plotted. The latter method is preferable in the sense of ease of calculation.

From figures 3.2 to 3.4 it can be seen that all of the theoretical solutions considered have reasonable agreement with the experimental velocity profiles. The exception is that Okabe's results deviate appreciably near the outer edge of the free shear layer. Considering the relative simplicity of the present analysis, the agreement with the experimental data is more than satisfactory.

Due to the fact that a Schlichting profile is assumed in the free shear layer a method of graphically determining the Schlichting jet profile parameters (i.e., γ/Re_c , X_{cv}) as well as an estimate of the potential core radius is possible directly from experimental data. This method is somewhat similar to that employed by Andrade and Tsien [A3] to determine the virtual origin of the jet from the experimental velocity profile data far downstream. By rearranging equation 3.5 the following is obtained.

$$R = 4(\gamma/Re_c) (U_0^{-0.5} - 1)^{0.5} + B \quad (3.17)$$

Defining $Z = (U_0^{-0.5} - 1)^{0.5}$ we get:

$$R = 4(\gamma/Re_c)Z + B \quad (3.18)$$

This means that if experimental values of R are plotted against Z the resulting curve should be a straight line with a slope of $4(\gamma/Re_c)$ and an R axis intercept of B . One such plot is shown in Fig. 3.5. Near the central portion of the plot the relationship seems to be linear. The line of best fit for the data points in the range $0.233 \leq Z \leq 1.11$, which corresponds to $0.2 \leq U \leq 0.9$, is shown as the solid line in Fig. 3.5. This was obtained by a linear least square regression of Z on R because Z has considerably more uncertainty than R . The data points outside the range mentioned above deviate from the line.

This behaviour could be explained in part by the fact that the uncertainty in Z is dependent upon the uncertainty in U in a non-linear manner as shown in Fig. 3.6. Uncertainty is magnified at large and small values of Z . This substantiates the selection of a central range of Z for determining the line of best fit which is used to obtain approximate values of γ/Re_c and B .

The resulting values of B are plotted (Method A) on Fig. 3.7 along with the present theoretical prediction and that of Hatta and Nozaki [H1]. The other theoretical analyses do not yield B explicitly and hence are not shown. It is seen that the present theoretical line agrees more closely with the experimental data than the other theoretical line shown. One could, however, question whether there is a bias introduced by the technique used especially the effect of the assumed velocity profile in the free shear layer. Values of B obtained by fitting the experimental data points to Hatta and Nozaki's [H1] assumed velocity profile are also shown (Method B) on Fig. 3.7. The method is similar to the previous one, however, it involves a convergent trial and error procedure. Even this new set of points lie closer to the present theoretical line than that of Hatta and Nozaki.

The values of γ/Re_c found in the manner illustrated in Fig. 3.5 are plotted against X_c in Fig. 3.8. Again the agreement is reasonable considering the uncertainty involved in obtaining γ/Re_c . In the developed flow region γ/Re_c is independent of X_c .

The distance, X_{cv} , to the virtual origin of the Schlichting free shear layer as described in Fig. 3.1 is considered next. Using experimental values of γ/Re_c and X_c , X_{cv} can be found from equation 3.4. Figure 3.9 is a plot of X_{cv} versus X_c including the theoretical variation. The agreement between experiment and theory is not quite as good as in the other figures. The experimental data seem to follow a straight line, passing through the origin having a slightly higher value for the slope than the theoretical line. An attempt to find the significance of the apparent difference should be carried out when more experimental information is available.

This plot serves another important purpose in that it shows the almost exact linear theoretical relationship between X_{cv} and X_c which is the basis for the simplified form of the present solution as given in section 3.4.

It is possible to compare the present solution with other experimental and theoretical results as follows.

A plot of centre line velocity variation with axial distance is shown in Fig. 3.10. This information cannot be extracted from Greene's data. It is possible, however, to compare the experimental data of Hrycak et al. as well as Pai and Hsieh's numerical results. Pai and Hsieh's solution for the parabolic exit condition is also shown for reference. The data of Hrycak et al. is not close to the analytical results for the uniform exit profile case. The disagreement may be due to the slight nonuniformity of the velocity profile at the nozzle

exit. A value of 0.96 is given for the ratio of average to centre line velocity. This explanation seems reasonable in view of the tendency of the data to fall closer to that of the parabolic exit velocity profile than the uniform case.

Pai and Hsieh's numerical method predicts a potential core length that is considerably shorter than the other methods. This length seems unreasonable in view of the plot of potential core width of Greene's experimental data as shown in Fig. 3.7.

The variation of $R_{m/2}$ with axial distance is presented in Fig. 3.11. It was not possible to obtain Pai and Hsieh's solution in the developing region due to inaccuracies in extracting data from their figure. As well, Hrycak et al. did not report values of $R_{m/2}$. Greene's results seem to diverge from the theoretical predictions as the distance downstream increases. A possible exception is that of Hatta and Nozaki. It should be noted that the discrepancies between the theory and experiments are magnified by the choice of scale. Also, the increased spread of the jet at large distances downstream may be due, in part, to the increased chance of turbulent eddies appearing in the flow at these locations.

3.4 Simplified Theory

In most problems X_c is the independent variable, in which case it becomes necessary to either solve equation 3.16 by trial and error or to take values from a graph. Clearly, it is desirable to obtain equations

which give X_{cv} , γ/Re_c and B explicitly in terms of X_c . As shown in Fig. 3.9, X_{cv} is almost exactly a linear function of X_c with a proportionality constant of approximately 630/307. This fact enables us to make an excellent approximation to the solution previously given. The resulting equations are considerably simpler than those mentioned above. Also, they are explicit in the variables needed to obtain the velocity profiles, namely, X_{cv} , γ/Re_c and B as shown below.

$$X_{cv} = \frac{630}{307} X_c \quad (3.19)$$

Using equation 3.19 in 3.4, we get

$$\frac{\gamma}{Re_c} = \sqrt{\frac{X_c}{2} \left(1 + \frac{630}{307}\right)} \quad (3.20)$$

Using equation 3.20 in 3.12, we get

$$B = -\frac{5\pi}{8} \sqrt{\frac{X_c}{2} \left(1 + \frac{630}{307}\right)} + \sqrt{X_c \left(1 + \frac{630}{307}\right) \left(\frac{25\pi^2}{128} - \frac{8}{3}\right) + \frac{1}{4}} \quad (3.21)$$

The accuracy of the above equations in describing the preceding theory may be shown by calculating the root mean square difference between the approximate and original solution. In order to provide these values 154 points were chosen in the developing region at equally spaced intervals of X_c . The resulting values are:

$$(\Delta X_{cv})_{RMS} = 0.000217$$

$$(\Delta Y/Re_c)_{RMS} = 0.000402$$

$$(\Delta B)_{RMS} = 0.000943$$

(3.22)

3.5 Conclusions

- (1) A closed form analytical solution for the developing region of an axisymmetric laminar jet with an initially uniform velocity profile is given.
- (2) The solution presented agrees reasonably well with the available experimental data and most of the previous analytical solutions.
- (3) The simplified solution is much easier to apply than those available in the literature.
- (4) A graphical method for obtaining the potential core width and Schlichting velocity profile parameters in the free shear layer is also presented.

CHAPTER IV

ANALYSIS FOR PARABOLIC EXIT CONDITION

4.1 Introduction

In this Chapter an approximate solution to the velocity distribution in a submerged axisymmetric, laminar jet which issues from a long tube is presented. The solution method is a combination of that of Okabe [02] and Thomas [T1] and takes into account the parabolic profile that exists at the jet exit. Comparisons are made with experimental data taken from the literature and other approximate theories.

4.2 Theoretical Analysis

The basic form of the velocity profile used by Thomas has already been given in equation 2.22 and is repeated here for convenience.

$$U_o = \frac{u}{u_{mo}} = (1-\psi^2)(1-\varepsilon e^{\psi/\lambda})^3 + \alpha\psi + \beta\psi^2 + \gamma\psi^3 + \sigma\psi^4 \quad \text{for } 0 < \psi < 1$$

and

$$U_o = 0 \quad \text{for } 1 < \psi < \infty \quad (2.22)$$

where $\psi = r/\Delta$ and Δ is the radial distance to where the velocity is zero. Also $\varepsilon = e^{-1/\lambda}$ and λ is an unknown function of x which is to be determined along with Δ . Figure 4.1 is an aid to define the variables as well as the flow development regions. α , β , γ and σ are values to

be determined such that the following boundary conditions are satisfied.

$$\text{At } \psi = 0, \quad \frac{\partial u}{\partial \psi} = 0$$

$$\text{and at } \psi = 1, \quad u = \frac{\partial u}{\partial \psi} = 0 \quad (4.1)$$

which gives $\partial^2 u / \partial \psi^2 = 0$ from the differential momentum equation.

By applying these conditions it can be shown that

$$3\alpha = -\beta = \gamma = -3\sigma = \frac{9\epsilon(1-\epsilon)^2}{\lambda} \quad (4.2)$$

Substituting these into equation 2.22 and simplifying yields:

$$u_0 = (1-\psi^2)(1-\epsilon e^{\psi/\lambda})^3 + \frac{3\epsilon\psi(1-\epsilon)^2}{\lambda} (1-\psi)^3 \quad (4.3)$$

This profile is used in conjunction with two equations, each of which expresses a flow condition that must be satisfied. These are the integral momentum equation over the complete jet and the momentum equation in differential form along the x axis.

The integral momentum equation, in a constant pressure region without contacting solid surfaces and subject to the boundary layer approximations is given by:

$$\frac{d}{dx} \int_0^{\infty} r u^2 dr = 0 \quad (4.4)$$

Accordingly, the momentum is constant and the value at the tube exit is equal to that in the jet at any axial distance, x , from the nozzle. Expressing this in convenient nondimensional terms gives

$$\int_0^{\frac{1}{2}} U_0^2 R dR \Big|_{x=0} = \int_0^1 U_0^2 \delta^2 \psi d\psi \Big|_x \quad (4.5)$$

where $\delta = \Delta/d$.

Using the condition that at $x = 0$; $U_0 = 1 - 4R^2$ and equations 4.3 and 4.5 it can be found, as shown in Appendix F, that

$$\delta^2 = \left[24 \sum_{n=0}^6 (F_n + G_n) \epsilon^n \right]^{-1} \quad (4.6)$$

where $F_n = \sum_{m=-2}^5 f_m \lambda^m$ (4.7)

and

$$G_n = \sum_{m=-1}^7 g_m \lambda^m \quad (4.8)$$

The coefficients of λ , f_m and g_m , are given in Table 4.1 and 4.2 respectively.

The momentum equation in differential form, along the x axis and including the boundary layer approximations may be written as

$$u_m \frac{du_m}{dx} = v \left(\frac{\partial^2 u}{\partial r^2} + \frac{1}{r} \frac{\partial u}{\partial r} \right)_{r=0} \quad (4.9)$$

or in convenient nondimensional terms as

$$U_m \frac{dU_m}{dX_c} = \left(\frac{\partial^2 U_0}{\partial R^2} + \frac{1}{R} \frac{\partial U_0}{\partial R} \right)_{R=0} \quad (4.10)$$

Making use of equation 4.3 and integrating both sides of equation 4.10 it is shown in Appendix F that

$$X_c = \frac{1}{2} \int_0^\lambda \frac{\epsilon(1-\epsilon)^4 \delta^2 d\lambda}{[\epsilon(1-3\epsilon) + \frac{2\lambda^2(1-\epsilon)^2}{3} + 6\lambda\epsilon(1-\epsilon)]} \quad (4.11)$$

The value of X_c can be determined by using equations 4.11 and 4.6 and a Simpsons rule integration scheme. Hence, values of λ and δ can be found as functions of X_c . This plot is shown in Fig. 4.2.

4.3 Comparison with External Experimental and Theoretical Results

Using equation 4.3 it can be shown that the dimensionless centre line velocity decay can be found as

$$U_m = (1-\epsilon)^3 \quad (4.12)$$

This quantity is plotted versus X_c in Fig. 4.3 along with Okabe's solution for the uniform case as well as other theoretical and experimental results. The effect that the initial velocity profile has on centre line velocity decay can readily be seen to be significant by comparing Okabe's solution for the uniform case with the present theory. The excellent agreement of the present theory with Dmitriev and Kulesova's theory for $X_c < 0.015$ is particularly noteworthy in view of the fact that theirs was taken from a finite difference solution of the boundary

layer equations. Pai and Hsieh's numerical solution does not agree as well within this region, however, it is close to Dmitriev and Kulesova's far downstream. The difference between Tsang's experimental results and the theory mentioned above could possibly be due to an uncertainty in the value of the kinematic viscosity of the fluid used in their experiments [T2]. Such an uncertainty could possibly shift the data points to X_c values that are 16% greater which would show a better agreement with the present theory. The data of Symons and Labus exhibits a considerable degree of scatter. This could possibly be due to uncertainties in their velocity measurements caused by the size of their pitot tube relative to the tube diameter. It is also questionable whether all of the data points are taken from within the laminar region of the jet. The correlation of Abramovich and Solan is in reasonable agreement with the lower Reynolds number data, however, does not predict the higher Reynolds number data accurately. It appears that although the simple centre line velocity matching scheme of Chang does not agree with either the present theory or that by Dmitriev and Kulesova, it does give a rough estimate of the centre line velocity decay.

Figure 4.4 shows the variation of $R_{m/2}$ along the jet. $R_{m/2}$ is the nondimensional radial coordinate of the point where the jet velocity is one half of the centre line velocity. This parameter is a measure of the spread of the jet. The present theory seems to predict this parameter quite accurately. Pai and Hsieh's numerical

result could not be extracted, accurately, from their graphs in the region near the jet exit. The result indicated is that of the straight line obtained from their graph for large X_c . It appears to give smaller values for $R_{m/2}$ than the other methods.

Figures 4.5, 4.6, 4.7 and 4.8 give velocity profile comparisons within the jet at progressively larger nondimensional distances downstream of the nozzle exit. The first three figures include profiles that are within the developing region of the jet while those in Fig. 4.8 are either fully developed or very close to being so.

In all of these figures the velocity is normalized with the jet centre line velocity and plotted against the radial distance normalized with the radial coordinate to the point where the nondimensional velocity is 0.5. Consequently, all curves pass through the point (1.0, 0.5) in these figures. This method of plotting allows a comparison of profile shapes, independent of $R_{m/2}$ and U_m . The parabolic and fully developed similarity profile are included on each figure.

In general it can be seen that the agreement between the present assumed velocity profile shape and the experiments becomes increasingly worse as the value of X_c becomes larger.

Chang's correlation is seen to be in fair agreement in Fig. 4.5. however, in Fig. 4.6 it reduces to the Schlichting similarity profile since $x/d > 10$. Relatively poor agreement with the experimental data is evident.

Dmitriev and Kulesova's curve is coincident with the similarity profile due to the fact that they only adjusted the centre line velocity and jet spread parameters of this profile in their model.

The results of the present theory for X_c values of 0.035 and 0.060 are plotted on Fig. 4.8. This shows that the present theory almost exhibits a similarity characteristic, however, not that of the experimental data. The classical similarity solution of Schlichting is in good agreement with the data beyond the initial development region.

Chang's correlation is also unable to accurately predict the particular case of $Re_c = 340$ and $x/d = 5$. This again emphasizes that X_c rather than x/d is the proper nondimensional x coordinate.

4.4 Conclusions

- (1) An approximate analytical solution for the axisymmetric laminar jet has been found to predict the jet spread and centre line velocity decay in the initial development region. That is in the approximate range $0 \leq X_c \leq 0.015$.
- (2) The assumed velocity profile shape is exact at the nozzle exit for the case of fully developed pipe flow and is reasonably accurate in the region of the jet immediately downstream. However, beyond the development region, the Schlichting's similarity solution

is preferable.

- (3) Although the velocity profile shape almost exhibits a similarity condition at large axial distances downstream of the nozzle exit, this profile does not reduce to the exact boundary layer solution of Schlichting.

CHAPTER V

EXPERIMENTAL INVESTIGATION

5.1 Objectives

The following experimental program was undertaken in order to provide additional information that either does not exist in the literature or for various reasons cannot be extracted from the published data. The use of a Laser Doppler Anemometer is particularly advantageous in this study in view of the unstable nature of the laminar jet and the destabilizing effect that obstacles submerged in the jet present [P2]. The jet inevitably becomes turbulent at some distance downstream and hence, extreme care should be exercised to ensure that measurements are taken only in the laminar region.

These experiments are specifically designed to obtain accurate velocity profiles in the laminar jet for the purpose of:

- (1) determining whether the proper nondimensional coordinate is X_c or X^* , which is used by Abramovich and Solan [A1].
- (2) determining the jet momentum from the basic, integral definition
- (3) providing additional experimental data to be used in evaluating the current analytical solution for the case of a parabolic exit condition.
- (4) determining quantities such as the virtual origin and development length.

5.2 Experimental Equipment

5.2.1 General Test Facility

This section includes a general description of the closed loop flow circuit used in the present study. Equipment requiring a more detailed description will be considered separately in subsequent sections. The closed loop design permits the use of a wide variety of working fluids, however, only ordinary tap water was used in the present investigation.

A schematic diagram of the facility is presented in Fig. 5.1.

Water from a 50 cm square by 30 cm deep reservoir was pumped to the upstream constant head tank. This tank consisted of a 43 cm diameter by 25 cm deep plexiglass tank with a 5 cm diameter overflow tube located in the centre.

It was supported on a wall approximately 5 m above the laboratory floor. The overflow from the constant head tank was returned to the reservoir. The test fluid from the tank passed through a rotameter, regulating valve and settling chamber before entering the supply tube. These items were fastened onto a laboratory table that was bolted to the floor. This was done in order to maintain alignment with the jet chamber and downstream constant head tank which were located on another stand, also bolted to the floor, some distance away. The measuring volume of the Laser Doppler Anemometer could be positioned at almost any point within the jet chamber using the traverse mechanism upon which it was fastened. The entire Laser Doppler arrangement and

traverse mechanism was situated under the stand which held the jet chamber. A thermometer was located inside the downstream constant head tank for measuring the fluid temperature. This tank was 25 cm in diameter and 24 cm deep with a 5 cm diameter overflow tube located in the centre, similar to the upstream constant head tank. The flow from this tank was returned to the reservoir, at which point it could be either recirculated or directed into a graduated cylinder and weighed in order to determine the mass flowrate.

Figure 5.2 is a photograph of the test facility with the exception of the upstream constant head tank.

5.2.2 Jet Chamber

The jet of interest was formed inside the jet chamber, shown schematically in Fig. 5.3. The end of the supply tube was flush with the inner wall of the jet chamber. Although the chamber is not infinite in lateral extent there is little doubt that it is large enough to simulate an unconfined jet, especially in the region just downstream of the tube exit. The chamber was constructed of plexiglass to allow the laser beams to be positioned as shown. Bleed connections were made on the upper surface and drains on the lower (not shown) to facilitate removal of air bubbles and the working fluid respectively. The fluid flowed out of the chamber through a 50 mm diameter by 30 cm long tube which was connected to the hole in the end plate. This tube was on the same axis as the supply tube. The top plate was covered with black paper except for a 2 mm wide strip along the centre. A

fluorescent light was positioned above this slit to illuminate the dyed laminar jet during flow visualization tests.

5.2.3 Supply Tube

The supply tube consisted of a 2.43 m length of 6.35 mm I.D. stainless steel seamless tubing giving an L/d of approximately 383. According to the equation developed by Langhear [L3] for the laminar development length, the exit velocity profile remains parabolic for Reynolds numbers, Re , below 6600. In order to prevent this long tube from bending, it was placed inside of a 3.18 cm diameter copper pipe with spacers located approximately every 30 cm along the length. An additional aluminium box section was subsequently fastened along approximately 2 m of the supply tube length when excessive bending was detected. The box section was approximately 10 cm square.

5.2.4 Settling Chamber

The settling chamber was connected to the supply tube by means of a bellmouth entrance section as shown in Fig. 5.4. Extreme care was taken to ream the bellmouth neck to the same size as the inner diameter of the supply tube to make the joint as smooth as possible.

As shown, the settling chamber consisted of a plexiglass tube of approximately 14 cm internal diameter and 1.22 m long. A plexiglass tube was chosen in order to locate any air that may be trapped inside. Bleed connections were provided along the top for removal of any such air. One bleed hole was connected to a plastic syringe which contained a weak solution of Meriam No. D-2930 (Green) manometer fluid and water for use in the flow visualization study.

5.2.5 Traverse Mechanism

The traverse mechanism is shown in Fig. 5.2. The Laser Doppler Anemometer components, receiving optics and transmitting optics are located on an angle iron frame which is horizontal and perpendicular to the jet axis. Adjustment in this direction (z direction) is limited to approximately 5 cm from the jet centre line by means of a plexiglass slide mechanism. This adjustment is only used for alignment. The entire angle iron frame that was previously mentioned is fastened onto a carriage which travels on tracks which are parallel to the jet axis (x direction). Each of the above mentioned tracks is in the form of a tee section made by joining two 1.27 cm by 5 cm cold rolled steel bars together. This provides a sturdy track that deflects a negligible amount due to the weight it carries. The carriage is prevented from moving in a direction lateral to the track by roller bearings adjusted to give zero backlash. The tracks just mentioned are securely fastened to the top of a hydraulic table which allows positioning in the vertical direction (y direction). The hydraulic table is bolted to the floor after being positioned relative to the jet chamber.

5.2.6 Laser Doppler Anemometer Arrangement

Figure 5.5 shows a schematic diagram of the Dual Beam Laser Doppler Anemometer arrangement. This is a top view of the equipment as seen in Fig. 5.2. The jet chamber is shown as a dashed line for reference. The details concerning each piece of equipment may be found in the Equipment Table given in Appendix A.

The light from the 15 mW He-Ne laser first passes through a polarization rotator and then an aperture before entering the beam splitter. The beam diameter was 1.1 mm between the $1/e^2$ points. The beam splitter divides the beam into two equal parts that are separated by a distance of 50 mm. The two beams enter the Acousto-optic cell housing. One beam is passed through the cell while the other is sent through a path length equalizer. Both the shifted and unshifted beams exit the Acousto-optic cell housing and are focused onto a point in the jet chamber by the focusing lens. These beams intersect with an included angle of $2\alpha = 27.52^\circ$.

The two beams pass through the chamber and strike a mask. Only scattered light is allowed to enter the collecting lens which collimates the light before it strikes the focusing lens. The lens focuses the scattered light onto the aperture of the photodetector which converts the light intensity variation into electrical variation.

The frequency shifter provides a 40 MHz frequency shift signal to drive the Acousto-optic cell. It also receives the photomultiplier signal and downmixes it to give effective frequency shifts from 10 KHz to 40 MHz in 12 shift increments. The shifted signal is then passed through a high pass filter and into the Frequency Tracker which converts the frequency into a proportional voltage. This voltage is then displayed on the digital voltmeter. An oscilloscope was also used to display the photodetector output signal. The laser and transmitting optics, receiving optics, signal processor and oscilloscope.

are shown in Figs. 5.6 to 5.8 inclusive.

5.3 Experimental Procedure

5.3.1 Initial Setup, Adjustments and Calibration

This section deals with procedures that were necessary to make the equipment ready for the collection of data.

The jet chamber, supply tube and settling chamber were levelled and aligned by "eye" during construction of the equipment, with the aid of a chalk line and carpenters level. The traverse mechanism was levelled in a similar manner and the x axis movement aligned to the side of the jet chamber using a vernier.

The flow system was filled with ordinary tap water until the open air bleeds overflowed. Large plastic syringes were used to aid in the removal of the air from both the settling and jet chambers and afterwards were also used as stoppers.

The Dual Beam Laser Doppler Anemometer arrangement was setup according to the procedures given by Thermo System Inc. in references T3 to T5 inclusive. These procedures are standard and hence will not be repeated here. The use of the Laser Doppler Anemometer requires knowledge of the laser light wavelength, focal distance of the lens and beam spacing. The focal distance and beam spacing given by the manufacturer were checked using a millimeter scale and found to be reasonable and hence the manufacturers values were utilized in all calculations.

The rotameter was calibrated by passing a steady flow of water through it, and recording the time required for a certain mass of fluid to be collected. The calibration curve is given in Appendix B.

5.3.2 Velocity Profiles

The following procedure was employed when recording velocity profile data. The temperature of the water was measured to the nearest tenth of a degree celsius and recorded. The flowrate was set to approximately the desired value using the regulating valve and the rotameter calibration curve. A quantity of water was collected over a certain time and the actual flowrate calculated. This value along with the tube diameter and viscosity of the water were then used to calculate the Reynolds number. If this number was different from the desired by more than 3 percent the flow was adjusted and measured again and the procedure repeated. Once the desired Reynolds number was set, a flow visualization study was conducted to determine the laminar region of the jet. A photograph of the dyed laminar jet is shown in Fig. 5.9. The syringes, dye and florescent lamp were used for this purpose. At this point the positions, in the x direction, at which velocity profiles were to be taken were decided. The first distance was then set on the x axis of the traverse mechanism. The value of the frequency shift and signal processor sensitivity were noted and the measuring volume raised to approximately the centre of the jet in the y direction.

The jet was traversed in the z direction while holding y constant. The centre of the jet in the z direction was determined by using the maximum voltage reading. The z position was set at this value.

The measuring volume was then traversed in the y direction while voltage and distance values were recorded at intervals of 0.25mm over most of the jet. Intervals of 0.50 and 1.25 were used where velocity gradients were small.

5.4 Results and Discussion

5.4.1 Velocity-Frequency-Voltage Relationship

An equation relating the signal processor output voltage and the fluid velocity is required in order to process the raw experimental data. This is partly determined by the Frequency Tracker range setting and partly by the optical arrangement. The fluid velocity is related to the doppler frequency according to equation 5.1 which was taken from reference T3 .

$$f_d = \frac{2 u \sin \kappa}{\lambda} \quad (5.1)$$

It should be noted that the variables κ and λ are quantities that depend upon the working medium. Hence, at first glance it seems that κ and λ must be calculated for the working medium in question. It can easily be shown, however, that the ratio $(\sin \kappa)/\lambda$ is independent of the medium. The insertion of the Acousto-optic cell in the circuit

shifts the frequency indicated to the Frequency Tracker according to equation 5.2:

$$f_i = f_d + f_s \quad (5.2)$$

Also, the tracker converts this frequency into a proportional voltage as expressed in equation 5.3 where S is the range switch setting.

$$E = S f_i \quad (5.3)$$

Combining equations 5.1, 5.2 and 5.3 it can be shown that:

$$u = \frac{\lambda}{2 S \sin \kappa} [E - S f_s] \quad (5.4)$$

The present experimental arrangement had values for the variables in equation 5.4 as given below:

$$\left. \begin{array}{l} \lambda = 632.8 \text{ nm} \\ \kappa = 13.76^\circ \end{array} \right\} \text{ for air}$$

$$f_s = 0.05 \text{ MHz}$$

$$S = 20 \text{ volts/MHz}$$

These values result in the following equation:

$$u = 66.51 [E - 1] \text{ mm/s} \quad (5.5)$$

The value of 1 in this equation is the theoretical voltage that would be recorded when $u = 0$. Zero velocity conditions were

established and the voltage, averaged over at least five minutes was 1.025. Hence, the equation that was used to process the data was

$$u = 66.51 [E - 1.025] \text{ mm/sec.} \quad (5.6)$$

5.4.2 Measuring Volume Dimensions

A diagram showing the details of the focusing optics and measuring volume is shown in Fig. 5.10. As illustrated, the measuring volume is an ellipsoid with minor and major axis of d_m and λ_m respectively. The diameter of the laser beam exiting the laser is D_{e-2} and that at the waist is d_{e-2} .

Reference T3 gives the following equations to be used for estimating these dimensions:

$$d_{e-2} = 4\lambda\lambda_f/\pi D_{e-2} \quad (5.7)$$

$$d_m = d_{e-2}/\cos \kappa \quad (5.8)$$

and

$$\lambda_m = d_{e-2}/\sin \kappa \quad (5.9)$$

In this case D_{e-2} and λ_f are given as 1.1 and 102.1 mm respectively. The other quantities required for the calculations have been given previously. Calculation results in the following dimensions; $d_{e-2} = 0.075$ mm, $d_m = 0.078$ mm and $\lambda_m = 0.315$ mm. It should be noted that these quantities are approximate in view of the fact that λ , κ and λ_f are functions of the fluid medium and this fact

has not been taken into account. It can be shown, however, that the corrections required are small. The length of the measuring volume is approximately the same as a standard subminiature hot wire probe (0.45 mm).

5.4.3 Verification of Laminar Jet

Although the laminar jet length was not measured explicitly in the current set of experiments, the readings were taken well within the laminar region. In order to substantiate this claim it seems appropriate to compare the current measurement locations with the natural laminar length information of independent investigators. The correlations of McNaughton and Sinclair [M2] and Marsters [M1] are used for this purpose. Their results are presented in Fig. 5.11 which is a plot of nondimensional axial distance along the jet, x/d , against the Reynolds number, Re_c . The data points indicate measurement locations used in the current study. It can be seen that all of these points lie within the laminar region indicated by McNaughton and Sinclair whose experiments closely resembled the present case. The points are also within the more restricted laminar region predicted by Marster's correlation.

5.4.4 Centre Line Velocity

The variation of centre line velocity with dimensionless axial distance, X_c , is presented in Fig. 5.12. The agreement with the present theory is excellent near the tube exit. Further downstream this agreement becomes progressively worse. The numerical solution of

Pai and Hsieh falls slightly closer to the experimental data. A fourth order polynomial was used to fit a curve to the data and is plotted on Fig. 5.12. The curve was chosen such that it gave $U_m = 1$ at $X_c = 0$. The resulting equation will be used in a later section and is given below.

$$U_m = 1.00 - 17.94X_c - 176.9X_c^2 + 1.343 \times 10^4 X_c^3 - 1.561 \times 10^5 X_c^4. \quad (5.10)$$

It can be seen that the present data possesses less scatter than the external data shown previously in Fig. 4.3. This fact is an indication that $\frac{x/d}{Re_c}$ is the proper nondimensional coordinate along the jet. When consideration is given to a plot of the same data using X^* as the coordinate this point becomes even more obvious. Such a graph is shown in Fig. 5.13. Considerable scatter is evident, even though only a relatively narrow range of Reynolds numbers, Re_c , is plotted.

5.4.5 Jet Half-Radius

The variation of the so called half-radius, $R_{m/2}$ with X_c is presented in Fig. 5.14 along the current theoretical result and that of Pai and Hsieh's asymptotic line. As in the comparison with the external experiments, their result predicts a considerably narrower jet. Due to the fact that this experimental data is to be used in a subsequent section it has been fitted in a manner similar to the centre line velocity case. A sixth order polynomial was used and the equation is given below.

$$R_{m/2} = 0.3534 - 7.227X_c + 2.328 \times 10^3 X_c^2 - 1.675 \times 10^5 X_c^3 + 6.496 \times 10^6 X_c^4 - 1.237 \times 10^8 X_c^5 + 9.076 \times 10^8 X_c^6. \quad (5.11)$$

The lack of any appreciable scatter is also evident in this diagram.

5.4.6 Velocity Profiles

Dimensionless velocity profiles are presented in Figures 5.15 to 5.18 inclusive. The radial coordinate is nondimensionalized with the half-radius, $r_{m/2}$ which provides an excellent means of comparing profile shapes. The current theoretical velocity profile, the parabolic exit velocity profile and that of Schlichting are also plotted for comparison. The results for $x/d = 4$ and $Re_c = 4000$ are presented in Fig. 5.15. Such a combination of x/d and Re_c yields a value of $X_c = 0.001$ which, according to the current theory, is considerably undeveloped. This is particularly evident in the figure presented since the major portion of the jet flowfield is parabolic. The current theory diverges slightly from the experimental data at the outer edge of the jet. It should also be mentioned that not all of the experimental data have been shown on this diagram or on those which follow. This is done to eliminate overcrowding of data points in the figures. The eliminated data in no way affects the interpretation of the results. A complete set of experimental values is included in tabular form in Appendix C. Samples of data from the complete velocity profile (i.e., both positive and negative values of y) are included in Figures 5.15 to 5.18. This fact in conjunction with a slight asymmetry in the velocity profile data is one reason for the small amount of scatter that appears. An Uncertainty Analysis is presented in Appendix D.

Data from three different Reynolds numbers, Re_c are plotted on Fig. 5.16. The x/d values are chosen so that $X_c = 0.005$ in all three

cases. The fact that all of the curves collapse reasonably onto one substantiates further the earlier claim that X_c is the proper nondimensional coordinate. The disagreement of the present theory at the outer edge of the jet is greater in this figure than that previously shown. The experimental points in the region $r/r_{m/2}$ greater than 1 are approaching Schlichting's solution. In a contrary manner, those points in the region where $r/r_{m/2}$ is less than 1 fall almost on the nondimensional parabola. It appears that, at least in a dimensionless manner, the velocity profile adjustment from the tube conditions to the free jet conditions take place at the jet outer edges first. Further adjustment in the outer region is evident also in the data at $X_c = 0.01$, presented in Fig. 5.17. The collapse of the experimental data and an increased difference between theory and experiment are also apparent in this figure.

Figure 5.18 contains experimental data from three different X_c conditions, namely, 0.018, 0.025 and 0.035. These results seem to fall reasonably close to the Schlichting velocity profile. This indicates that fully developed conditions exist at an axial distance given approximately by $X_{cd} = 0.018$. This value is in reasonable agreement with the values found in the references.

5.4.7 Jet Momentum Flux and Virtual Origin

The velocity profile data in this investigation was collected at sufficiently small radial increments so that the basic definition could be used to determine the momentum flux in the axial direction. The

kinematic momentum flux will be used here and is defined below:

$$K = \frac{J}{\rho} = 2\pi \int_0^{\infty} u^2 r dr \quad (5.13)$$

In order to use this definition directly, it is necessary to perform the integration numerically. It is also convenient to modify the equation as follows

$$K = \pi \int_0^{\infty} u^2 d(r^2) \quad (5.14)$$

This equation is now approximated using the trapezoidal rule as shown below:

$$K = \pi \sum_{i=1}^{n-1} \frac{(r_{i+1}^2 - r_i^2)(u_i^2 + u_{i+1}^2)}{2} \quad (5.15)$$

where n is the number of data points. It should also be mentioned that the profile was integrated between the points where $u = 0.05 u_m$. If such data points did not exist, they were generated using an interpolation procedure. This step was taken to avoid error accumulation due to possible inaccuracies near the jet boundaries.

The momentum flux is made dimensionless by dividing it by the value at the tube exit, K_0 . In the case of a parabolic exit profile this value can be shown to be:

$$K_0 = \frac{\pi d^2}{12} u_{m0}^2 \quad (5.16)$$

The value of u_{m0} is determined using the mass flowrate information. A plot of the variation of K/K_0 with axial distance is shown on Fig. 5.19.

Considerable scatter of the data can be seen, however, there seems to be a general trend. An initial decrease in K/K_0 is followed by an increase to a value greater than one. A constant value is reached farther downstream. The occurrence of this trend is strengthened by the determination of the dashed line which is now considered.

One reason for the scatter of the data in Fig. 5.19 can be readily seen by considering equation 5.14, rearranged as follows:

$$\begin{aligned}
 K &= \pi r_{m/2}^2 u_m^2 \int_0^\infty (u/u_m)^2 d(r/r_{m/2})^2 \\
 &= \pi r_{m/2}^2 u_m^2 \beta
 \end{aligned}
 \tag{5.17}$$

and nondimensionally as

$$\frac{K}{K_0} = 8 R_{m/2}^2 U_m^2 \beta/\beta_0
 \tag{5.18}$$

where $\beta_0 = 2/3$ for a parabolic exit velocity profile. This equation separates the determination of K/K_0 into three parts: the half-radius, $r_{m/2}$; the local maximum velocity, u_m and a nondimensional integrated value, β which is referred to as a momentum flux coefficient. Each of these quantities is determined with some degree of uncertainty and the combination is more uncertain. A method of obtaining K/K_0 with less uncertainty is to arrive at the values in equation 5.18 separately. Empirical equations have already been given for $R_{m/2}$ and U_m as a function of X_c . A plot of β/β_0 versus X_c is presented in Fig. 5.20. The degree of scatter that is evident on the graph is considerably less

than that of K/K_0 . It is also noticed that this curve seems to indicate a development length longer than that mentioned previously.

A curve was fit to this data in a manner similar to that of U_m and $R_m/2$. The form of the equation that yields a good representation of the data is that presented below:

$$\beta/\beta_0 = 1.37 (5.79 \times 10^{-4} + X_c)^{0.0419} \quad (5.19)$$

The empirical relations mentioned above were used in conjunction with equation 5.18 to plot the dashed line in Fig. 5.19. The trend that this line indicates has two aspects which are particularly interesting. One is the increase in momentum far downstream. This observation is contrary to that of Abramovich and Solan [A1] who noticed a decrease in momentum. The possibility of an increase in momentum is certainly a point that one may question. The conditions under which such an increase can occur are considered as follows.

A control volume is chosen, which completely includes the developing region of the jet. It is infinite in radial extent. The x-component of the momentum theorem applied to this control volume yields the following equation

$$\int_{\infty} \frac{p_0}{\rho} dA_0 - \int_{\infty} \frac{p_d}{\rho} dA_d = - \int_{\infty} u^2 dA_0 + \int_{\infty} u^2 dA_d \quad (5.20)$$

or

$$\frac{F_0 - F_d}{\rho} = -K_0 + K_d \quad (5.21)$$

However, the (gauge) pressure forces on planes within the fully

developed region must be zero and therefore

$$\frac{K_d}{K_0} = \frac{F_0}{\rho K_0} + 1 \quad (5.22)$$

This equation indicates that the ratio K_d/K_0 can be greater than one if the pressure force across the exit plane is positive. Such a condition may occur if some pressure adjustment occurs outside of the tube. This is an hypothesis which is in need of verification.

The second point of interest on this graph is the initial decrease of the momentum ratio. By assuming that the pressure gradient at the exit of the tube is approximately zero, and that, the wall shear stress persists an infinitesimal amount outside of the tube, it is possible to show that

$$\left. \frac{d(K/K_0)}{dX_c} \right|_{X_c=0} = -48 \quad (5.23)$$

This equation gives the slope of the curve in Fig. 5.19, at $X_c=0$ and is observed to be in fair agreement with the data. This result also seems reasonable when it is considered that the velocity profiles must approach a parabolic shape as the distance downstream tends to zero. Caution should be exercised in using the correlations for U_m , $R_{m/2}$ and β/β_0 with equation 5.18 in order to determine this slope due to inherent inaccuracies near $X_c=0$.

The jet momentum as well as the virtual origin can be determined using the Schlichting velocity profile and experimental data at large distances downstream. In this investigation, the developing region is of particular interest and hence not much data is available far

downstream. These methods are, however, applied to the data as follows.

The first method of determining K/K_0 and X_{cv} makes use of centre line velocity data, Schlichting's velocity profile (equation 2.1) and the virtual origin concept of Andrade and Tsien [A3]. The following equation may be obtained:

$$X_c = \frac{K/K_0}{32 U_m} - X_{cv} \quad (5.24)$$

If the experimental data, taken from the region far from the tube exit, is plotted on a graph with X_c as ordinate and $1/U_m$ as abscissa a straight line results. The slope of the line is $\frac{K/K_0}{32}$

while the intercept on the X_c axis is $-X_{cv}$. Such a graph is plotted in Fig. 5.21. The resulting values of K/K_0 and X_{cv} are found to be 0.997 and 0.028 using linear regression. The standard deviations of these quantities are also found to be 0.034 and 0.0018 respectively. The value of K/K_0 found above is in agreement with the assumption of a constant momentum and not too different from that previously found in this work. The X_{cv} value is extremely close to that given by du Plessis et al. [D2].

The second method of determining K/K_0 and X_{cv} is similar to the first, however, use is made of the $R_{m/2}$ variation with axial distance instead of centre line velocity. The following formula can be derived in a manner similar to equation 5.24 :

$$R_{m/2} = \left[\frac{(\sqrt{2} - 1) 256}{K/K_0} \right]^{3/2} [X_c + X_{cv}] \quad (5.25)$$

This equation indicates a linear variation of $R_{m/2}$ with X_c in the fully developed region and can be expressed as shown below:

$$R_{m/2} = A + B X_c \quad (5.26)$$

A and B can be determined from the experimental data and K/K_0 and X_{cv} calculated as follows:

$$K/K_0 = \frac{(\sqrt{2} - 1) 256}{B^2} \quad (5.27)$$

and

$$X_{cv} = \frac{A}{B} \quad (5.28)$$

The values determined using linear regression on the last seven data points are $K/K_0 = 0.738$ and $X_{cv} = 0.022$. The standard deviations are found to be 0.0314 and 0.00072 respectively. The K/K_0 and X_{cv} values found above are considerably different than those found using the centre line velocity method, however, the standard deviations are almost the same. A Student's t test of the values indicate a significant difference. This result is not that which would have been expected, especially in view of the velocity profile similarity conditions. Explanation of this point should be attempted after obtaining more data in the developed region.

5.5 Conclusions

1. X_c is the proper nondimensional coordinate for laminar jets.
2. The length of the developing region, virtual origin and K/K_0 are found to depend upon the method used to determine them.
3. The experimental results indicate a slight variation of the momentum flux along the jet, however, conservation of momentum is a reasonable approximation. An attempt to explain the trend of the variation is also presented.
4. The agreement between the experimental results and the present analytical solution is reasonable.

CHAPTER VI

SUMMARY OF CONCLUSIONS AND RECOMMENDATIONS

6.1 Summary of Conclusions

The most significant conclusions made at the end of the previous three chapters are now summarized. This effort will serve to consolidate the separate sections and relate them to the overall aims of the present work.

Relatively simple analytical solutions are presented which give the velocity fields in the developing regions of laminar jets with both uniform and parabolic exit velocity profiles. The solution given for the uniform case is the first of an integral type to be obtained in a closed form and also has the desirable feature of reducing to the exact solution of Schlichting in the fully developed region. In the case of an axisymmetric jet with a parabolic exit velocity profile the solution is the first of an integral type. Both of the analytical results agree reasonably well with experimental data and theoretical work that is available in the literature for the jet development region. The differences between the experimental and analytical results increase as the distance from the exit increases.

The present experimental results have considerably less scatter than most of those in the literature and are consistent with the relevant conclusions previously made concerning the current analytical method for

the parabolic exit velocity condition. Also, X_c is shown to be the proper nondimensional coordinate required to collapse the experimental data. This is contrary to that found by Abramovich and Solan [A1] but consistent with a dimensional analysis of the pertinent equations.

It is shown that the common assumption of conservation of momentum is only a reasonable approximation. An apparent trend of the variation of momentum along the jet axis is presented and the salient features discussed in relation to the equations of motion and appropriate assumptions. Finally, the constant value of the momentum in the fully developed region, the virtual origin and the length of the development region appear to depend upon the method of determination. Further verification and an explanation of this point are left for a future study.

6.2 Recommendations

It appears that additional work is required in the area of laminar axisymmetric jets. This work includes both experimental and analytical studies as follows.

In the case of a uniform exit velocity profile additional experimental information is required. Both the development and fully developed regions should be investigated concurrently. The method of producing the uniform profile employed by Greene [G2] should be used along with the method of measuring velocity used in the present investigation. Also, precautions to ensure that a laminar jet exists

similar to those of the current investigation should be made.

Further experimental data should be collected for the case of a parabolic exit velocity profile. Emphasis should be given not only to the development region but also to the fully developed region. Such an investigation should focus on the momentum flux variation and the dependence of the fully developed momentum flux, virtual origin and development length on the method of determination.

Also, the momentum flux variation is consistent with a zero axial pressure gradient on the jet centre line at the nozzle exit as well as a positive value of gauge pressure at this point. It would be desirable to experimentally confirm this using direct pressure measurements, however, this would likely be difficult because of the small pressure differences likely to be encountered.

An analytical model which reduces to the Schlichting profile in the development region should be investigated. Such a study could possibly make use of the experimental fact that the central portion of the jet velocity profile remains parabolic when nondimensionalized with respect to the local centre line velocity.

Pai and Hsieh's [P1] numerical solution should be repeated in order to yield accurate information in the development and fully developed region. This would help to explain the apparent differences that exist. Use of the other available numerical methods; namely, that of du Plessis [D2] or Fox et al. [F2] would also suffice in this regard.

REFERENCES

- A1 Abramovich, S. and Solan, A., "The Initial Development of a Submerged Laminar Round Jet", *Journal of Fluid Mechanics*, Vol. 59, part 4, 1973, pp. 791-801...
- A2 Abramovich, S. and Solan, A., "Turn-on and Turn-off Times for a Laminar Jet", *ASME Journal of Dynamic Systems, Measurement and Control*, Vol. 95, 1973, pp. 155-160.
- A3 Andrade, E.N. and Tsien, L.C., "The Velocity Distribution in a Liquid into Liquid Jet", *Proceedings of the Physical Society, London*, Vol. 29, Part 4, 1937, pp. 381-391.
- B1 Bell, A.C., "An Analytical and Experimental Investigation of the Turbulence Amplifier", ScD thesis, Mechanical Engineering Department, Massachusetts Institute of Technology, 1969.
- B2 Birkhoff, G. and Zarantonello, E.H., Jets, Wakes and Cavities, Academic Press, New York, 1957, p. 274.
- B3 Brown, G.B., "The Vortex Motion in Gaseous Jets and the Origin of their Sensitivity to Sound", *Proc. of the Physical Society of London, England*, Vol. 47, 1935, pp. 703-732.
- C1 Chang, H., "An Analytical and Experimental Investigation of a Large-Scale Model of a Turbulence Amplifier", M.Sc. thesis, State University of New York at Buffalo, 1972.
- D1 Dmitriev, V.N. and Kulesova, N.A., "The Calculation of a Laminar Jet in the Surroundings of the Supply Nozzle", *Proceedings of the "Jablonna" Fluidics Conference*, Budapest, Hungary, Nov. 1974, pp. 83-91.
- D2 du Plessis, M.P., Wang, R.L. and Tsang, S., "Development of a Submerged Round Laminar Jet from an Initially Parabolic Profile", *ASME Journal of Dynamic Systems, Measurement and Control*, Vol. 95, 1973, pp. 148-154.

- F1 Foster, K. and Parker, G.A., Fluidics: Components and Circuits, Wiley-Interscience, London, 1970, pp. 94-96.
- F2 Fox, H., Sinha, R. and Weinberger, L., "An Implicit Finite Difference Solution for Jet and Wake Problems", *Astronautica Acta*, Vol. 17, 1972, pp. 265-278.
- G1 Gaunter, J.W., Livingood, J.N.B. and Hrycak, P., "Survey of Literature on Flow Characteristics of a Single Turbulent Jet Impinging on a Flat Plate", NASA TN D-5652, February 1970.
- G2 Greene, G.C., "Comparison of Measured and Calculated Velocity Profiles of a Laminar Incompressible Free Jet at Low Reynolds Numbers", NASA TN D-7510, May 1974.
- G3 Greene, G.C. and Brink, D.F., "Method for Producing a Uniform, Low Reynolds Number Jet", *J. of Spacecraft and Rockets*, Vol. 11, no. 8, August 1974, pp. 604-605.
- G4 Greene, G.C., "An Investigation of a Free Jet at Low Reynolds Numbers" M. Eng. thesis, Mech. Eng. Dept., Old Dominion Univ., Norfolk, Va., Aug. 1973.
- H1 Hatta, K. and Nozaki, T., "Two-Dimensional and Axisymmetric Jet Flows with Finite Initial Cross Sections", *Bull. of the J.S.M.E.*, Vol. 18, no. 118, April 1975, pp. 349-57.
- H2 Hrycak, P., Lee, D.T., Gaunter, J.W. and Livingood, J.N.B., "Experimental Flow Characteristics of a Single Turbulent Jet Impinging on a Flat Plate", NASA TN D-5690, March 1970.
- K1 Kennedy, J.B., and Neville, A.M., Basic Statistical Methods for Engineers and Scientists, 2nd ed., IEP, New York, N.Y., 1976.
- K2 Kline, S.J. and McClintock, F.A., "Describing Uncertainties in Single-Sample Experiments", *Mechanical Engineering*, Jan. 1953, pp.3-8.
- L1 Landau, L.D., "A New Exact Solution of the Navier-Stokes Equations", Collected Papers of L.D. Landau, 2nd ed., D. Ter Haar ed., Gordon and Breach, Science Publishers, 1967, pp. 383-386.
- L2 Landau, L.D., "A New Exact Solution of the Navier-Stokes Equations", *C.R. Acad. Sci., URSS*, Vol. 43, 1944, pp. 286-89.

- L3 Langhaar, H.L., "Steady Flow in the Transition Length of a Straight Tube", Journal of Applied Mechanics, June 1942, pp. A55-58.
- M1 Marsters, G.F., "Some Observations on the Transition to Turbulence in Small, Unconfined Free Jets", Report #1-69, Dept. of Mech. Eng., Queens University, Kingston, Ontario, Canada, Oct. 1969.
- M2 McNaughton, K.J. and Sinclair, C.G., "Submerged Jets in Short Cylindrical Flow Vessels", Jour. of Fluid Mechanics, Vol. 25, pt. 2, 1966, pp. 367-375.
- M3 Morton, B.R., "Entrainment Models for Laminar Jets, Plumes, and Wakes", The Physics of Fluids, Vol. 10, no. 10, October 1967, pp. 2120-2127.
- O1 Okabe, J., "Approximate Calculations of Laminar Jets", Rep. Res. Inst. Fluid Eng., Kyushu Univ., Vol. 5, 1948, pp. 1-13.
- O2 Okabe, J., "Approximate Calculations of Laminar Jets (continued)", Rep. Res. Inst. Fluid Eng., Kyushu Univ., Vol. 5, 1948, pp. 15-22.
- P1 Pai, S.I. and Hsieh, T., "Numerical Solution of Laminar Jet Mixing with and without Free Stream", Applied Scientific Research, Vol. 27, no. 1, October 1972, pp. 39-62.
- P2 Powell, A., "Vortex Action on Edgetones", Journal of the Acoustical Society of America, Vol. 34, 1962, pp. 163-166.
- R1 Rumer, Yu.B., "Problem of Submerged Jet", Prikladnaja Matematika i Mekani, Vol. 15, 1952, pp. 255-56.
- S1 Samuels, M.R. and Wetzel, D.M., "Velocity Profiles in the Exit Region of a Submerged Laminar Jet", The Chemical Engineering Journal, Vol. 4, 1972, pp. 41-45.
- S2 Sato, H., "The Stability and Transition of a Two-Dimensional Jet", Journal of Fluid Mechanics, Vol. 7, 1960, pp. 53-80.

- S3 Schlichting, H., Boundary Layer Theory, 6th ed., McGraw-Hill, New York, N.Y., 1968, pp. 218-221.
- S4 Squire, H.B., "The Round Laminar Jet", Quarterly Journal of Mechanics and Applied Mathematics, Vol IV, pt. 3, 1951, pp. 321-329.
- S5 Symons, E.P. and Labus, T.L., "Experimental Investigation of an Axisymmetric Fully Developed Laminar Free Jet", NASA TN D-6304, 1971.
- T1 Thomas, A.L., "Force and Mass Balances of the Incompressible, Isothermal, Planar Laminar Jet Issuing from a Finite Source", Chemical Engineering Science, Vol. 8, 1958, pp. 254-264.
- T2 Tsang, S., "A Study of Axisymmetric Submerged Jets Relevant to Turbulence Amplifier Design", Masters thesis, Dept. of Mechanical Engineering, Sir George Williams University, Montreal, Canada, August 1971.
- T3 Thermo Systems 900 Series Laser Optics Instruction Manual, TSI Incorporated, St. Paul, Minnesota.
- T4 Thermo Systems Model 1090 Tracker Instruction Manual, TSI Incorporated, St. Paul, Minnesota.
- T5 Thermo Systems Model 980 Frequency Shifter Instruction Manual, TSI Incorporated, St. Paul, Minnesota.
- Y1 Vaz, T., "An Experimental Investigation into the Response of a Turbulence-Type Amplifier, and Laminar/Turbulent Jet Study", M.A.Sc. thesis, Department of Mechanical Engineering, University of Windsor, Windsor, Ontario, Canada, 1970.

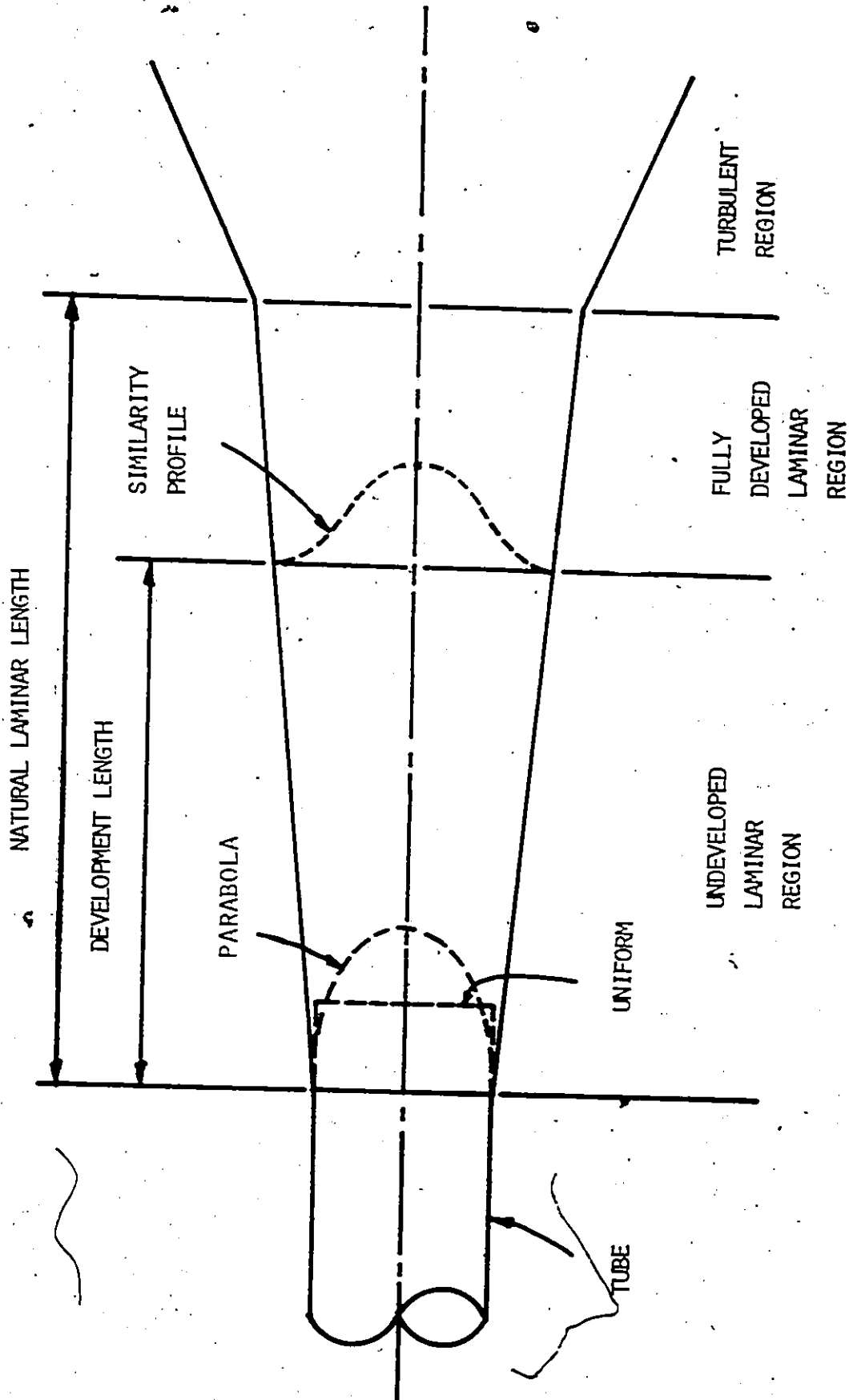


FIG. 1.1.1 CHARACTERISTIC JET LENGTHS

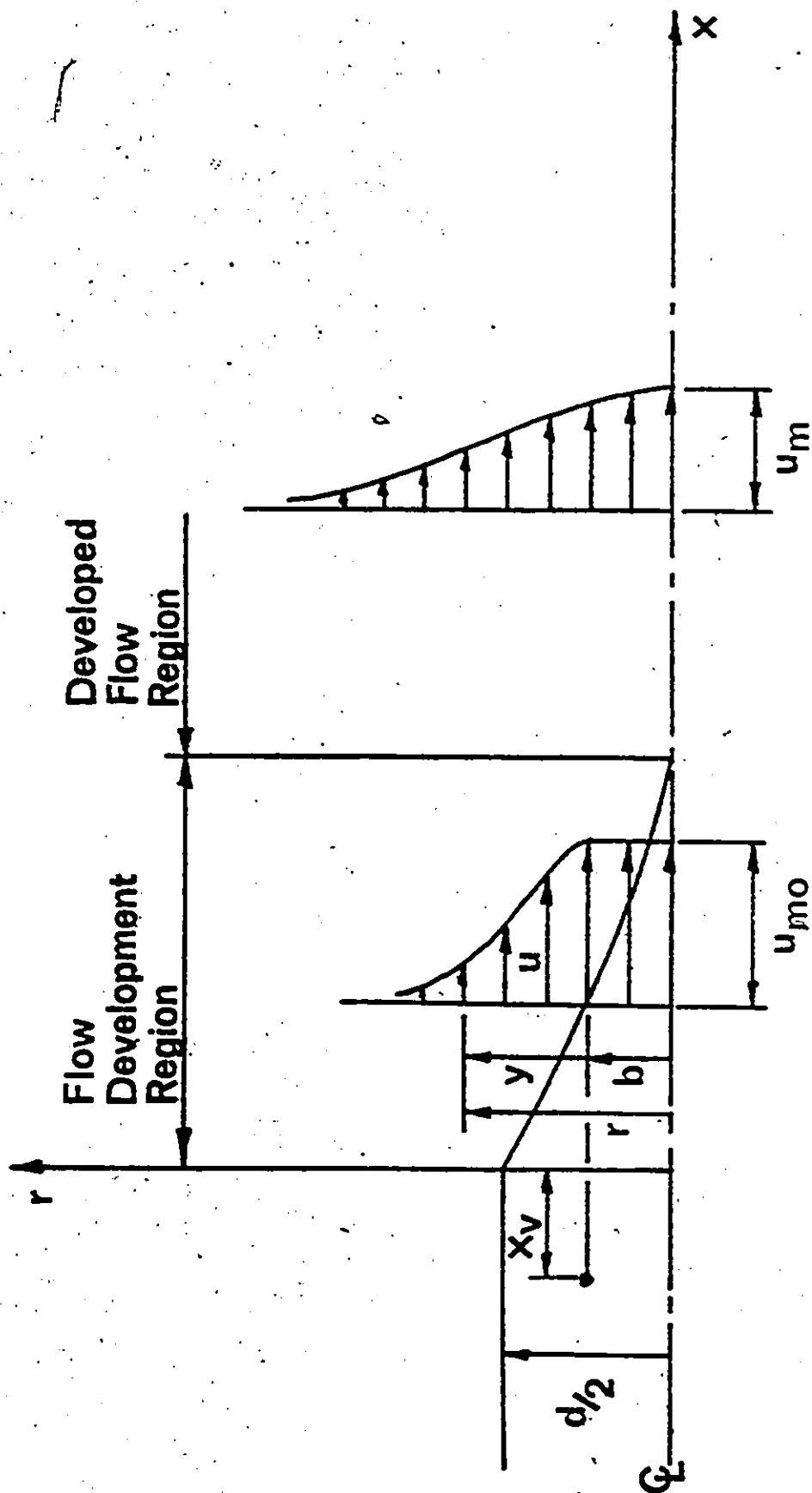


FIG. 3.1.1 DEFINITION OF THE FLOW MODEL

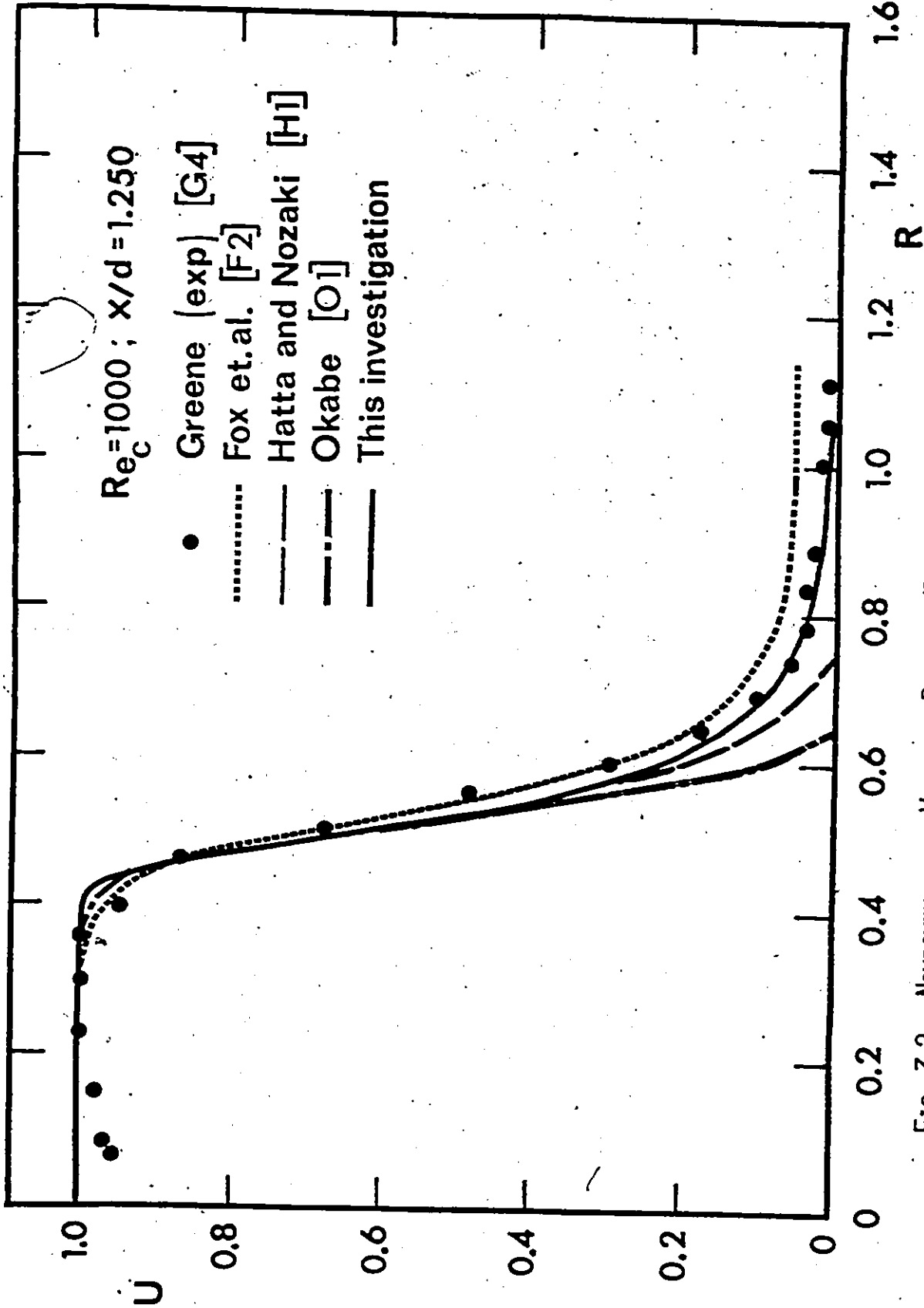
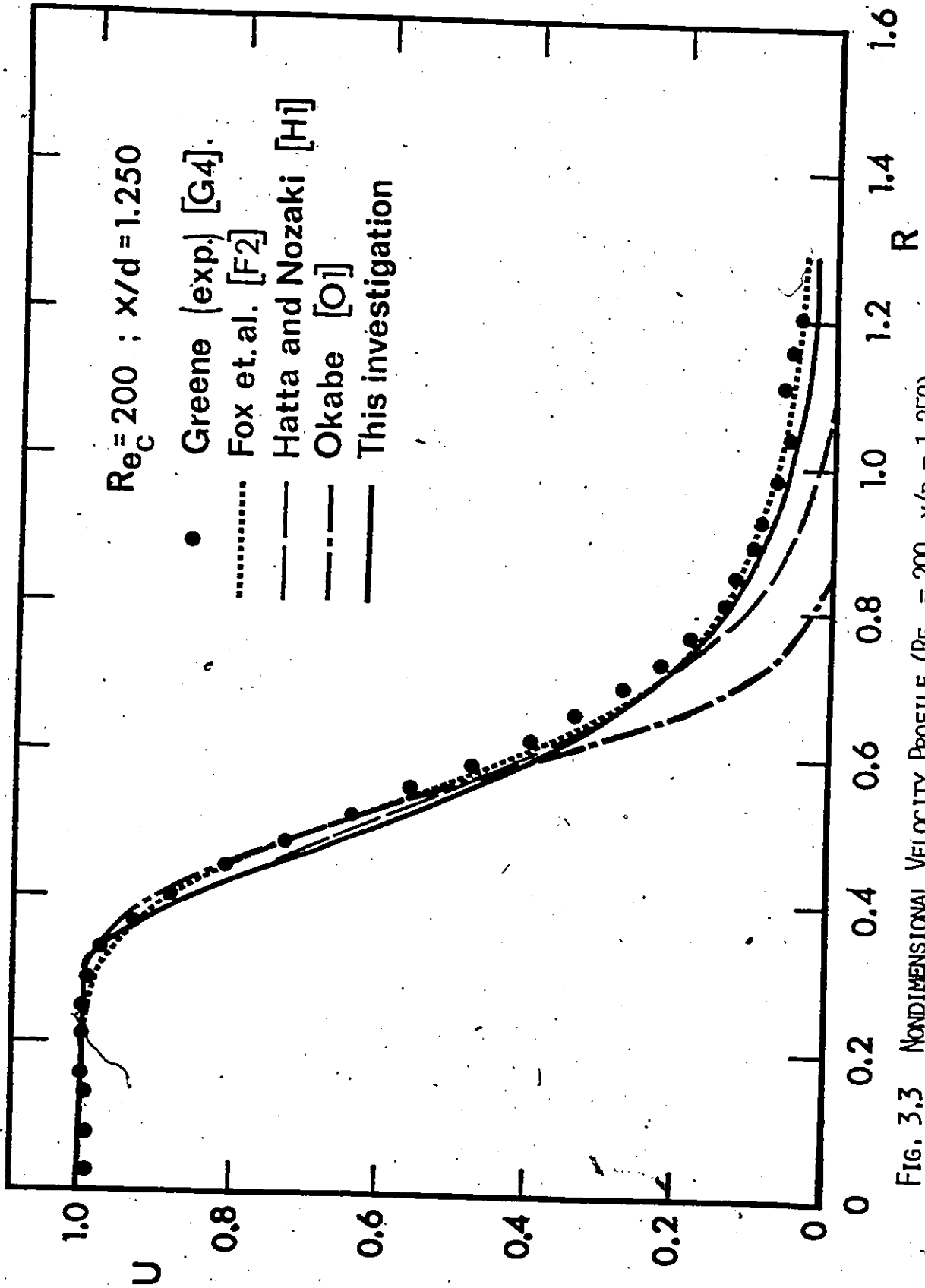


FIG. 3.2 NONDIMENSIONAL VELOCITY PROFILE ($Re_c = 1000, x/d = 1.250$)

FIG. 3.3 NONDIMENSIONAL VELOCITY PROFILE ($Re_c = 200, x/d = 1.250$)

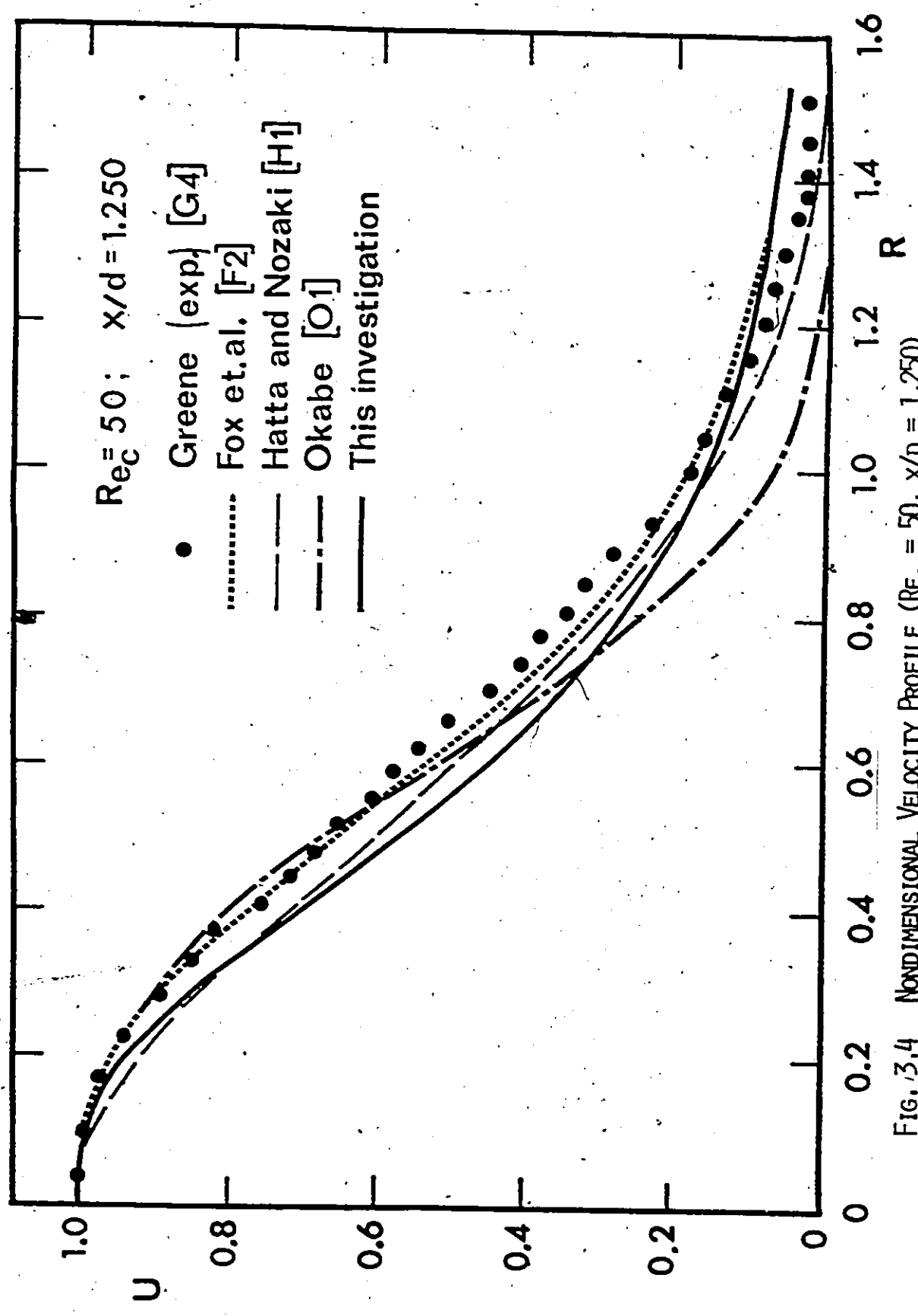


FIG. 3.4 NONDIMENSIONAL VELOCITY PROFILE ($Re_c = 50, x/d = 1.250$)

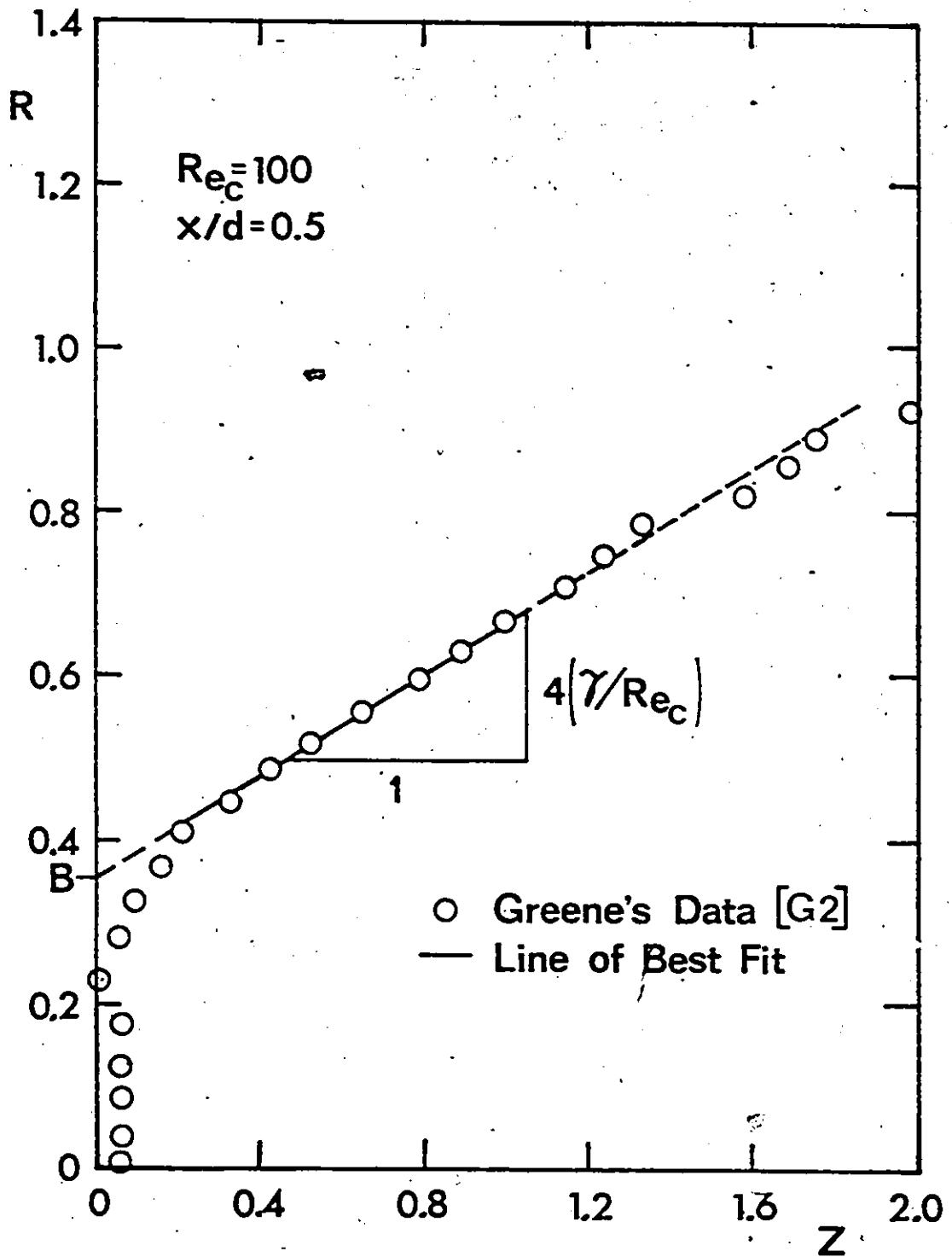


FIG. 3.5 MODIFIED VELOCITY PROFILE PLOT

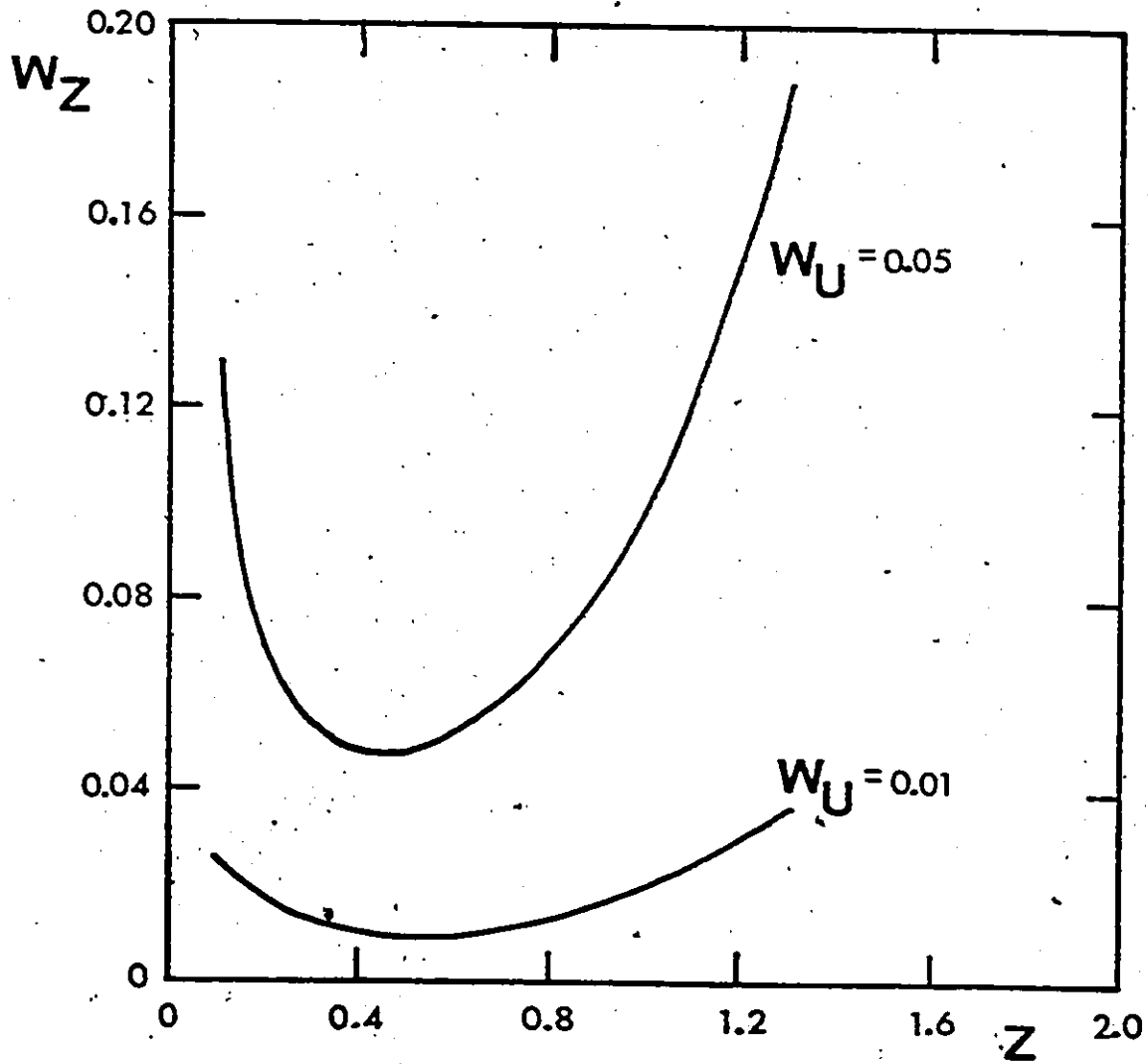


FIG. 3.6 VARIATION OF W_Z WITH Z FOR DIFFERENT VALUES OF W_U

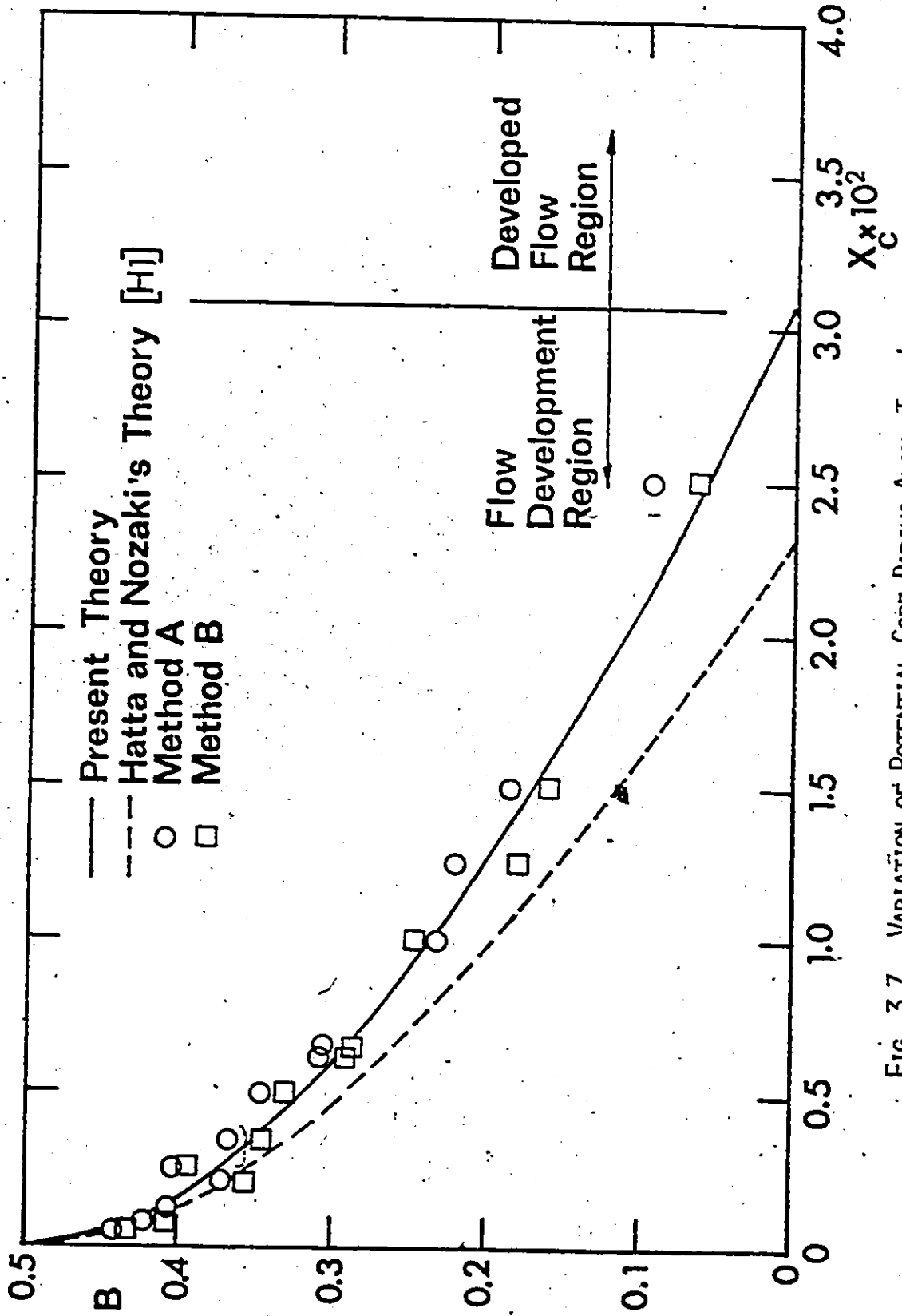


FIG. 3.7 VARIATION OF POTENTIAL CORE RADIUS ALONG THE JET

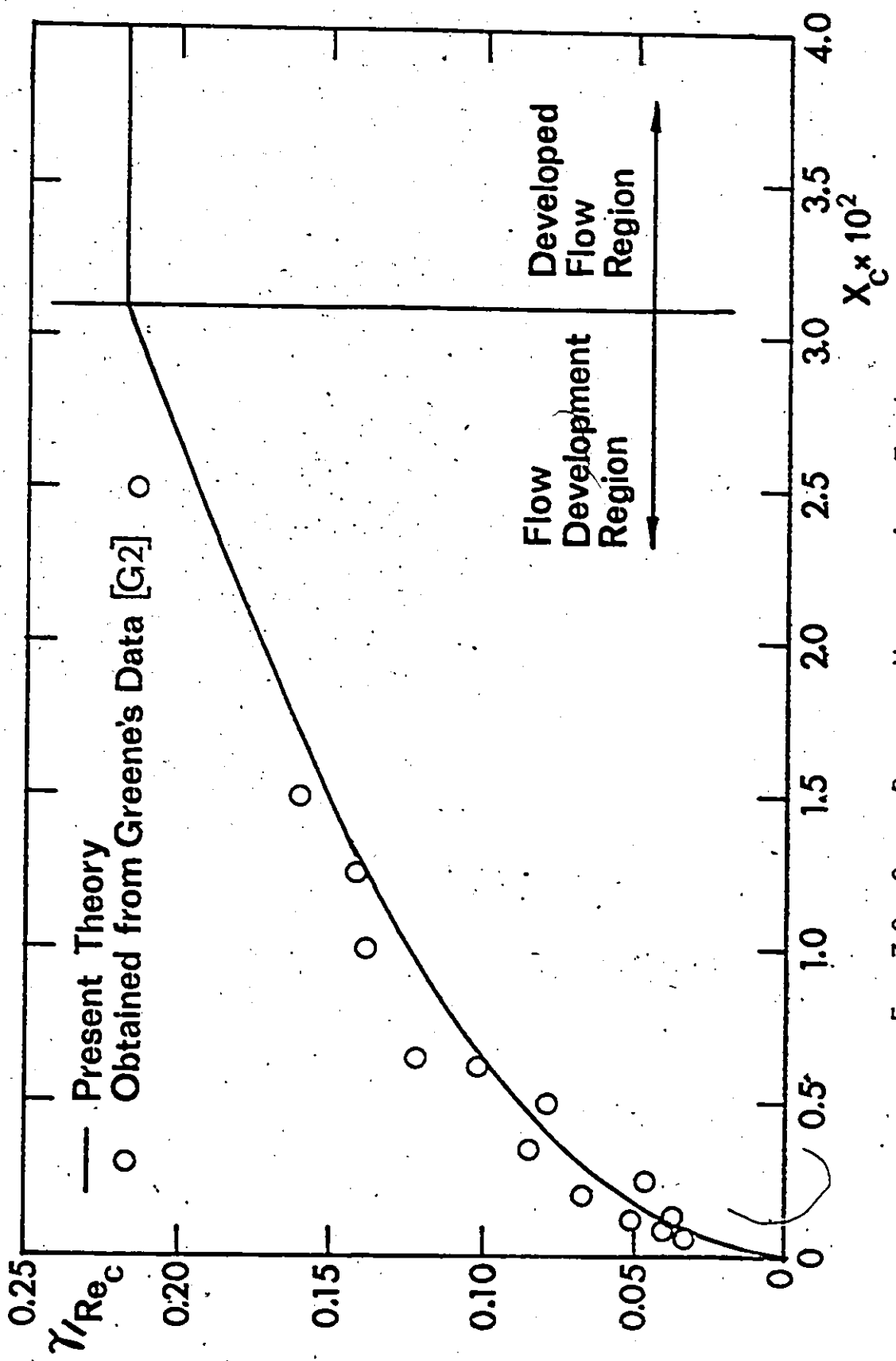


FIG. 3.8 SPREAD PARAMETER VARIATION ALONG THE JET

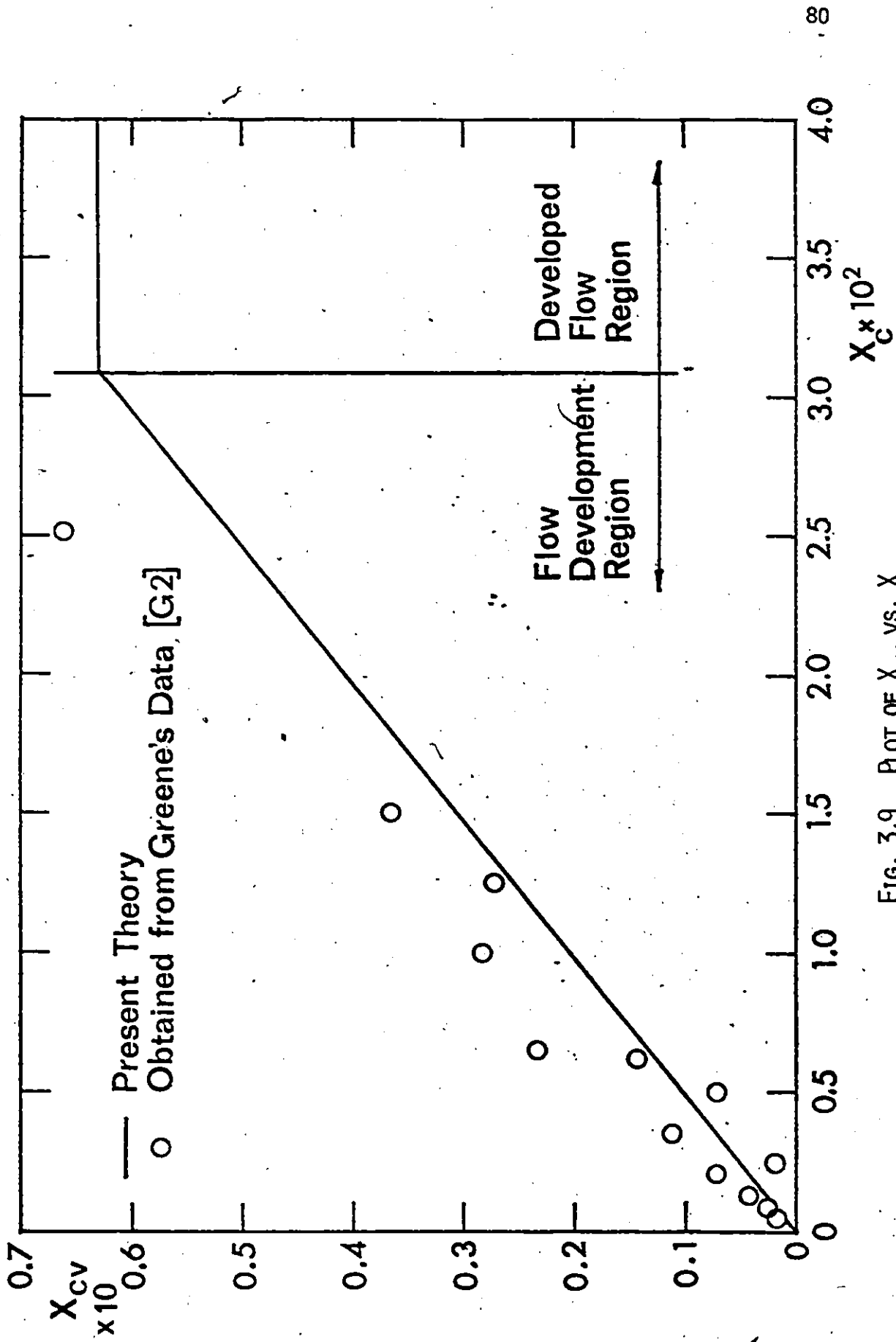


FIG. 3.9 PLOT OF X_{cv} VS. X_c

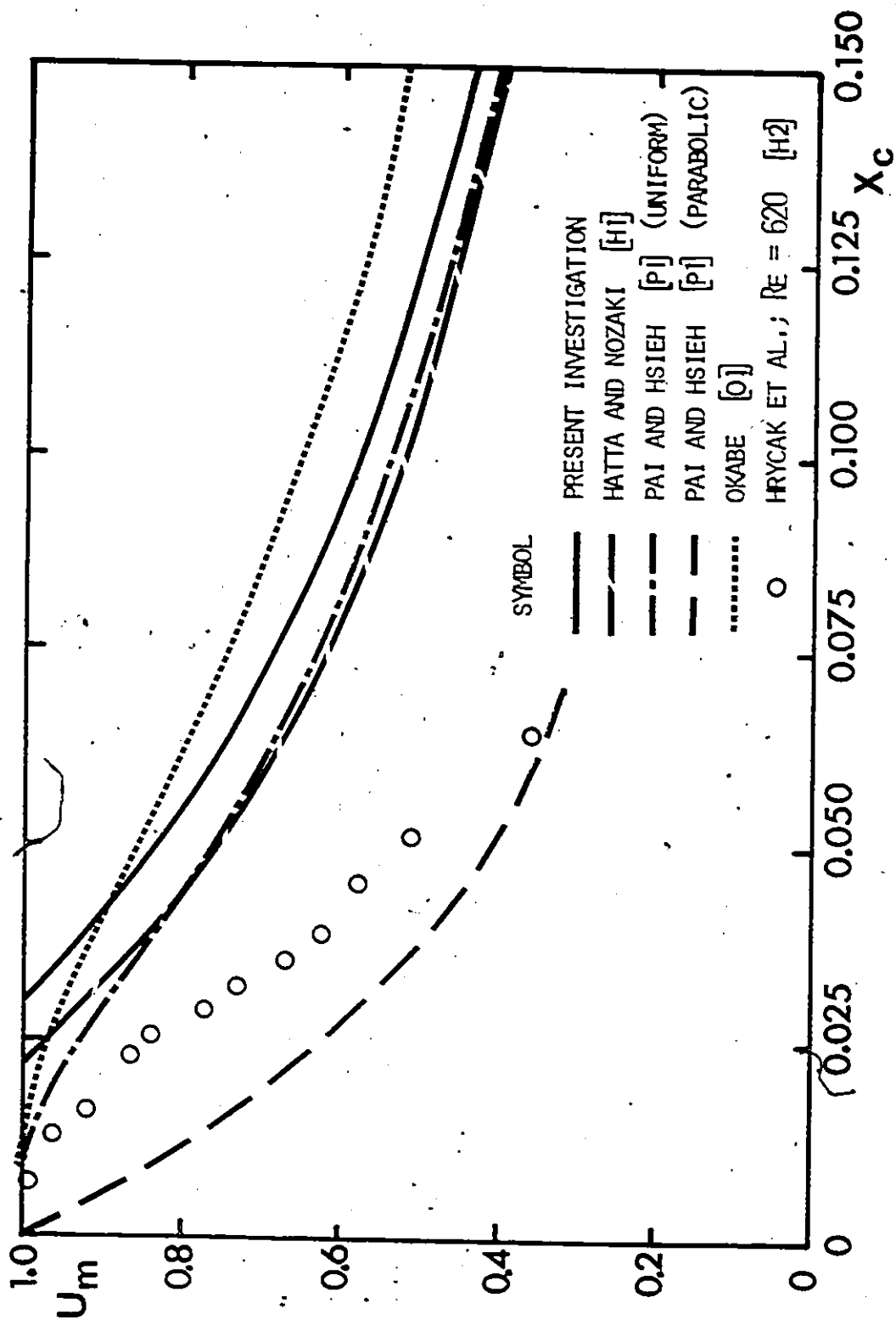


FIG. 3.10 CENTRE LINE VELOCITY DECAY

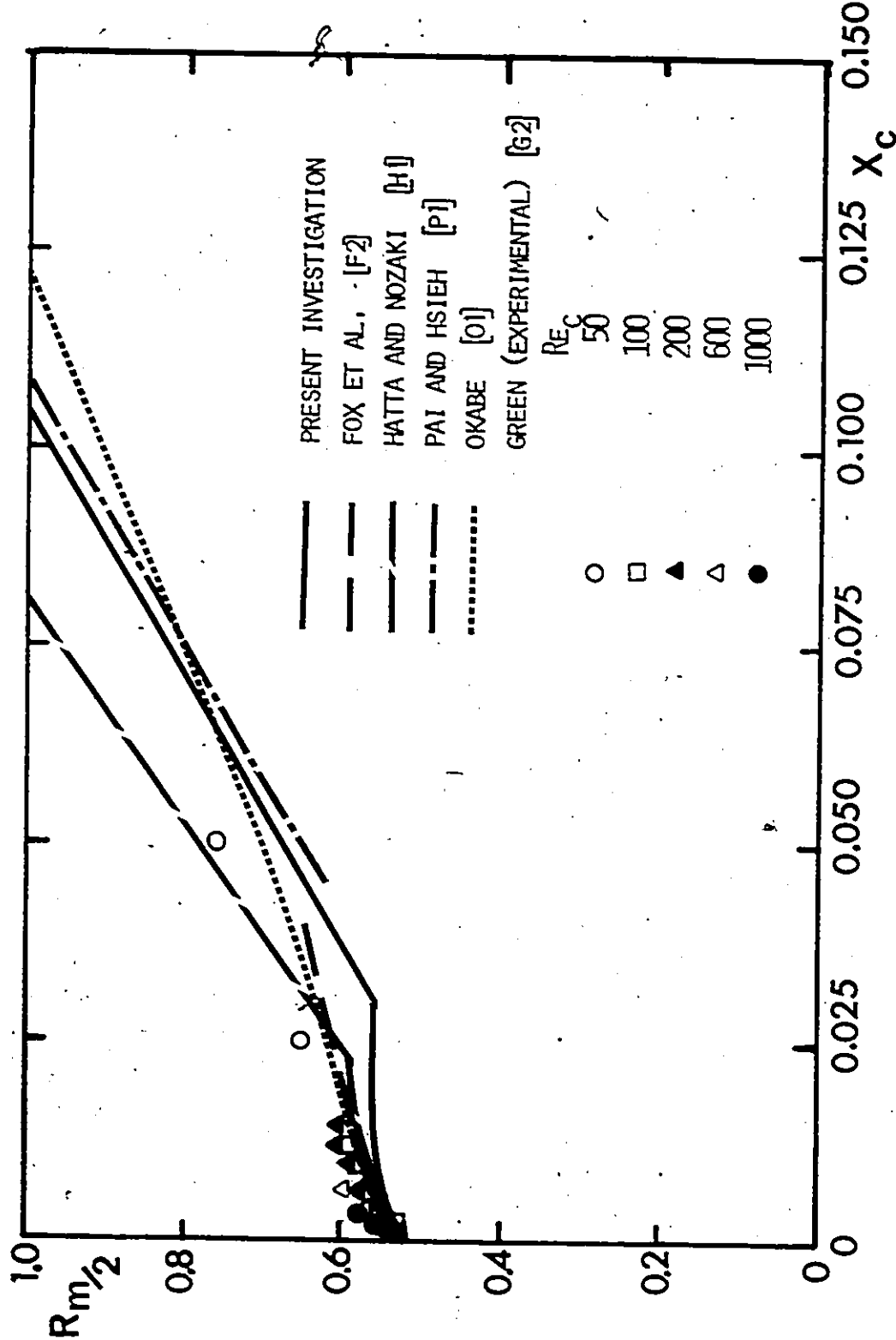


FIG. 3.11 JET HALF-RADIUS VARIATION ALONG THE JET

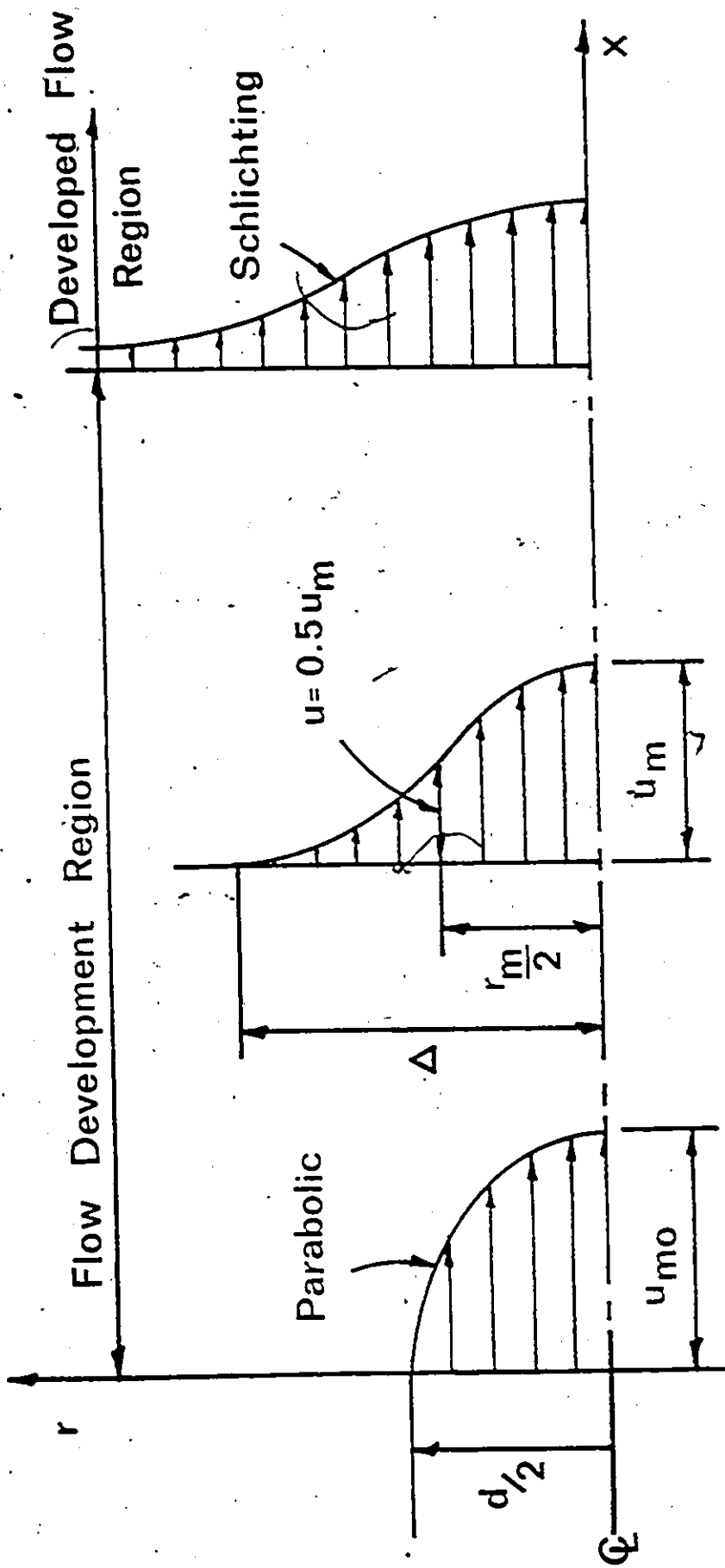


FIG. 4.1.1: JET FLOW REGIONS

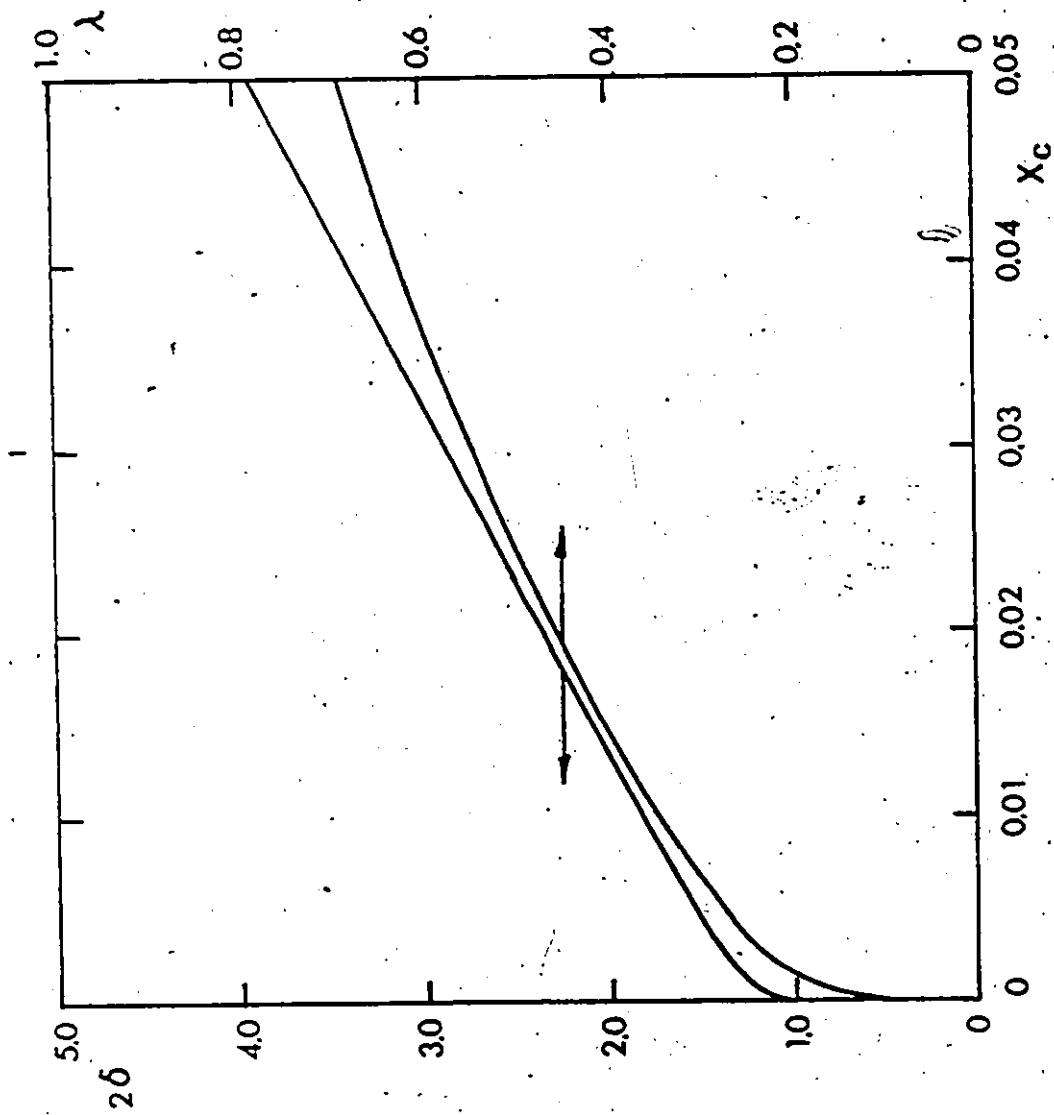


FIG. 4.2 VARIATION OF PROFILE PARAMETERS ALONG THE JET

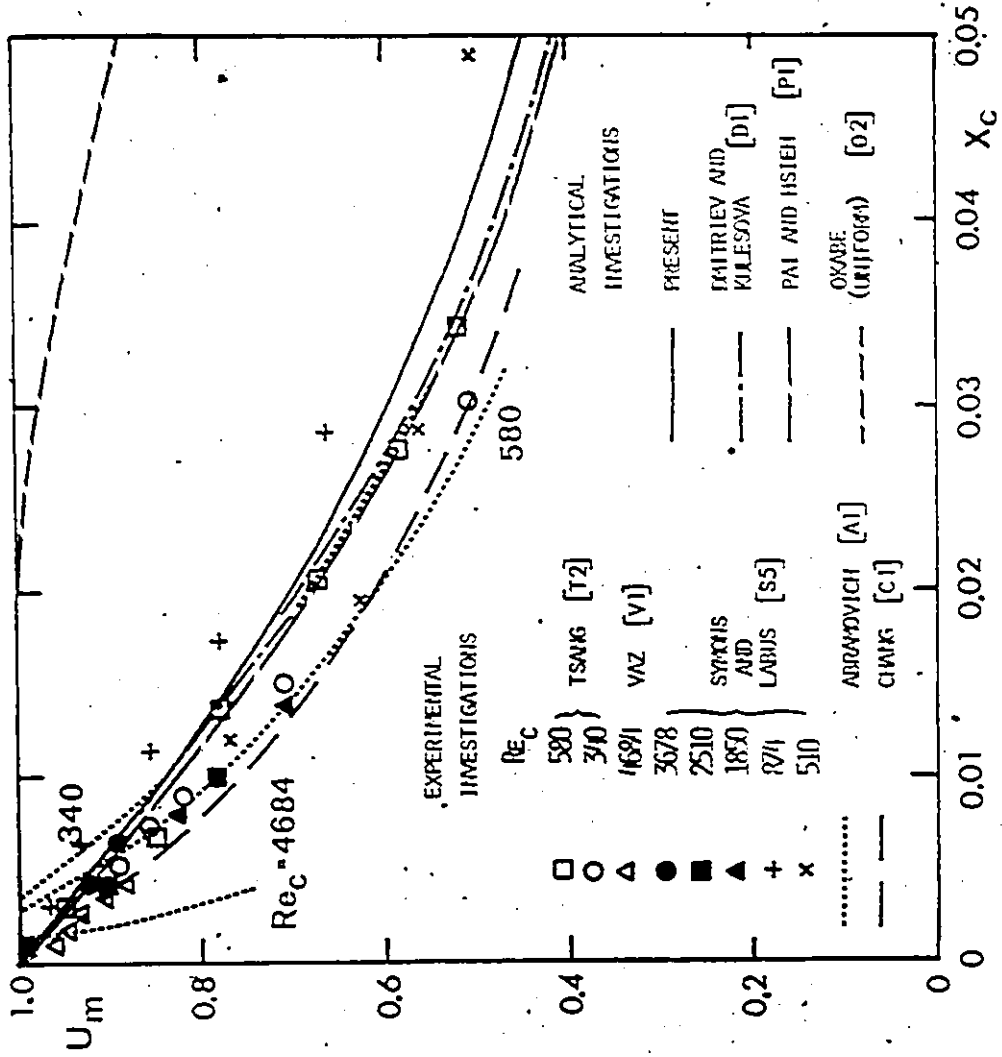


FIG. 4.3 CENTRE LINE VELOCITY DECAY

F

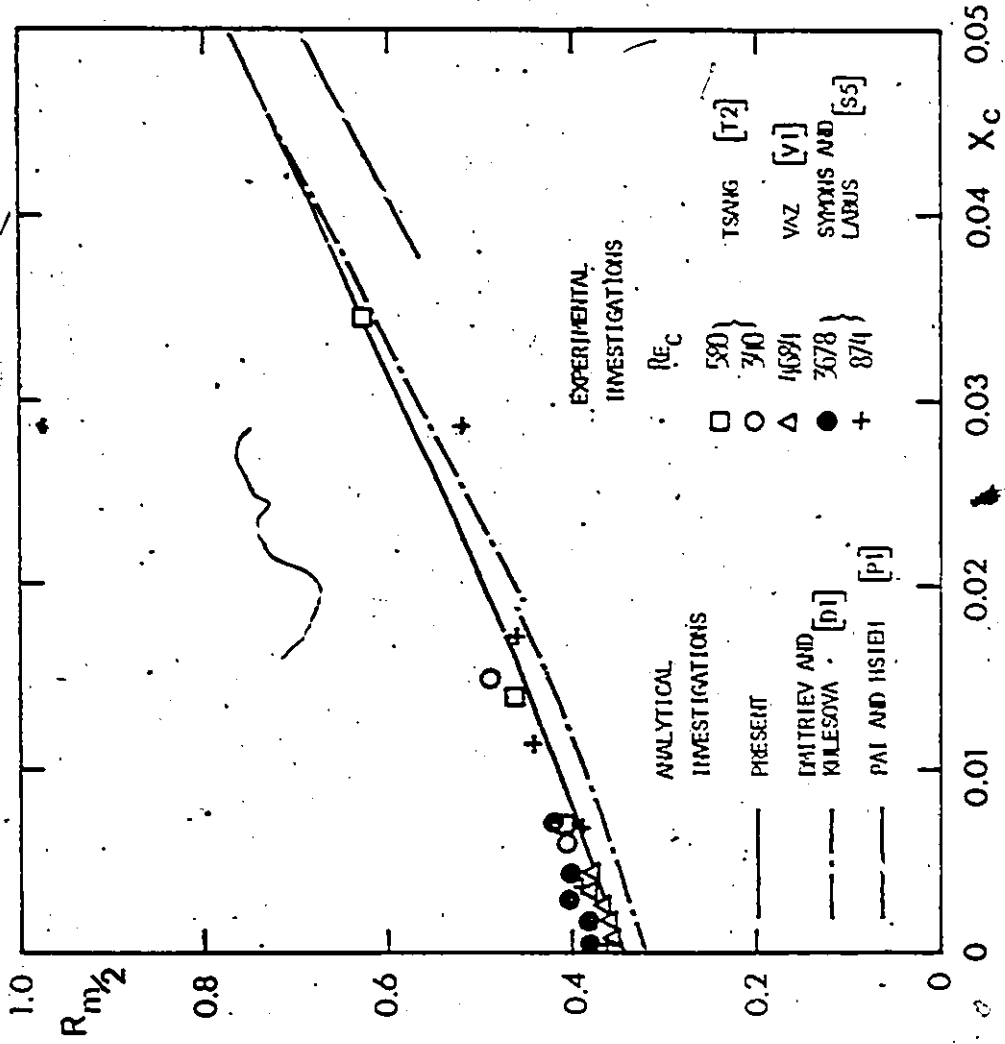


FIG. 4.4 JET GROWTH

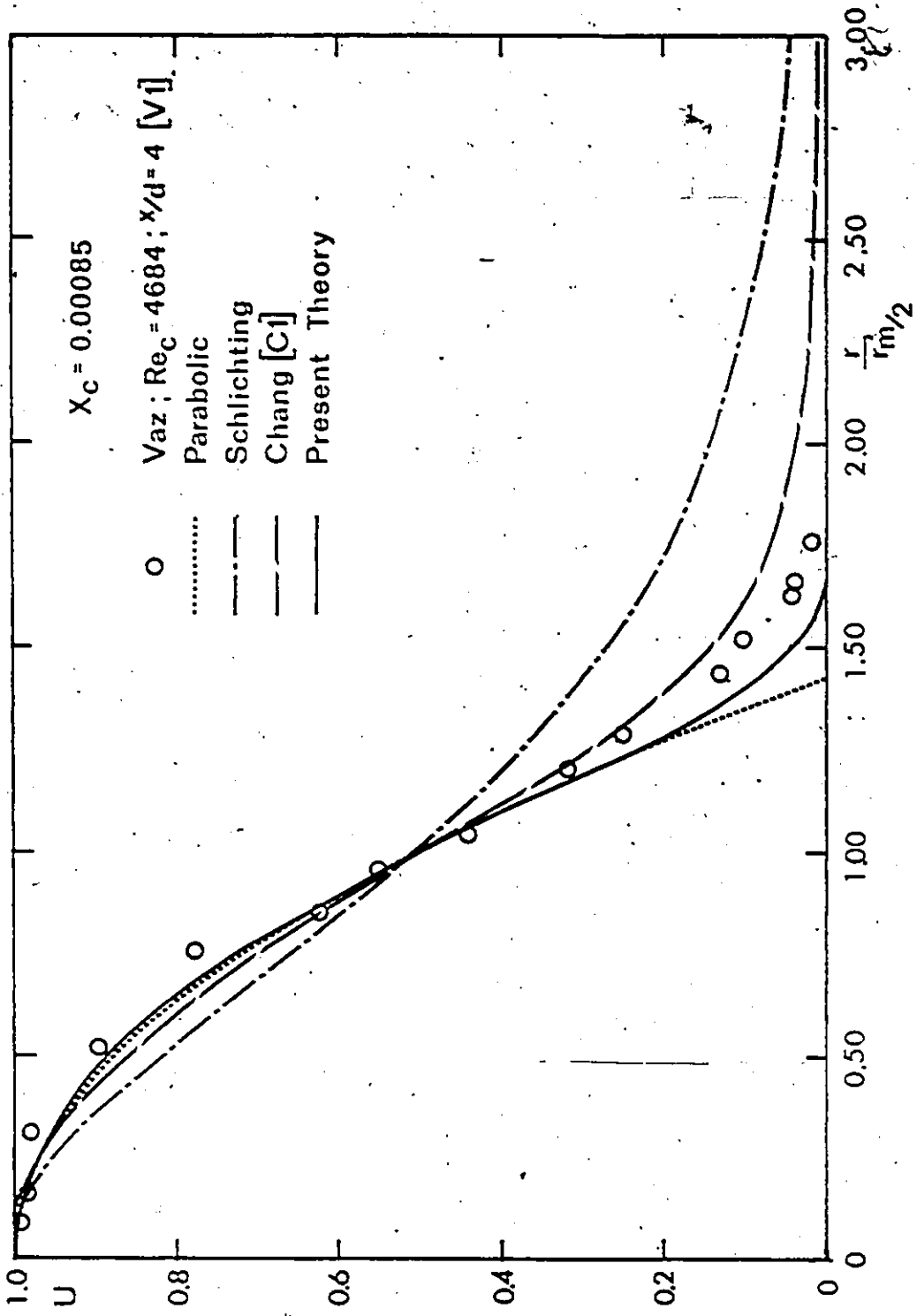


FIG. 4.5 NONDIMENSIONAL VELOCITY PROFILE ($X_c = 0.00085$)

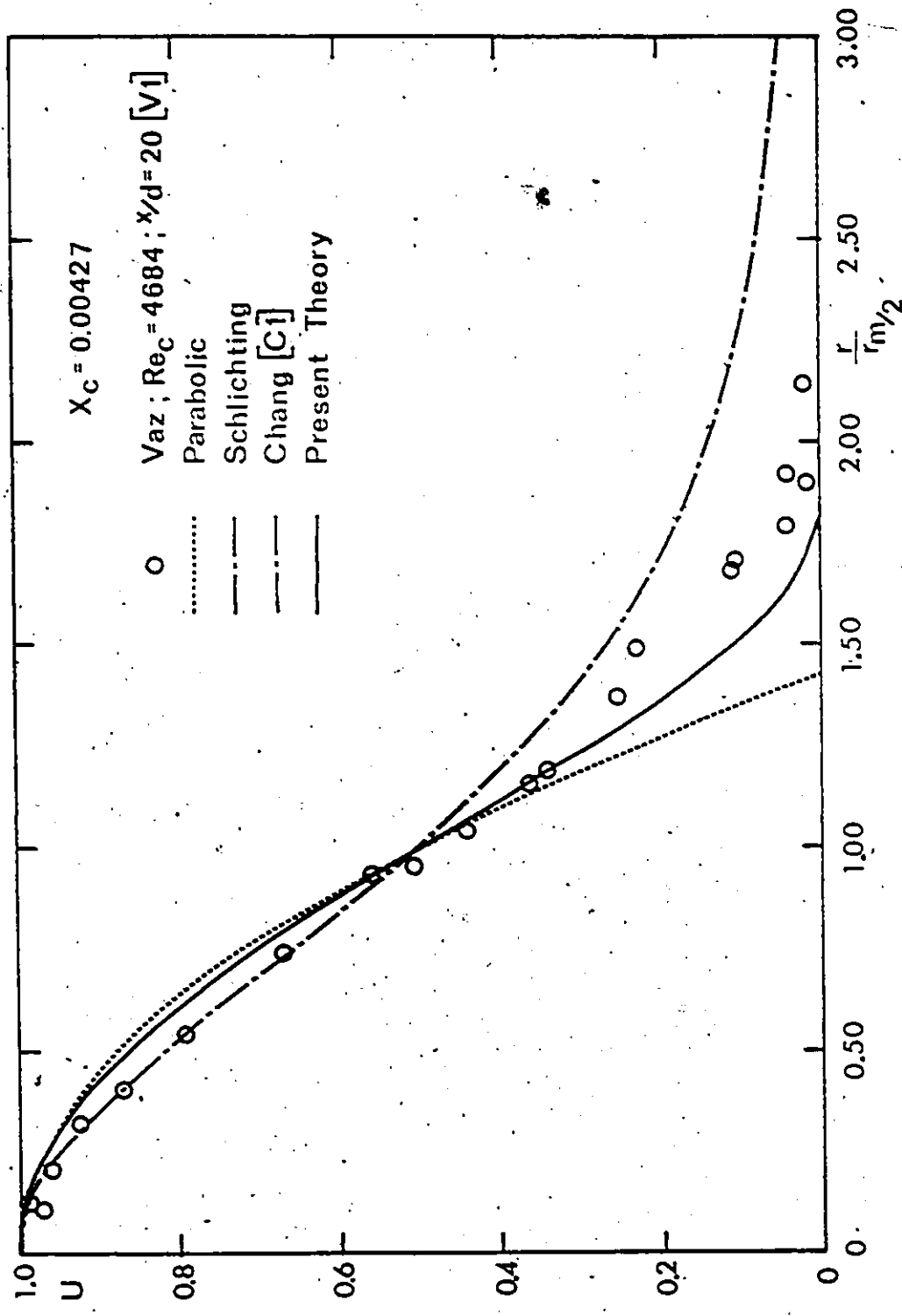


FIG. 4.6 NONDIMENSIONAL VELOCITY PROFILE ($X_c = 0.00427$)

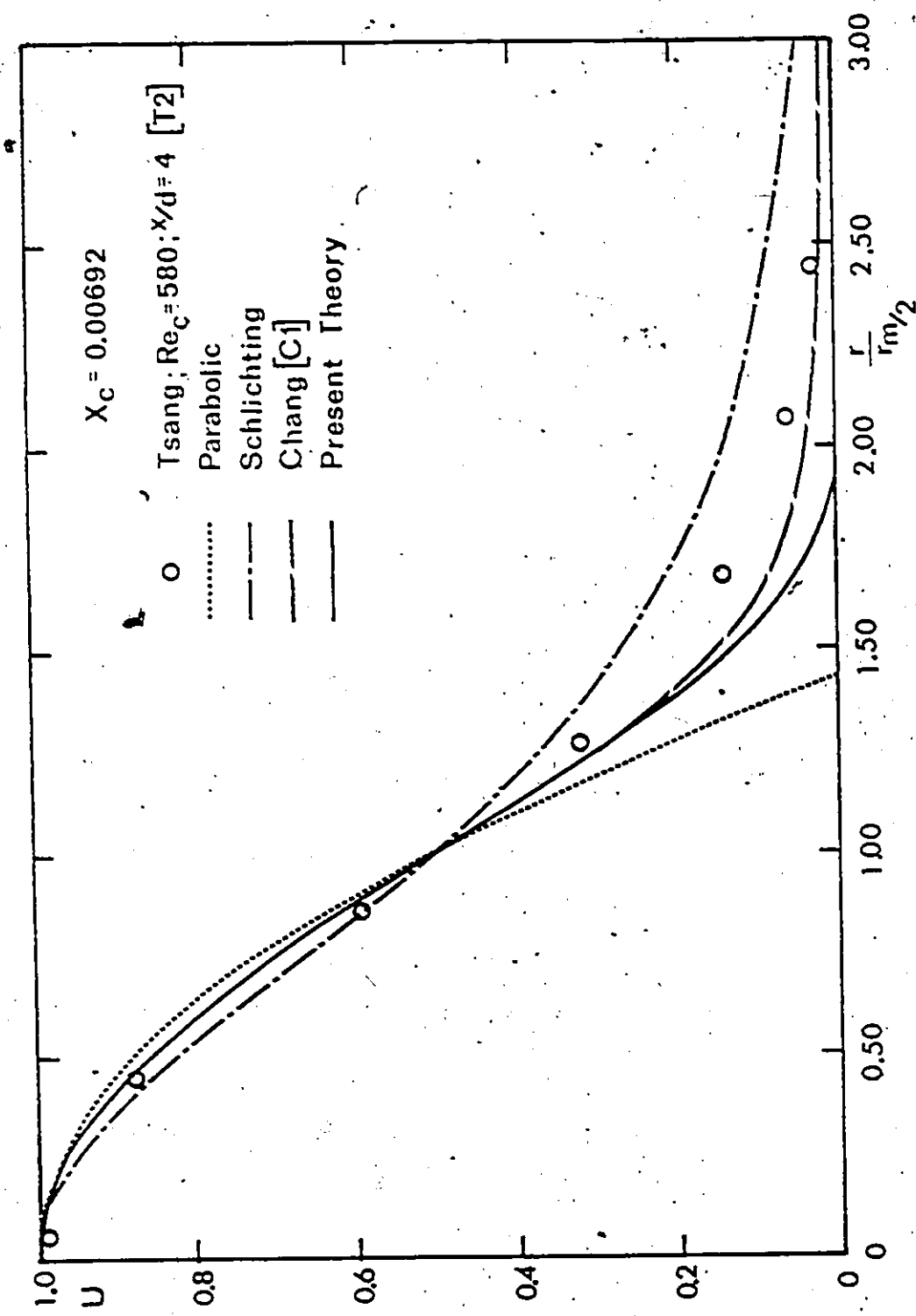


FIG. 4.7 NONDIMENSIONAL VELOCITY PROFILE ($X_c = 0.00692$)

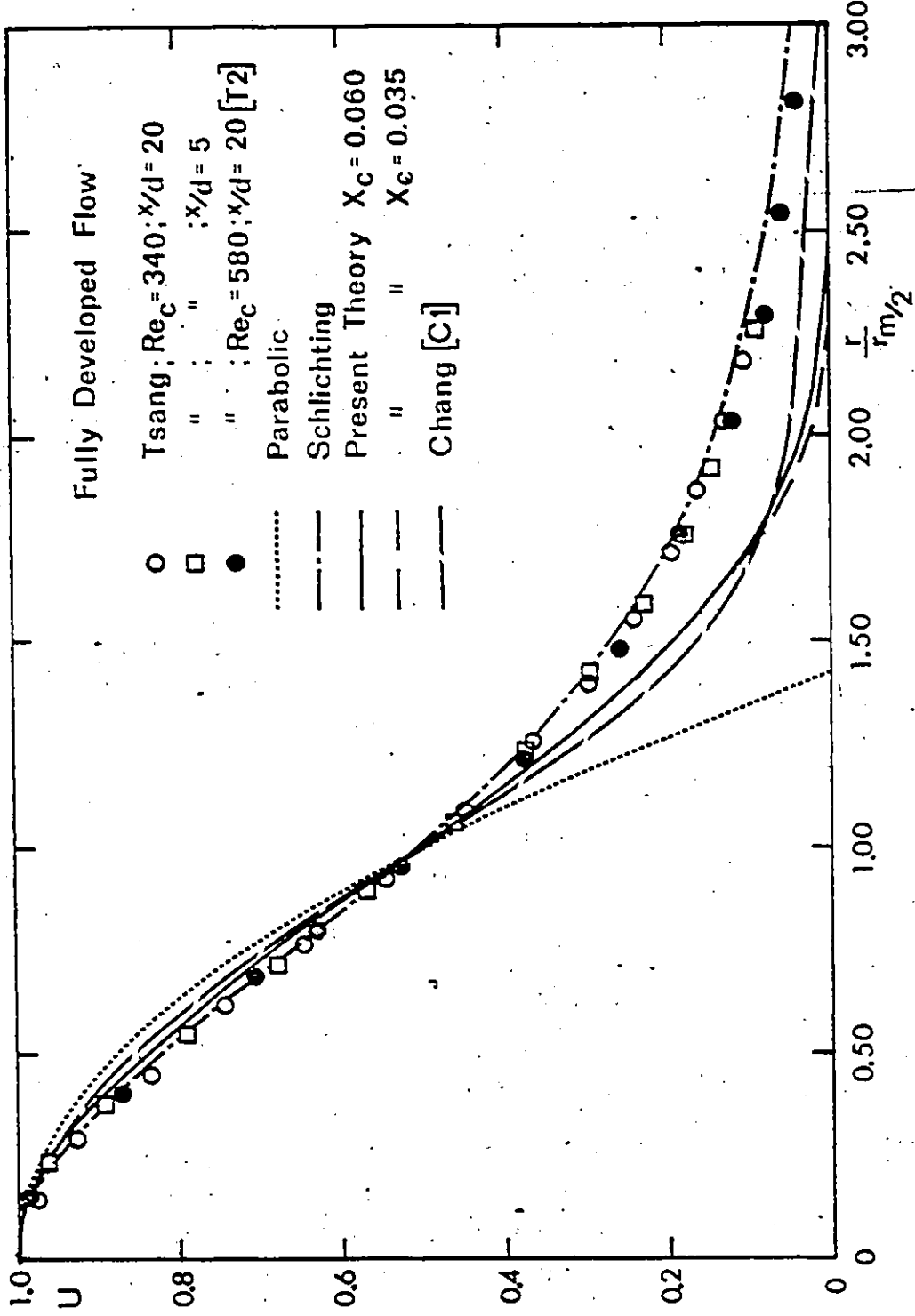


FIG. 4.8 NONDIMENSIONAL VELOCITY PROFILE (FULLY DEVELOPED)

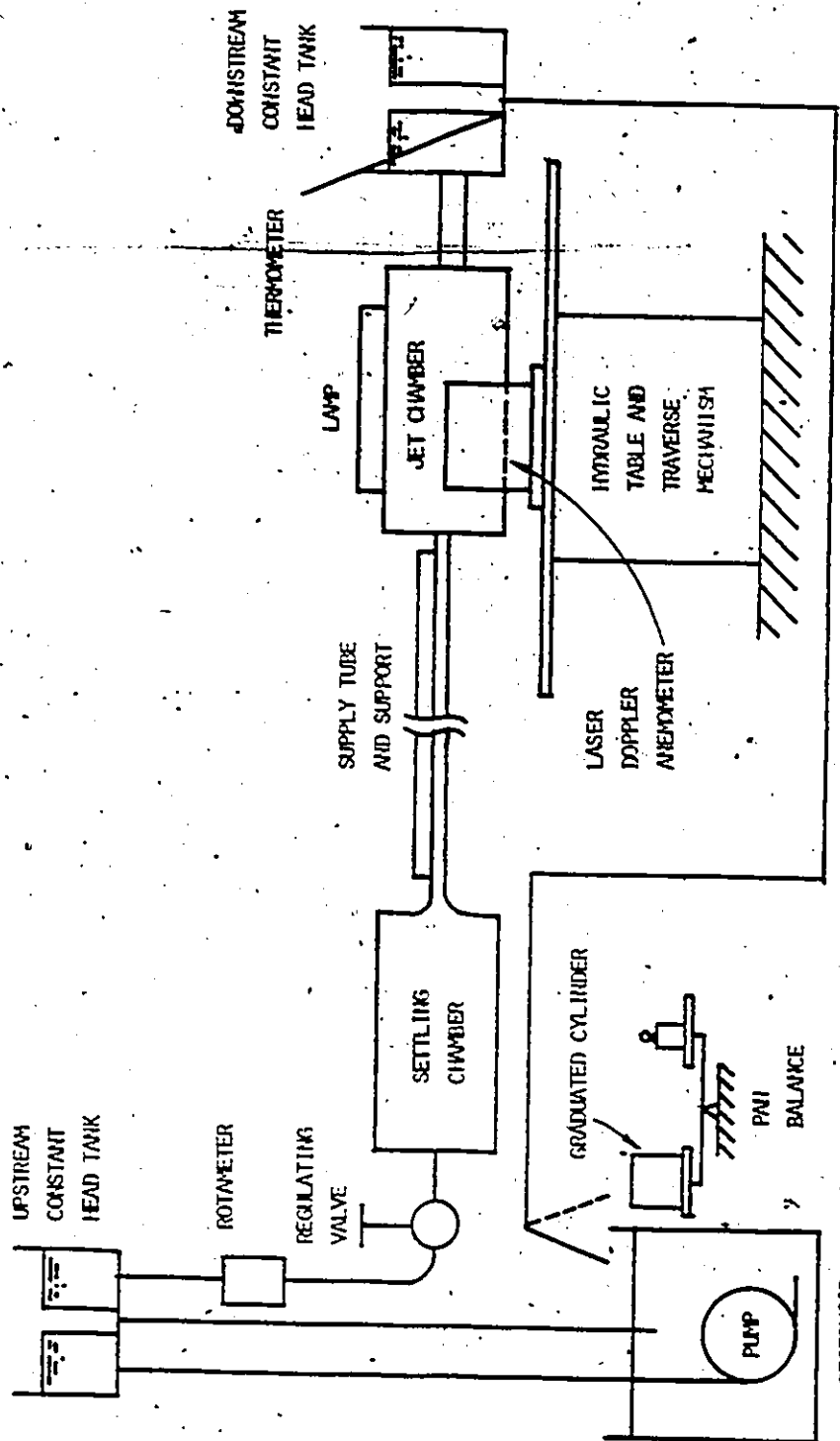


FIG. 5.1 FLOW TEST FACILITY



FIG. 5.2 OVERALL VIEW OF TEST FACILITY

COLOURED PAPER
PAPIER DE COULEUR

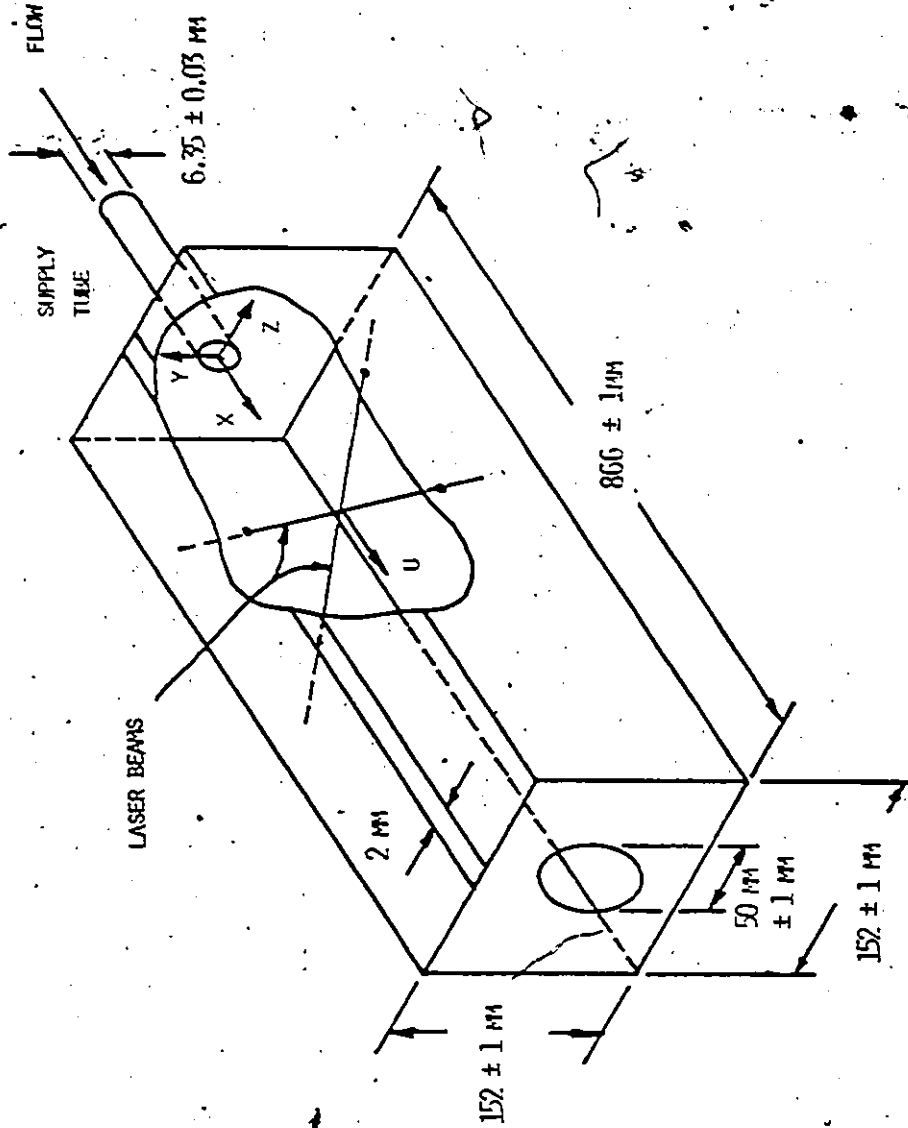
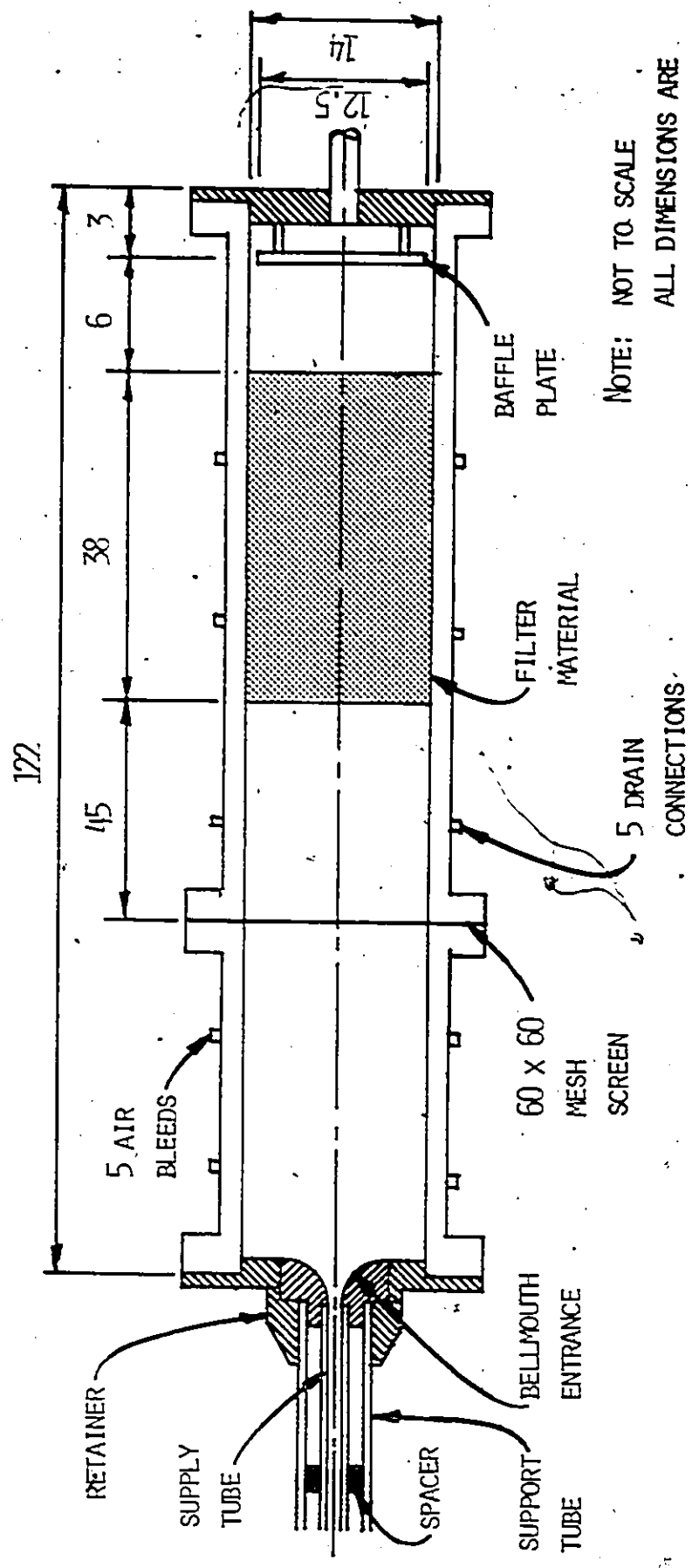


FIG. 5.3 JET CHAMBER



NOTE: NOT TO SCALE
 ALL DIMENSIONS ARE
 IN CENTIMETERS
 TOLERANCE ± 0.5 CM
 UNLESS OTHERWISE
 SPECIFIED.

Fig. 5.4 SETTLING CHAMBER

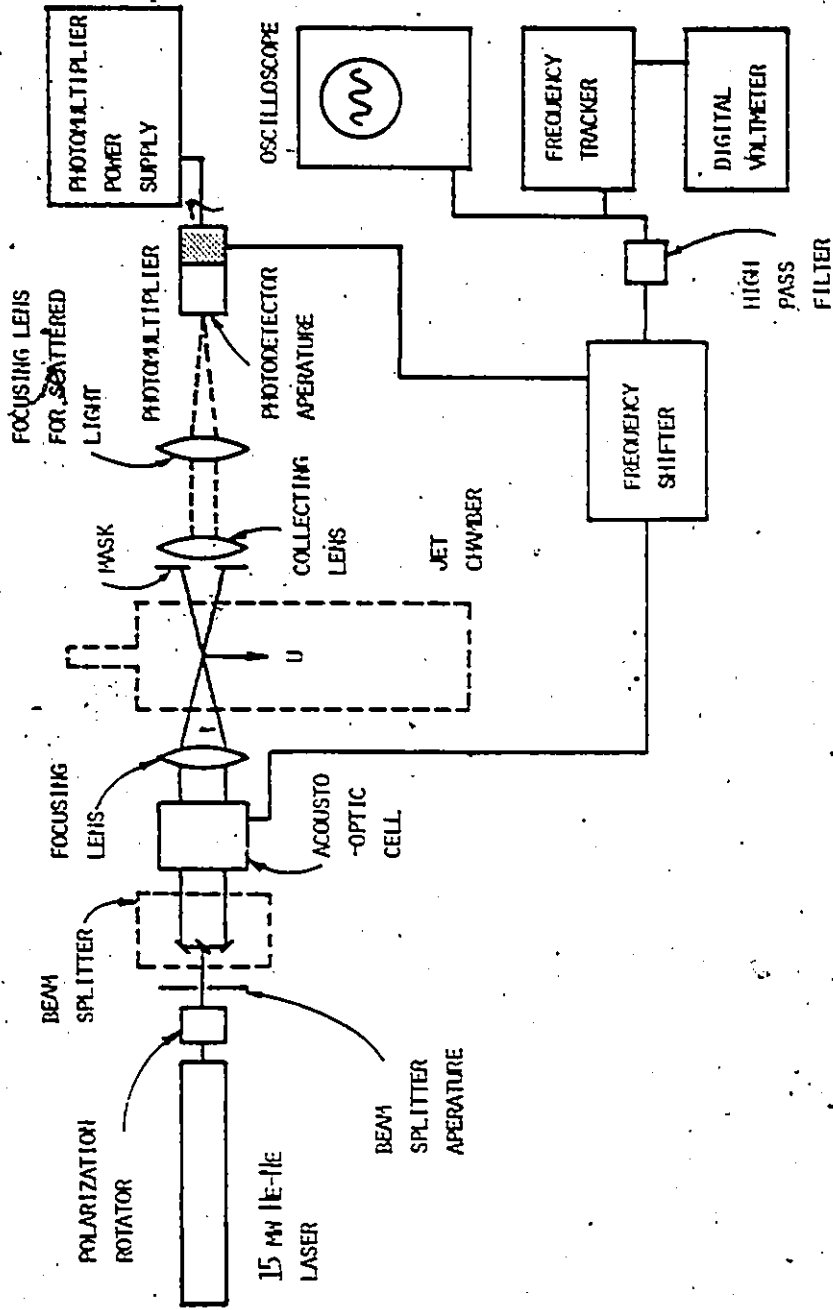


FIG. 5.5 LASER DOPPLER ANEMOMETER ARRANGEMENT

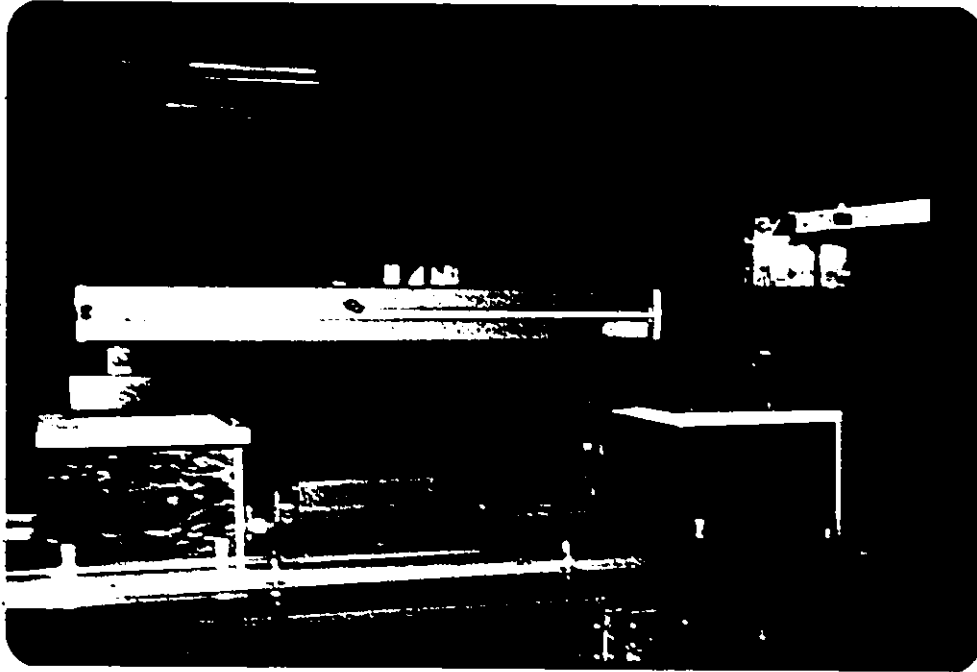


FIG. 5.6 LASER AND TRANSMITTING OPTICS

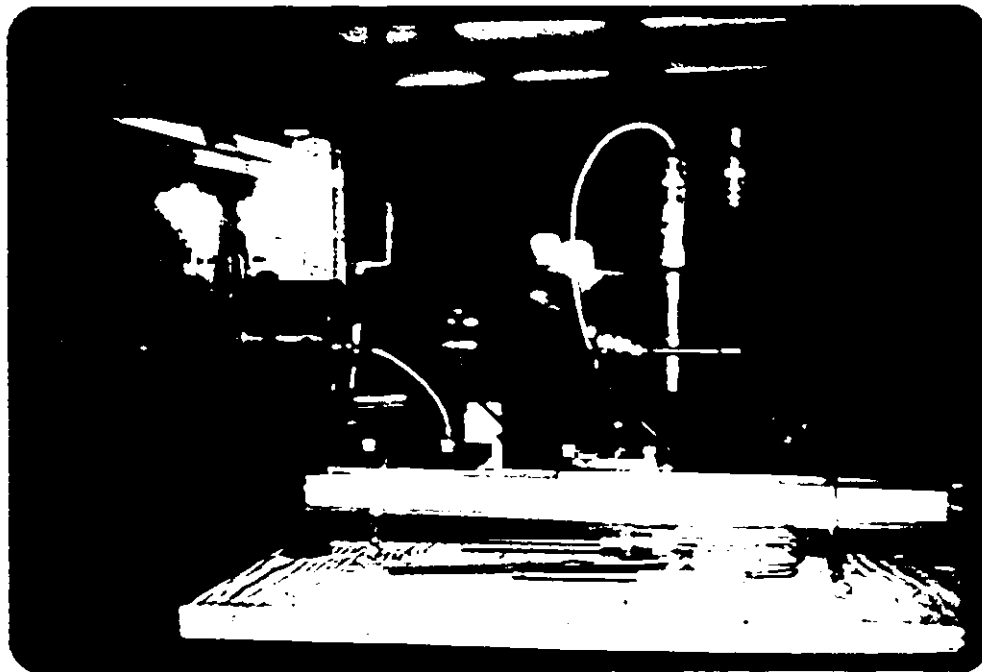


FIG. 5.7 RECEIVING OPTICS

COLOURED PAPER
PAPIER DE COULEUR

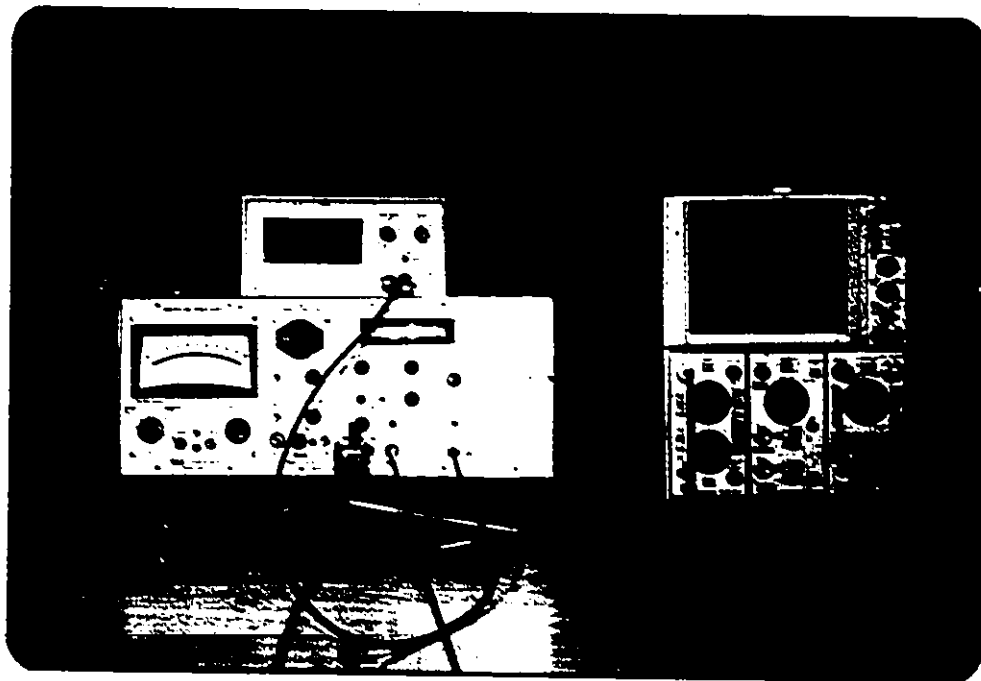


FIG. 5.8 SIGNAL PROCESSOR AND OSCILLOSCOPE

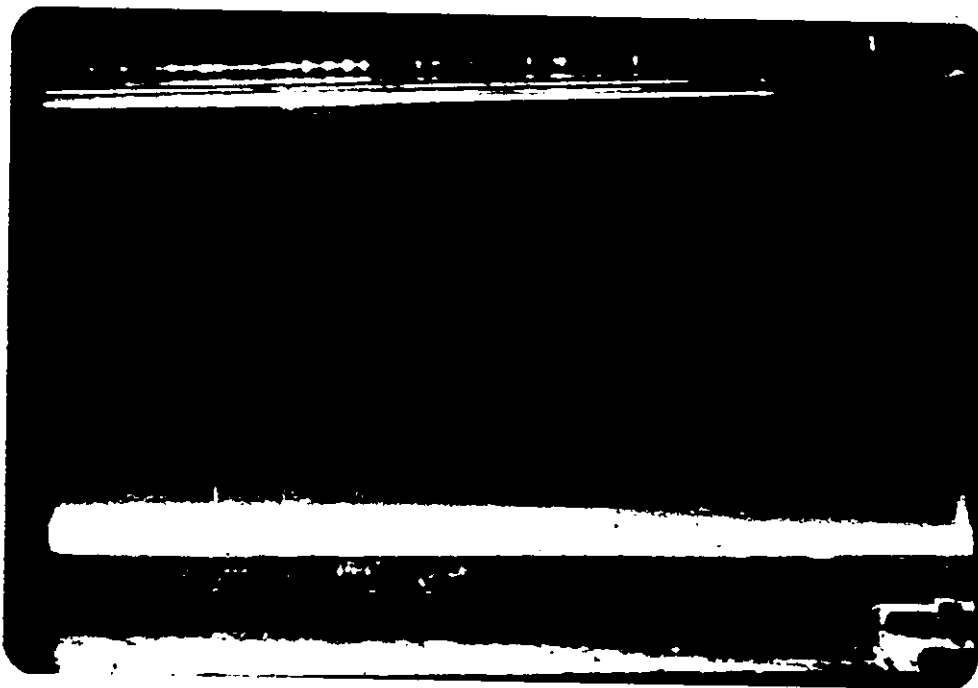


FIG. 5.9 FLOW VISUALIZATION OF LAMINAR JET

COLOURED PAPER
PAPIER DE COULEUR

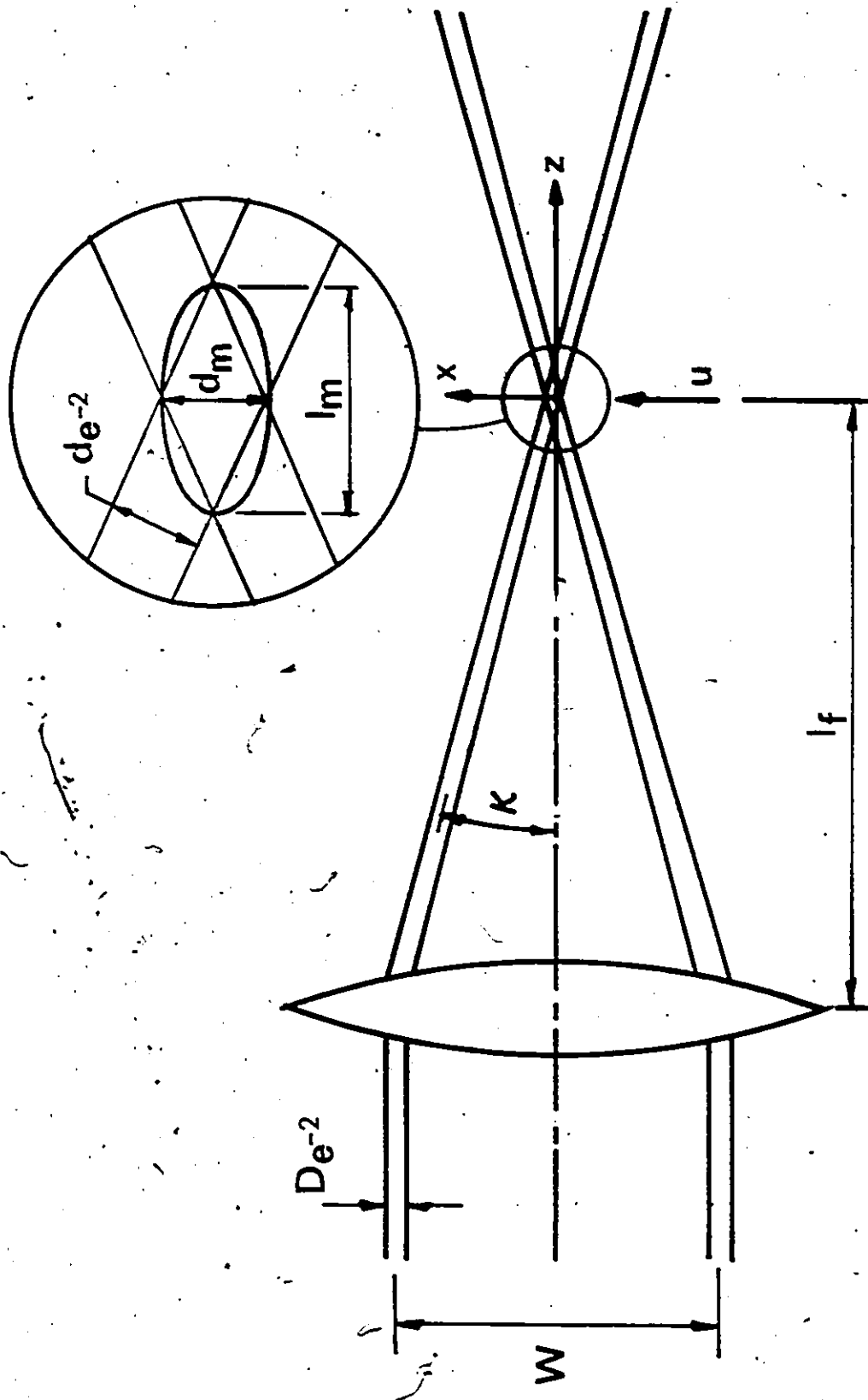


FIG. 5.10 DETAILS OF MEASURING VOLUME

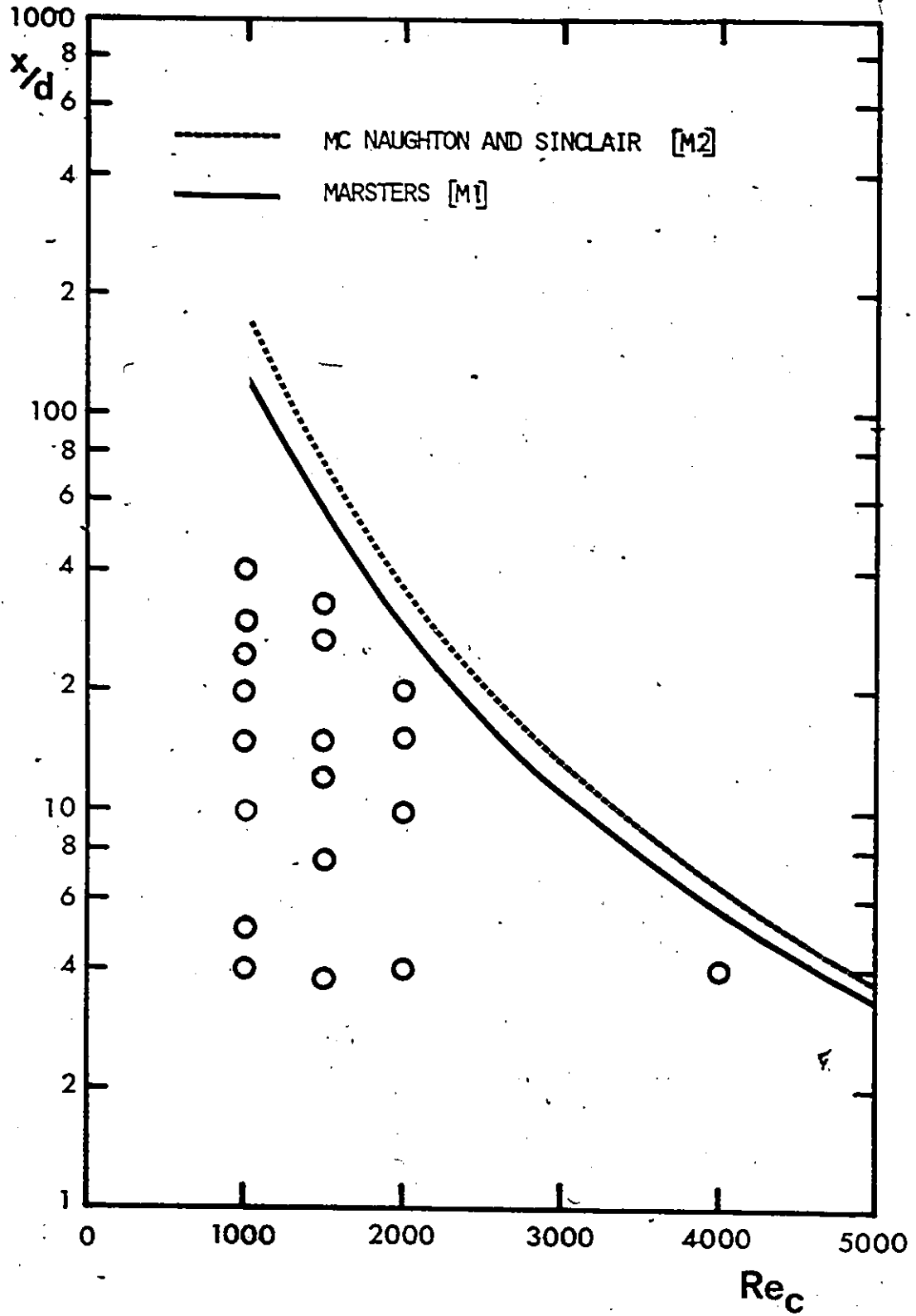


FIG. 5.11 VERIFICATION OF LAMINAR JET

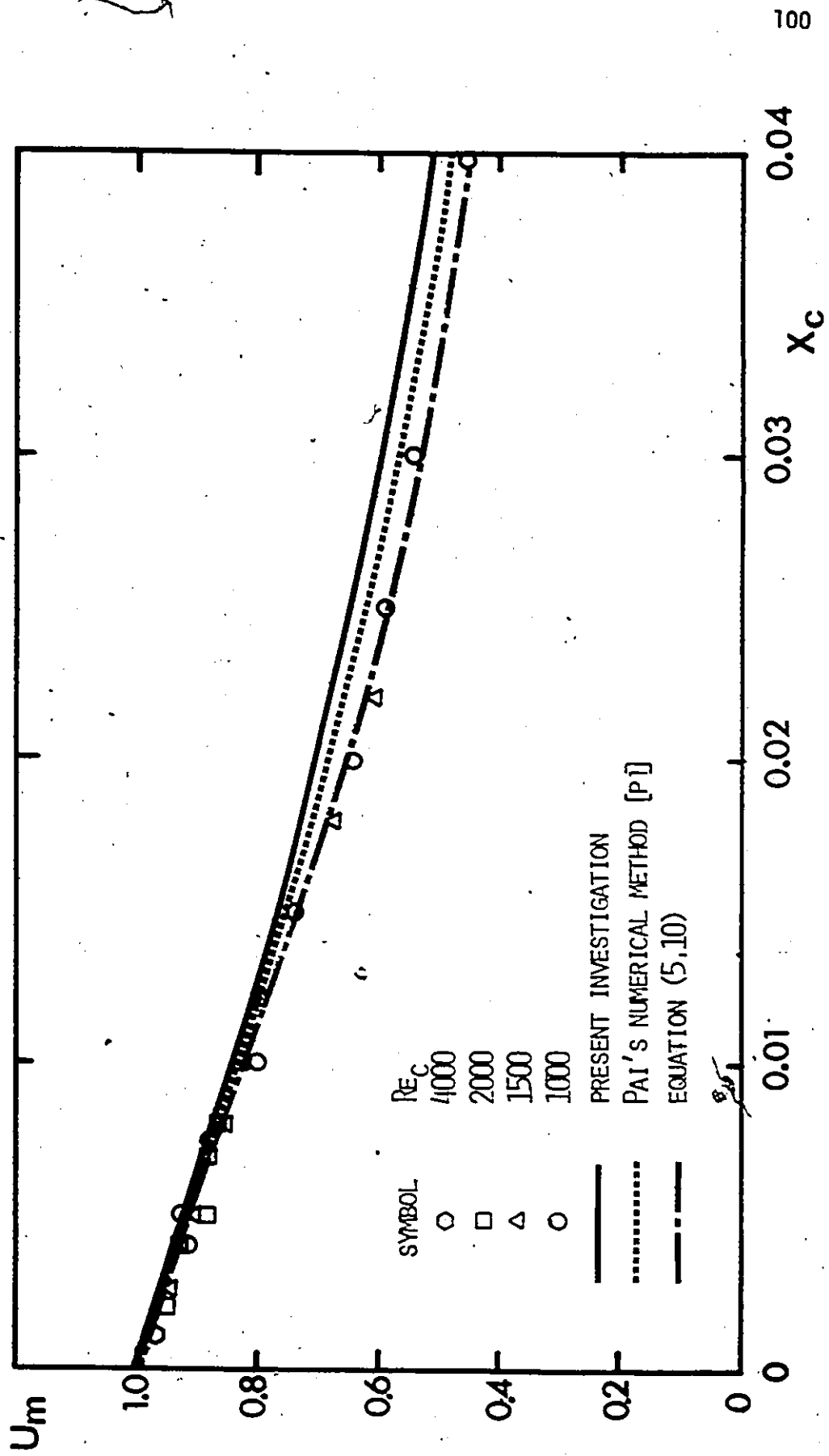


FIG. 5.12 CENTRE LINE VELOCITY VARIATION WITH AXIAL DISTANCE

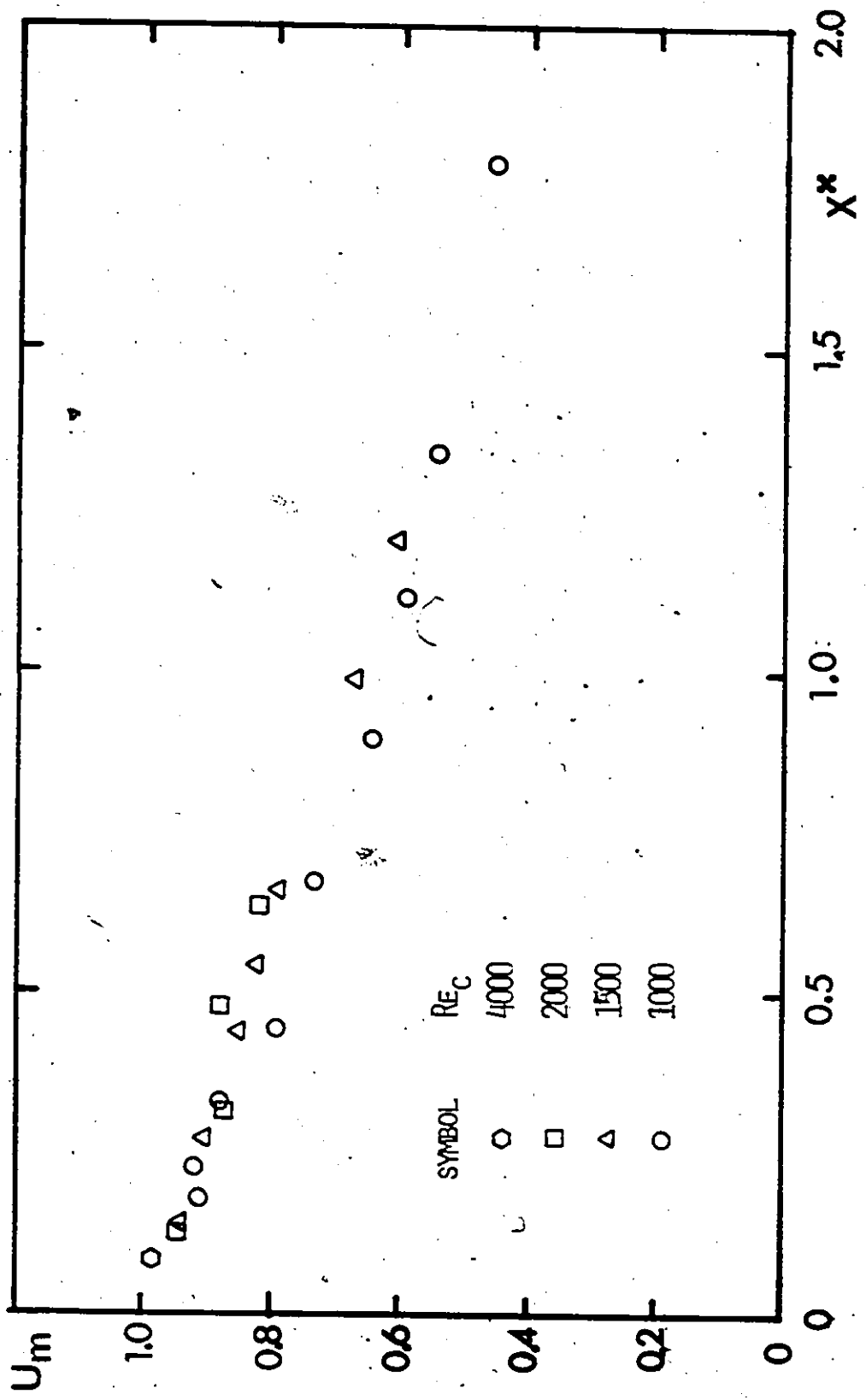


FIG. 5.13 CENTRE LINE VELOCITY VARIATION WITH X^*

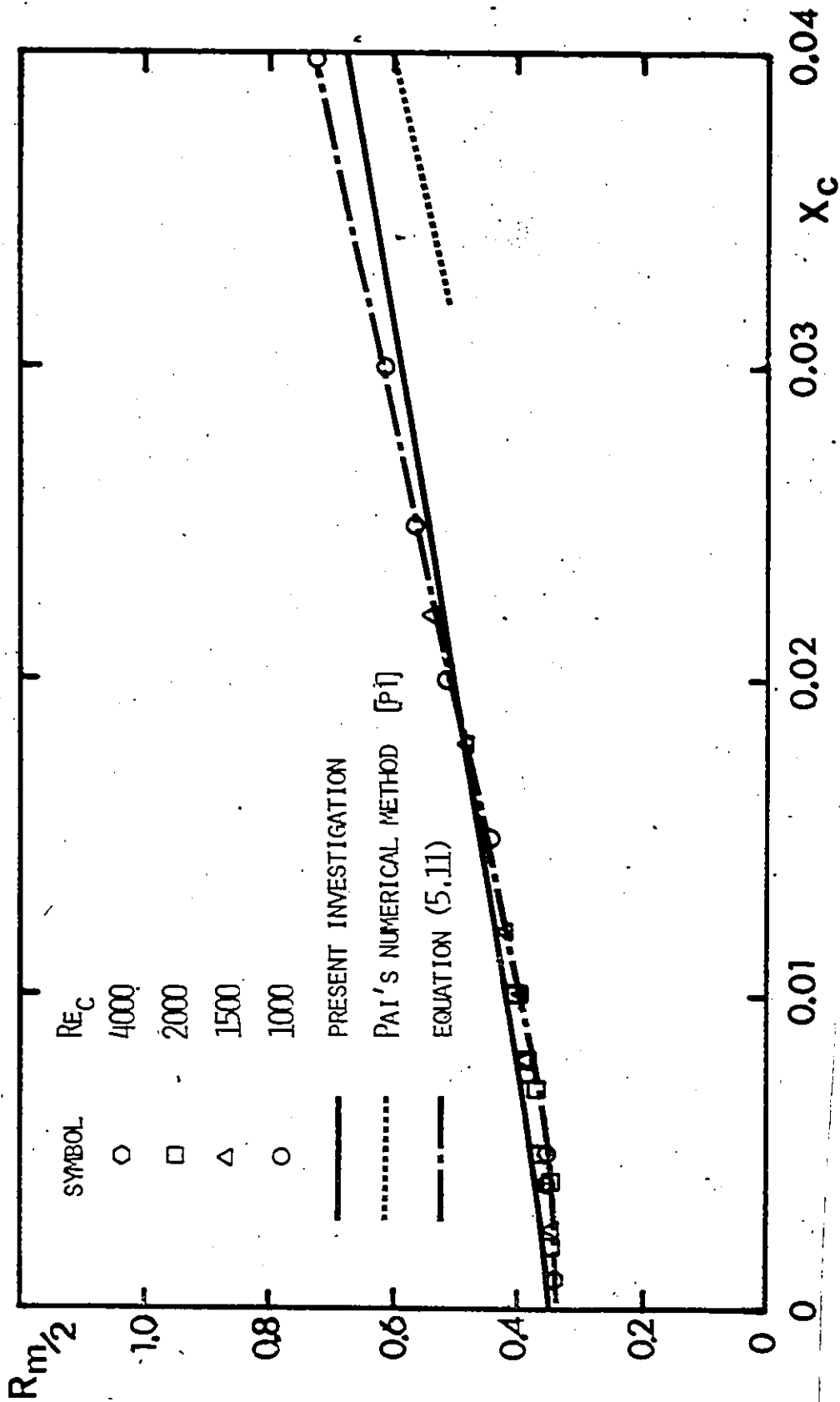
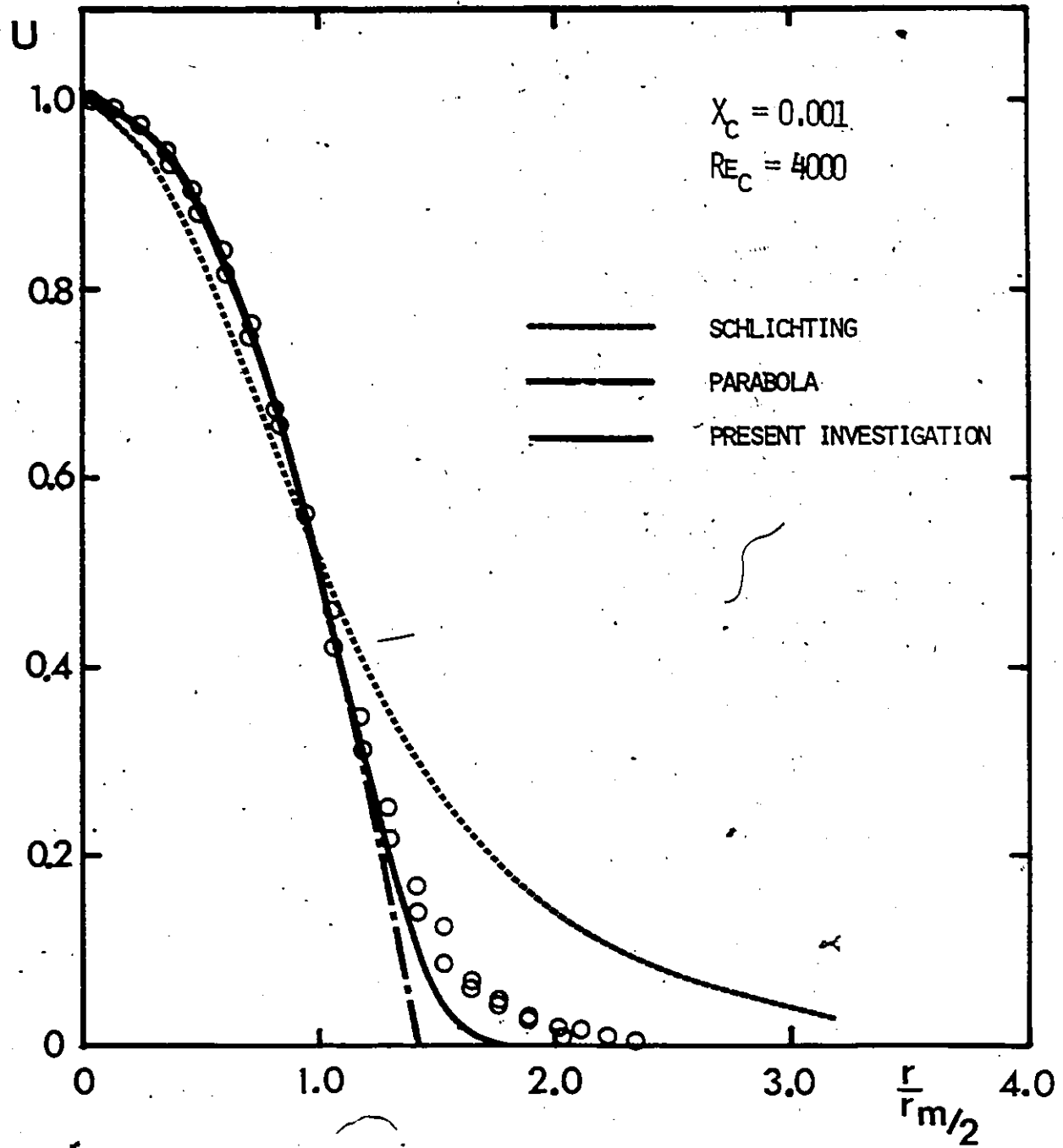


FIG. 5.14 HALF-RADIUS VARIATION WITH AXIAL DISTANCE

FIG. 5.15 NONDIMENSIONAL VELOCITY PROFILE ($X_c = 0.001$)

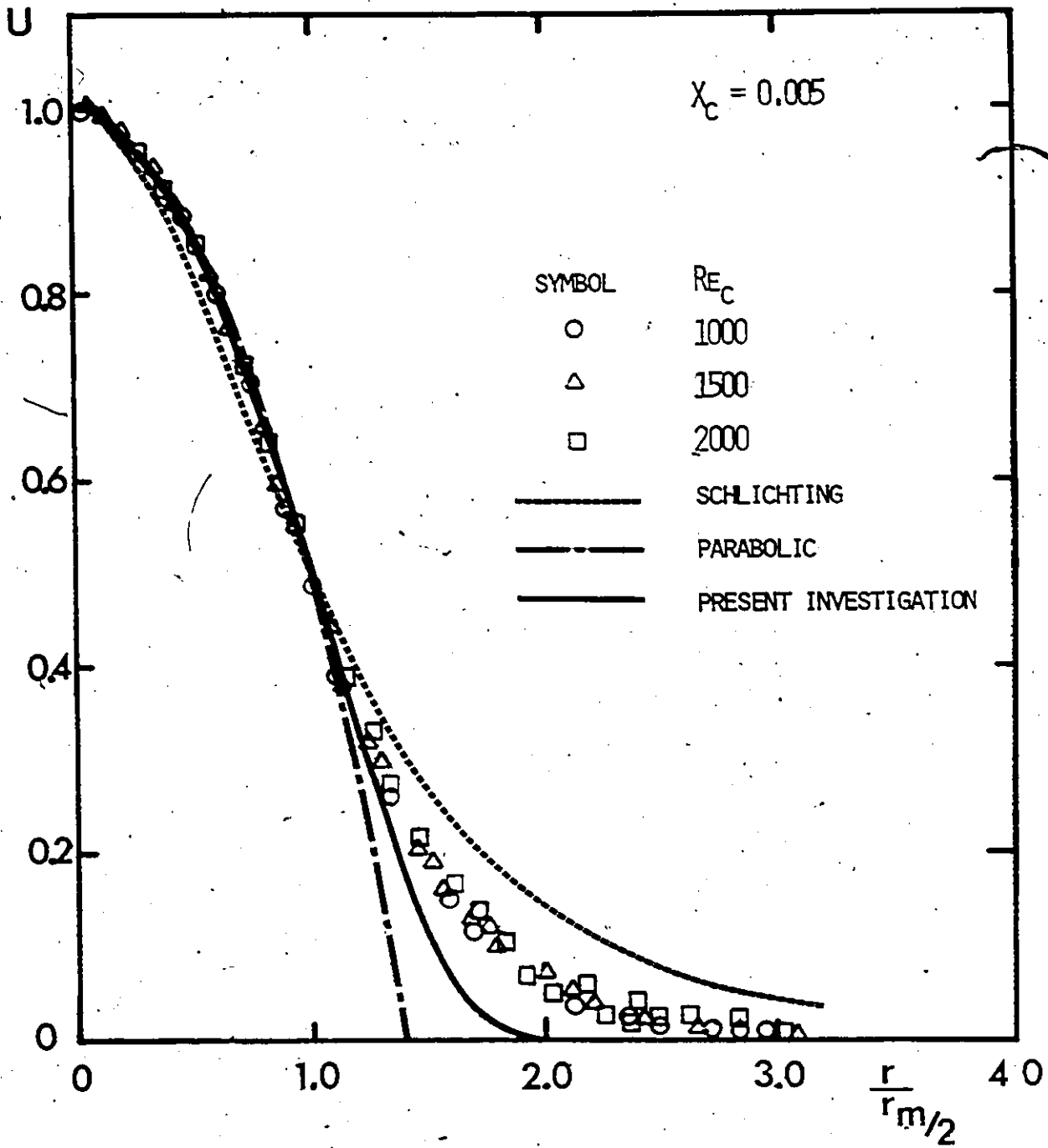


FIG. 5.16 NONDIMENSIONAL VELOCITY PROFILE ($\alpha_c = 0.005$)

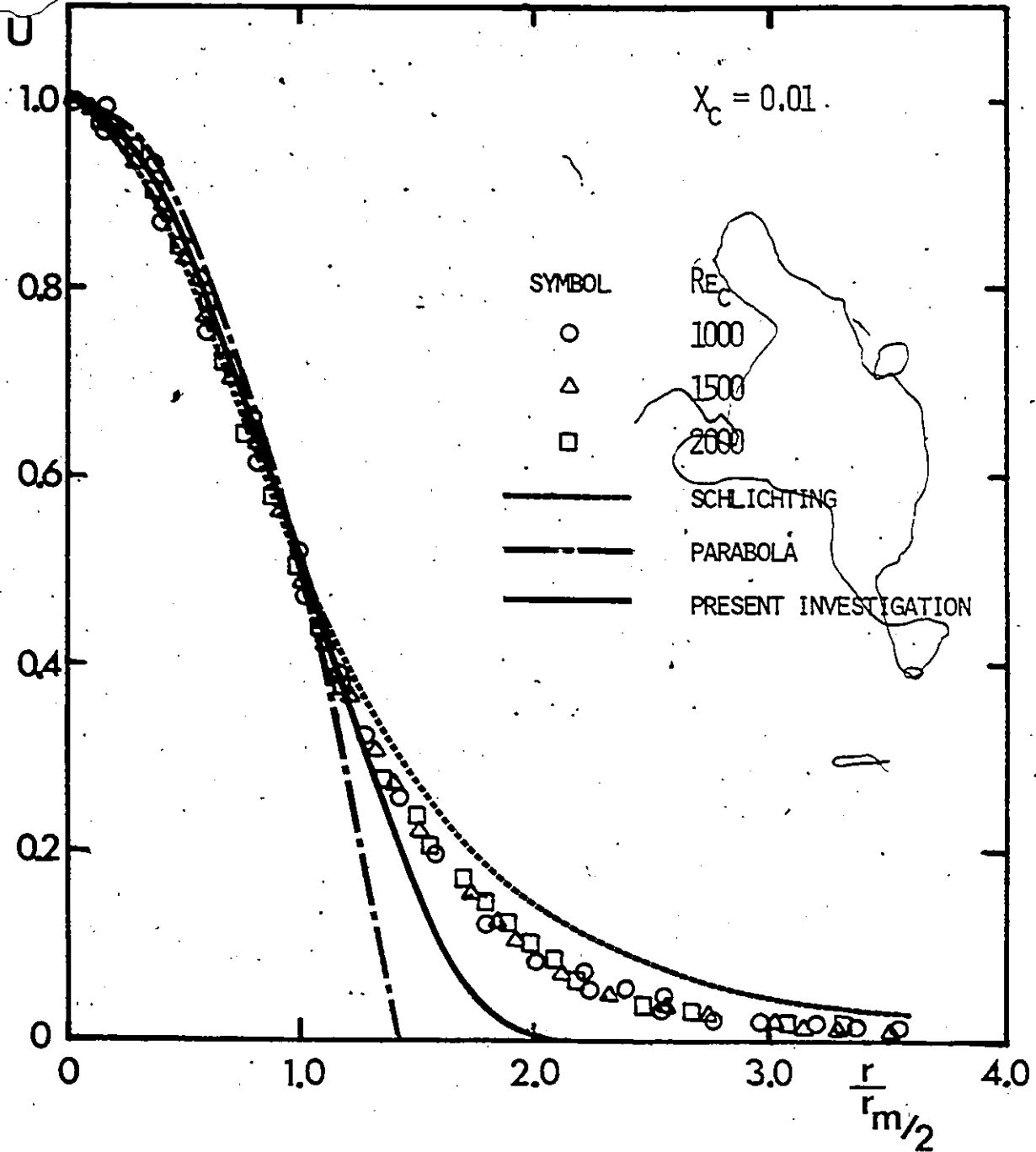


FIG. 5.17 NONDIMENSIONAL VELOCITY PROFILE ($X_c = 0.01$)

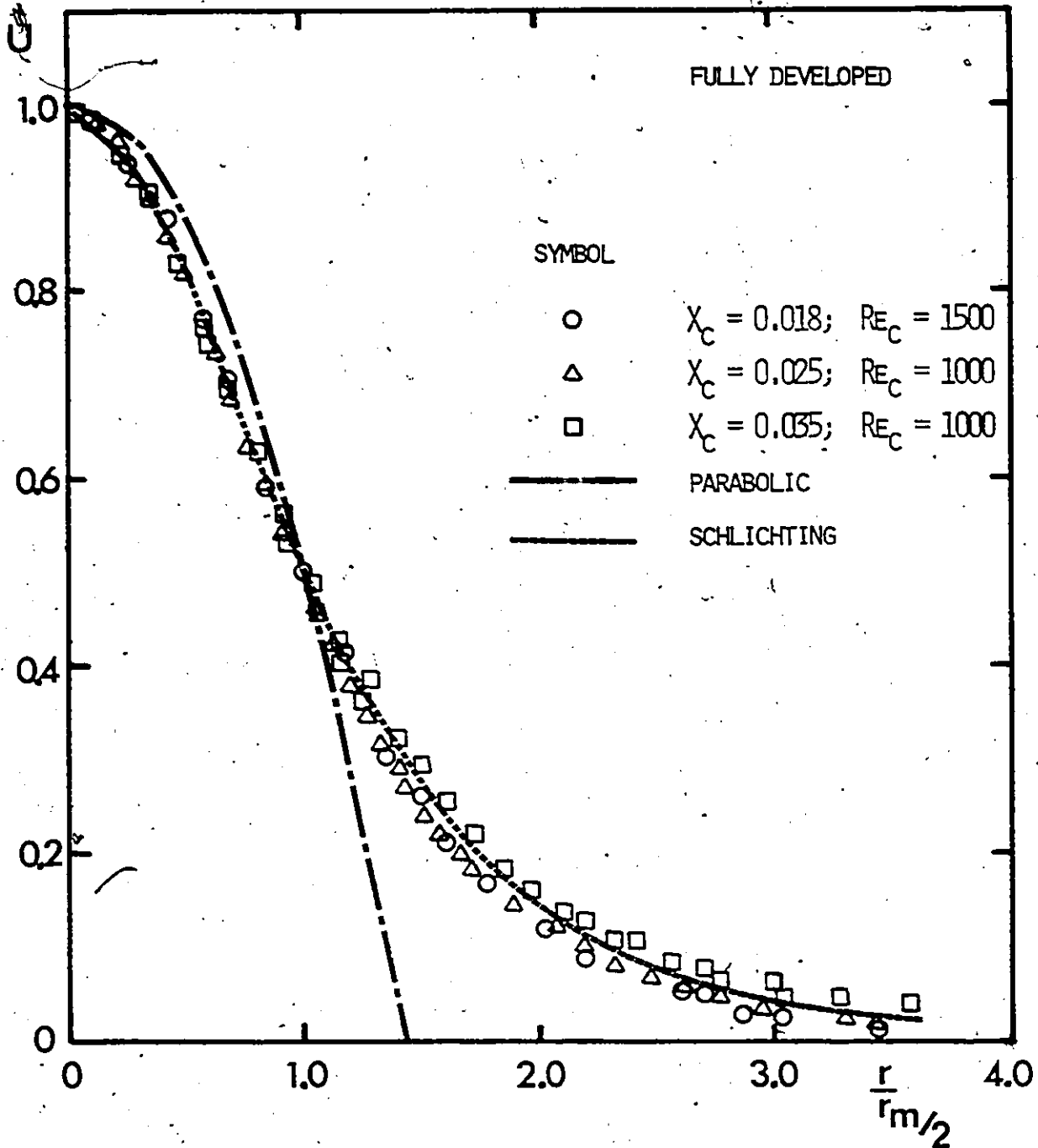


FIG. 5.18 NONDIMENSIONAL VELOCITY PROFILE (FULLY DEVELOPED)

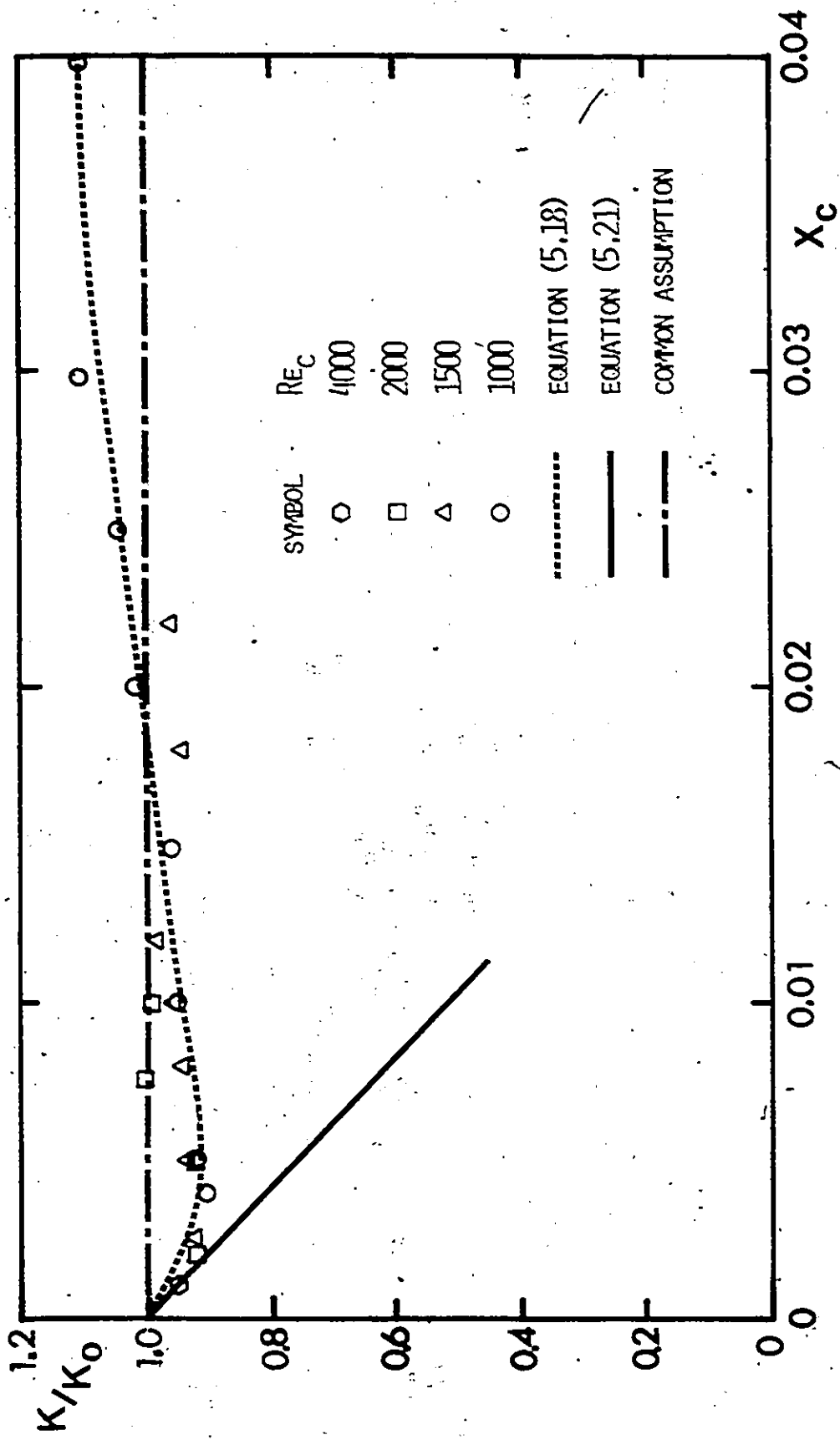


Fig. 5.19 VARIATION OF MOMENTUM RATIO WITH AXIAL DISTANCE

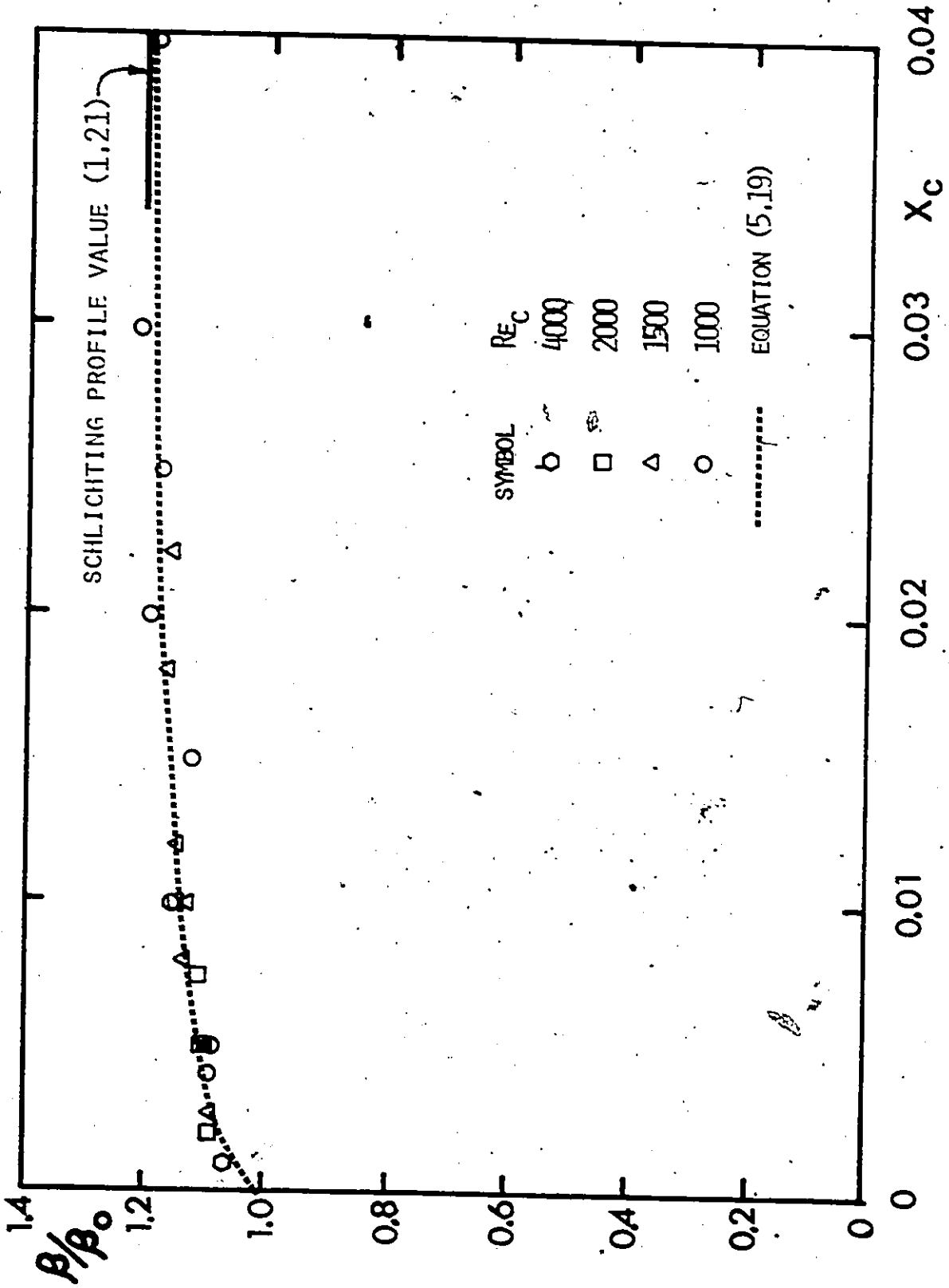


FIG. 5.20 MOMENTUM FLUX COEFFICIENT VARIATION WITH AXIAL DISTANCE

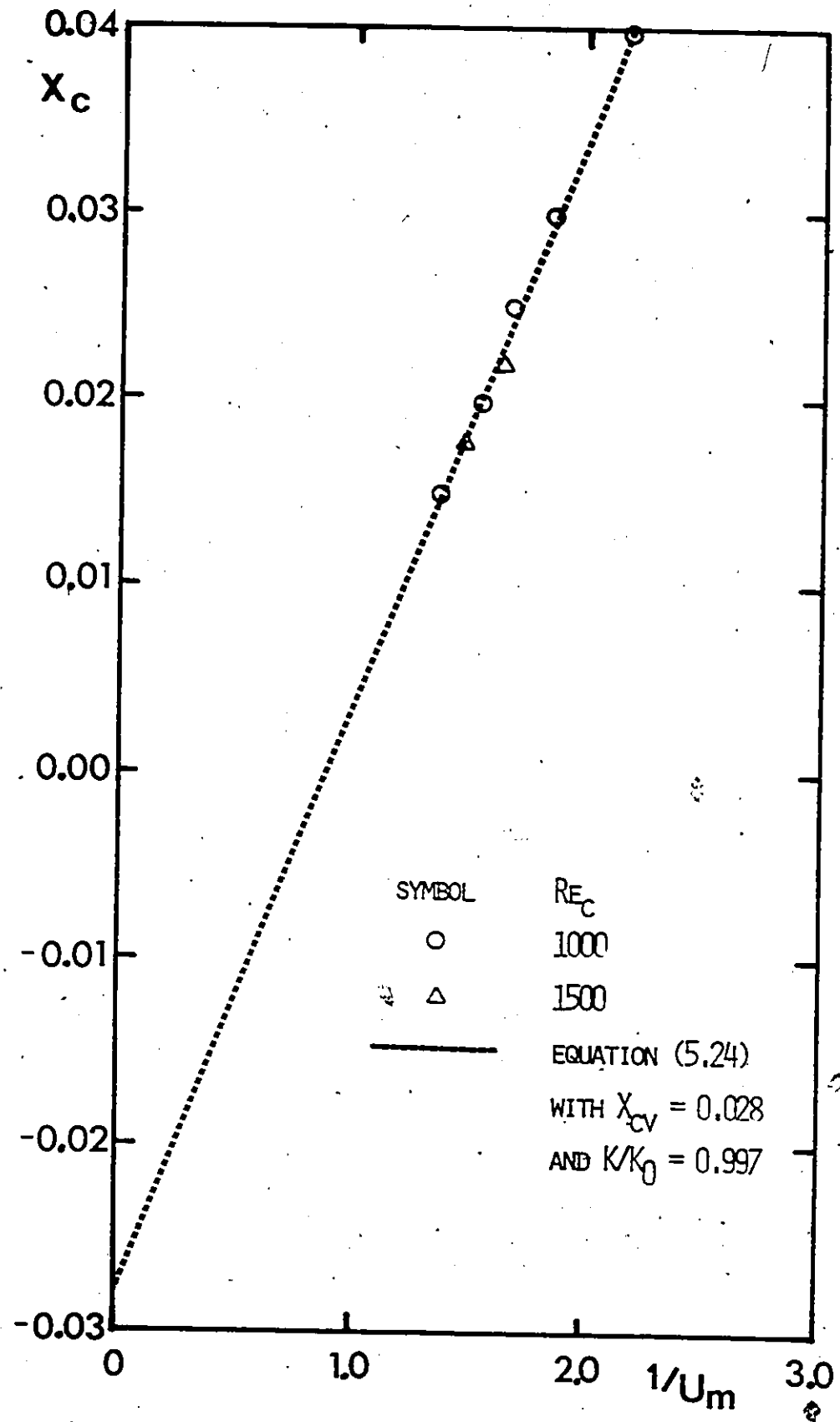


FIG. 5.21, DETERMINATION OF K/K_0 AND X_{cv} USING CENTRE LINE VELOCITY

Table 4.1 VALUES OF f_m IN EQUATION 4.7.

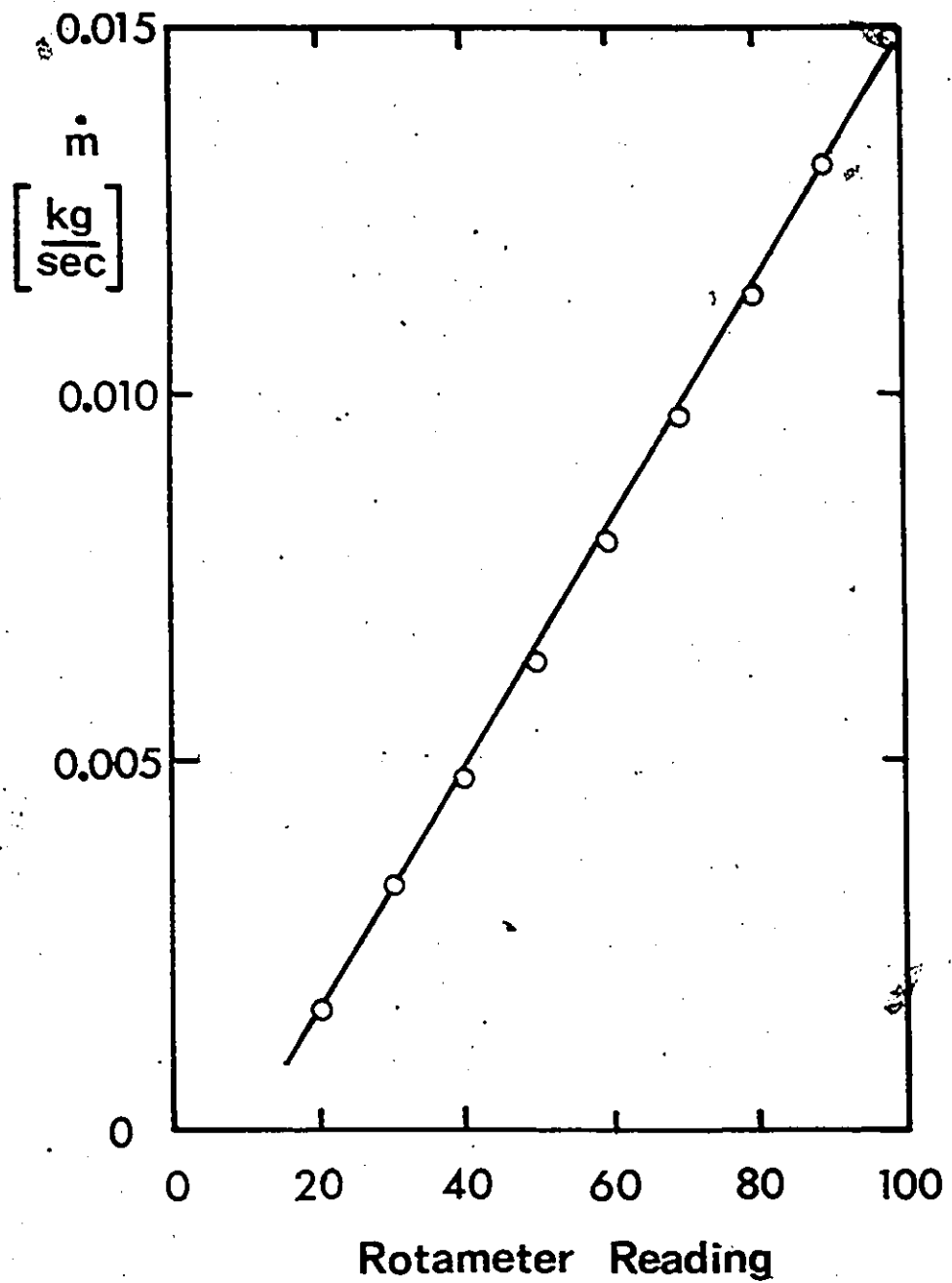
m	f_0	f_1	f_2	f_3	f_4	f_5	f_6
-2	0	0	$\frac{3}{280}$	$\frac{3}{70}$	$\frac{9}{140}$	$\frac{3}{70}$	$\frac{3}{280}$
-1	0	$\frac{1}{10}$	$\frac{1}{5}$	$\frac{1}{10}$	0	0	0
0	$\frac{1}{2}$	0	0	0	0	0	0
1	$-\frac{2}{20}$	0	0	0	0	0	0
2	$\frac{3}{3600}$	-6	$39\frac{3}{4}$	$78\frac{13}{18}$	$46\frac{55}{144}$	$-5\frac{283}{450}$	$\frac{17}{36}$
3	0	$-101\frac{25}{36}$	$527\frac{7}{18}$	$-769\frac{17}{18}$	$365\frac{5}{6}$	$-22\frac{11}{12}$	$1\frac{1}{3}$
4	0	$838\frac{5}{27}$	$-380\frac{10}{27}$	$-1794\frac{17}{54}$	$1378\frac{7}{9}$	$-44\frac{1}{18}$	$1\frac{7}{9}$
5	0	$-2127\frac{77}{324}$	$6414\frac{77}{162}$	$-6480\frac{80}{81}$	$2228\frac{79}{162}$	$-35\frac{235}{324}$	$\frac{80}{81}$

Table 4.2 VALUES OF gm IN EQUATION 4.8.

m	g_0	g_1	g_2	g_3	g_4	g_5	g_6
-1	0	$\frac{3}{140}$	$\frac{3}{70}$	$\frac{3}{140}$	0	0	0
0	$-\frac{1}{3}$	0	0	0	0	0	0
1	$2\frac{9}{20}$	0	0	0	0	0	0
2	$-3\frac{2689}{3600}$	0	0	0	0	0	0
3	$-37\frac{3581}{9000}$	$101\frac{25}{36}$	$-203\frac{7}{18}$	$101\frac{25}{36}$	0	0	0
4	$252\frac{125041}{270000}$	$-1604\frac{10}{27}$	$2909\frac{53}{108}$	$-795\frac{49}{54}$	$-460\frac{511}{1728}$	$14\frac{27013}{33750}$	$65\frac{-108}{-108}$
5	$-672\frac{81263}{720000}$	$12763\frac{23}{54}$	$-32006\frac{23}{27}$	$25824\frac{73}{108}$	$-6685\frac{75}{162}$	$107\frac{57}{324}$	$-2\frac{26}{27}$
6	$694\frac{299856579}{388800000}$	$-52162\frac{73}{81}$	$64033\frac{601}{648}$	$26617\frac{541}{972}$	$-39492\frac{13637}{13824}$	$315\frac{187573}{337500}$	$-5\frac{1795}{1944}$
7	0	$90370\frac{455}{1944}$	$-271460\frac{455}{972}$	$272164\frac{148}{243}$	$-91433\frac{3141}{8748}$	$363\frac{10377}{17496}$	$-4\frac{148}{243}$

APPENDIX A
EQUIPMENT TABLE

No.	Equipment	Model/ Type	Range and/or Comments	Manufacturer Supplier
1	15 mW He-Ne Laser	9126	$\lambda = 632.8 \text{ nm}$	Thermo- Systems Inc.
2	Polarization Rotator	9101-2	-----	
3	Beam Splitter	9115	W=50 mm	
4	Acousto-optic cell and Frequency Shifter	9180-2	-----	
5	Focusing Lens	9117	$f_f = 102.1 \text{ mm}$	
6	Photomultiplier System	9160	-----	
7	Frequency Tracker	1090	2 kHz-50 MHz	
8	High Pass Filter	10095	0-10 MHz	
9	Photodetector Aperature	9161-11	Aperature Diameter=0.28 mm	
10	Oscilloscope	5103N	-----	Tektronics Inc.
11	Digital Voltmeter	55031	0-1 ± 0.001 Volt 0-10 ± 0.01 " 0-100 ± 0.1 "	DISA Elektronik
12	Pan Balance	-----	$\pm 0.003 \text{ Kg}$	Central Scientific Ltd.
13	Thermometer	15-000A	1-51 $\pm 0.1^\circ\text{C}$	Fisher Scientific
14	Rotameter	D314	see Appendix B	Roger Gilmont
15	Electronic Stopwatch	100	$\pm 0.01 \text{ sec}$	Premer

APPENDIX BROTAMETER CALIBRATION CURVE

APPENDIX CEXPERIMENTAL DATA

The number of significant figures presented in the following tables is not indicative of the data uncertainty. An uncertainty analysis is presented in Appendix D.

$$X_c = 0.001$$

$$Re_c = 4000$$

$$x/d = 4$$

$$u_m = 579.1 \text{ mm/sec}$$

$$r_{m/2} = 2.16 \text{ mm}$$

$$\dot{m} = 0.00932 \text{ kg/sec}$$

$$u_{m0} = 588.5 \text{ mm/sec}$$

r (mm)	u (mm/sec)	r (mm)	u (mm/sec)
-7.112	-1.00	-.508	563.09
-6.858	-.33	-.254	573.07
-6.604	-.33	0.000	579.06
-6.350	1.00	.254	576.40
-6.096	1.66	.508	567.08
-5.842	1.66	.762	549.79
-5.588	1.66	1.016	525.18
-5.334	.33	1.270	488.59
-5.080	2.33	1.524	443.36
-4.826	6.32	1.778	390.14
-4.572	11.64	2.032	321.62
-4.318	11.64	2.286	245.13
-4.064	18.29	2.540	181.27
-3.810	29.60	2.794	126.06
-3.556	38.25	3.048	80.82
-3.302	75.50	3.302	50.22
-3.048	100.11	3.556	35.59
-2.794	146.68	3.810	24.28
-2.540	201.22	4.064	15.63
-2.286	266.41	4.318	4.32
-2.032	326.95	4.572	1.66
-1.778	384.15	4.826	.33
-1.524	436.04	5.080	-.33
-1.270	476.62	5.334	-1.00
-1.016	512.54	5.588	-1.66
-.762	541.81		

$$X_c = 0.002 \quad Re_c = 2000 \quad x/d = 4$$

$$u_m = 268.4 \text{ mm/sec} \quad r_{m/2} = 2.18 \text{ mm} \quad \dot{m} = 0.00447 \text{ kg/sec}$$

$$u_{m0} = 282.6 \text{ mm/sec}$$

r (mm)	u (mm/sec)	r (mm)	u (mm/sec)
-7.112	-.33	.254	267.74
-6.604	-.33	.508	264.42
-6.096	-.33	.762	255.77
-5.588	1.00	1.016	243.80
-5.080	3.66	1.270	227.17
-4.572	8.31	1.524	207.21
-4.318	10.98	1.778	183.26
-4.064	14.30	2.032	155.99
-3.810	20.95	2.286	126.06
-3.556	28.94	2.540	98.12
-3.302	40.24	2.794	73.50
-3.048	55.54	3.048	53.55
-2.794	74.17	3.302	38.91
-2.540	97.45	3.556	27.61
-2.286	120.73	3.810	19.62
-2.032	147.34	4.064	14.30
-1.778	173.28	4.318	10.31
-1.524	197.23	4.572	7.65
-1.270	218.52	4.826	5.65
-1.016	235.15	5.080	4.32
-.762	249.78	5.334	2.33
-.508	259.10	5.588	1.66
-.254	265.75	6.858	.33
0.000	268.41	8.128	.33

$$X_c = 0.005$$

$$Re_c = 2000$$

$$x/d = 10$$

$$u_m = 251.1 \text{ mm/sec}$$

$$r_{m/2} = 2.32 \text{ mm}$$

$$\dot{m} = 0.00454 \text{ kg/sec}$$

$$u_{m0} = 286.5 \text{ mm/sec}$$

r (mm)	u (mm/sec)	r (mm)	u (mm/sec)
-9.550	.33	.102	250.45
-8.280	1.00	.356	247.12
-7.010	2.99	.610	241.80
-6.502	5.65	.864	231.16
-5.994	7.65	1.118	217.85
-5.486	10.31	1.372	200.56
-4.978	14.97	1.626	182.60
-4.470	22.28	1.880	160.65
-4.216	26.94	2.134	138.03
-3.962	34.26	2.388	119.40
-3.708	42.91	2.642	98.12
-3.454	53.55	2.896	82.15
-3.200	66.85	3.150	70.18
-2.946	84.15	3.404	55.54
-2.692	101.44	3.658	37.58
-2.438	119.40	3.912	29.60
-2.184	140.02	4.166	24.94
-1.930	157.98	4.420	18.29
-1.676	176.61	4.674	13.64
-1.422	197.23	4.928	9.65
-1.168	212.53	5.182	6.98
-.914	227.83	5.436	5.65
-.660	239.14	5.690	4.32
-.406	245.79	6.960	.33
-.152	249.78	8.230	-.33

$$X_c = 0.0075$$

$$Re_c = 2000$$

$$x/d = 15$$

$$u_m = 247.1 \text{ mm/sec}$$

$$r_{m/2} = 2.44 \text{ mm}$$

$$\dot{m} = 0.00445 \text{ kg/sec}$$

$$u_{m0} = 280.8 \text{ mm/sec}$$

r (mm)	u (mm/sec)	r (mm)	u (mm/sec)
-9.474	.33	.686	237.14
-8.204	1.66	.940	226.50
-6.934	4.99	1.194	213.20
-6.426	6.98	1.448	196.57
-5.918	10.31	1.702	177.94
-5.410	14.97	1.956	161.31
-5.156	18.29	2.210	142.02
-4.902	22.28	2.464	121.40
-4.648	26.94	2.718	105.43
-4.394	32.26	2.972	91.46
-4.140	38.91	3.226	74.17
-3.886	46.90	3.480	59.54
-3.632	56.21	3.734	47.56
-3.378	67.52	3.988	38.25
-3.124	82.15	4.242	30.27
-2.870	95.46	4.496	27.61
-2.616	110.09	4.750	18.29
-2.362	127.39	5.004	12.31
-2.108	144.68	5.258	8.31
-1.854	161.31	5.512	6.32
-1.600	177.28	5.766	4.99
-1.346	194.57	6.020	2.99
-1.092	209.87	6.274	2.33
-.838	224.50	6.782	2.33
-.584	235.15	7.290	2.33
-.330	242.47	7.798	1.00
-.076	246.46	8.306	.33
.178	247.12	9.322	.33
.432	243.80		

$$X_c = 0.010 \quad Re_c = 2000 \quad x/d = 20$$

$$u_m = 235.2 \text{ mm/sec} \quad r_{m/2} = 2.55 \text{ mm} \quad \dot{m} = 0.00454 \text{ kg/sec}$$

$$u_{m0} = 286.5 \text{ mm/sec}$$

r (mm)	u (mm/sec)	r (mm)	u (mm/sec)
-11.684	-.33	1.016	217.85
-10.414	1.00	1.524	191.24
-9.144	2.33	2.032	156.65
-8.636	2.99	2.540	124.06
-8.128	4.99	3.048	90.80
-7.620	5.65	3.556	62.86
-7.112	6.98	4.064	45.57
-6.604	12.31	4.572	28.27
-6.096	14.97	5.080	17.63
-5.588	18.96	5.588	12.97
-5.080	24.94	6.096	8.31
-4.572	37.58	6.604	6.98
-4.064	53.55	7.112	4.32
-3.556	64.19	7.620	2.99
-3.048	90.80	8.128	2.33
-2.540	111.42	8.636	1.66
-2.032	142.69	9.144	1.66
-1.524	178.61	9.652	1.00
-1.016	202.55	10.160	1.66
-.508	225.17	10.668	1.66
0.000	235.15	11.176	1.66
.508	233.15		

$$x_c = 0.0025$$

$$Re_c = 1500$$

$$x/d = 3.75$$

$$u_m = 199.2 \text{ mm/sec} \quad r_{m/2} = 2.20 \text{ mm} \quad \dot{m} = 0.00333 \text{ kg/sec}$$

$$u_{m0} = 210.3 \text{ mm/sec}$$

r (mm)	u (mm/sec)	r (mm)	u (mm/sec)
-12.217	-.33	.483	197.90
-10.947	-.33	.737	190.58
-9.677	-.33	.991	181.27
-8.407	-.33	1.245	170.62
-7.137	-.33	1.499	157.98
-5.867	1.00	1.753	138.03
-5.359	2.33	2.007	117.41
-5.105	3.66	2.261	94.79
-4.851	4.99	2.515	78.16
-4.597	5.65	2.769	60.20
-4.343	8.98	3.023	45.57
-4.089	12.31	3.277	33.59
-3.835	16.96	3.531	24.94
-3.581	23.61	3.785	18.96
-3.327	31.60	4.039	14.30
-3.073	41.57	4.293	10.98
-2.819	55.54	4.547	7.65
-2.565	71.51	4.801	5.65
-2.311	88.14	5.055	4.32
-2.057	106.76	5.309	3.66
-1.803	124.06	5.563	2.99
-1.549	142.69	5.817	1.65
-1.295	158.65	6.071	1.00
-1.041	171.25	6.325	1.00
-.787	183.26	6.579	1.00
-.533	191.24	6.833	.33
-.279	196.57	8.103	.33
-.025	199.23	9.373	.33
.229	199.23		

$$X_c = 0.005 \quad Re_c = 1500 \quad x/d = 7.5$$

$$u_m = 190.6 \text{ mm/sec} \quad r_{m/2} = 2.30 \text{ mm} \quad \dot{m} = 0.00333 \text{ kg/sec}$$

$$u_{m0} = 210.3 \text{ mm/sec}$$

r (mm)	u (mm/sec)	r (mm)	u (mm/sec)
-12.141	-1.00	1.575	141.35
-10.871	-.33	1.829	124.72
-9.601	-.33	2.083	107.43
-8.331	-.33	2.337	90.13
-7.061	1.00	2.591	74.17
-6.553	2.33	2.845	60.20
-6.045	2.99	3.099	48.89
-5.537	4.32	3.353	38.91
-5.029	7.65	3.607	30.93
-4.775	10.31	3.861	24.94
-4.521	13.64	4.115	20.29
-4.267	18.29	4.369	16.30
-4.013	23.61	4.623	12.97
-3.759	29.60	4.877	10.31
-3.505	36.92	5.131	8.31
-3.251	46.90	5.385	6.98
-2.997	57.54	5.639	5.65
-2.743	70.18	5.893	4.32
-2.489	84.15	6.147	3.66
-2.235	99.45	6.401	2.99
-1.981	114.08	6.655	2.33
-1.727	130.05	6.909	2.33
-1.473	145.35	7.163	2.33
-1.219	158.65	7.417	1.66
-.965	169.96	7.671	1.66
-.711	178.61	7.925	1.66
-.457	185.26	8.179	1.66
-.203	189.25	9.449	.33
.051	190.58	10.719	-.33
.813	177.94		
1.067	168.63		
1.321	155.99		

$$X_c = 0.008$$

$$Re_c = 1500$$

$$x/d = 12$$

$$u_m = 179.3 \text{ mm/sec}$$

$$r_{m/2} = 2.41 \text{ mm} \quad \dot{m} = 0.00333 \text{ kg/sec}$$

$$u_{m0} = 210.3 \text{ mm/sec}$$

r (mm)	u (mm/sec)	r (mm)	u (mm/sec)
-11.913	-1.00	.025	179.27
-10.643	-1.00	.279	178.61
-9.373	-.33	.533	175.95
-8.103	.33	.787	169.29
-7.849	1.00	1.041	160.65
-7.341	2.33	1.295	149.34
-6.833	2.99	1.549	138.03
-6.325	5.65	1.803	122.73
-5.817	8.31	2.057	109.43
-5.563	10.31	2.311	93.46
-5.309	12.31	2.565	79.49
-4.801	16.30	2.819	68.18
-4.293	24.94	3.073	57.54
-4.039	30.93	3.327	48.89
-3.785	37.58	3.581	40.91
-3.531	44.90	3.835	34.26
-3.277	53.55	4.089	28.94
-3.023	62.86	4.343	24.28
-2.769	73.50	4.597	20.29
-2.515	84.81	4.851	16.96
-2.261	97.45	5.105	13.64
-2.007	112.09	5.359	11.64
-1.753	124.06	5.613	9.65
-1.499	136.03	5.867	8.31
-1.245	148.01	6.375	4.99
-.991	158.65	6.883	2.99
-.737	167.30	7.391	1.66
-.483	173.95	7.899	.33
-.229	177.94	8.407	-.33

$$X_c = 0.010 \quad Re_c = 1500 \quad x/d = 15$$

$$u_m = 173.3 \text{ mm/sec} \quad r_{m/2} = 2.50 \text{ mm} \quad \dot{m} = 0.00333 \text{ kg/sec}$$

$$u_{m0} = 210.3 \text{ mm/sec}$$

r (mm)	u (mm/sec)	r (mm)	u (mm/sec)
-14.478	-1.00	.762	163.31
-11.938	.33	1.016	155.32
-10.668	.33	1.270	145.35
-9.398	1.00	1.524	133.37
-8.890	1.66	1.778	120.73
-8.382	1.66	2.032	108.10
-7.874	1.66	2.286	95.46
-6.858	5.65	2.540	83.48
-6.350	7.65	2.794	72.84
-5.842	8.31	3.048	62.86
-5.334	11.64	3.302	53.55
-4.826	18.29	3.556	44.90
-4.572	21.62	3.810	38.91
-4.318	26.28	4.064	32.93
-4.064	31.60	4.318	27.61
-3.810	38.91	4.572	23.61
-3.556	46.23	4.826	19.62
-3.302	54.21	5.080	16.30
-3.048	63.53	5.334	13.64
-2.794	73.50	5.588	11.64
-2.540	84.81	5.842	9.65
-2.286	97.45	6.096	8.98
-2.032	109.43	6.858	6.32
-1.778	122.06	7.366	4.32
-1.524	133.37	8.382	1.66
-1.270	144.02	9.398	2.33
-1.016	153.99	10.414	1.66
-.762	161.98	10.922	.33
-.508	167.96	13.462	-1.00
-.254	171.95		
0.000	173.28		
.254	171.95		
.508	168.63		

$$X_c = 0.012$$

$$Re_c = 1500$$

$$x/d = 18$$

$$u_m = 165.3 \text{ mm/sec}$$

$$r_{m/2} = 2.63 \text{ mm}$$

$$\dot{m} = 0.00330 \text{ kg/sec}$$

$$u_{m0} = 208.6 \text{ mm/sec}$$

r (mm)	u (mm/sec)	r (mm)	u (mm/sec)
-14.478	.33	.762	156.65
-13.208	1.00	1.016	149.34
-11.938	1.00	1.270	141.35
-10.668	1.66	1.524	131.38
-9.398	2.33	1.778	120.73
-8.382	3.66	2.032	109.43
-7.366	6.32	2.286	98.12
-6.858	7.65	2.540	86.81
-6.350	10.31	2.794	76.83
-5.842	13.64	3.048	67.52
-5.334	18.29	3.302	58.20
-4.826	24.28	3.556	51.55
-4.318	32.26	3.810	44.24
-4.064	37.58	4.064	37.58
-3.810	42.91	4.318	32.26
-3.556	49.56	4.572	28.27
-3.302	57.54	4.826	23.61
-3.048	64.86	5.080	20.29
-2.794	74.83	5.334	16.96
-2.540	84.81	5.588	14.97
-2.286	94.79	5.842	12.31
-2.032	106.10	6.096	10.31
-1.778	116.74	6.350	8.98
-1.524	126.72	6.858	6.98
-1.270	137.36	7.874	2.99
-1.016	146.01	8.890	1.00
-.762	153.33	9.906	.33
-.508	159.32		
-.254	163.31		
0.000	165.30		
.254	164.64		
.508	161.31		

$$x_c = 0.018 \quad Re_c = 1500 \quad x/d = 27$$

$$u_m = 141.4 \text{ mm/sec} \quad r_{m/2} = 3.01 \text{ mm} \quad \dot{m} = 0.00333 \text{ kg/sec}$$

$$u_{m0} = 210.3 \text{ mm/sec}$$

r (mm)	u (mm/sec)	r (mm)	u (mm/sec)
-12.954	-1.00	2.540	83.48
-11.684	1.00	2.794	76.17
-10.414	1.66	3.048	67.52
-9.144	3.66	3.302	60.87
-8.636	3.66	3.556	54.88
-7.874	7.65	3.810	48.23
-7.112	9.65	4.064	42.91
-6.604	12.31	4.318	37.58
-6.096	16.30	4.572	33.59
-5.588	20.29	4.826	30.27
-5.080	27.61	5.080	27.61
-4.572	36.92	5.334	23.61
-4.064	47.56	5.588	21.62
-3.556	58.87	5.842	18.29
-3.048	70.84	6.096	16.96
-2.540	84.81	6.604	13.64
-2.032	100.11	7.112	10.98
-1.524	116.08	7.620	8.98
-1.016	128.05	8.128	7.65
-.762	132.71	8.636	6.32
-.508	137.36	9.652	4.32
-.254	140.02	10.668	2.99
0.000	141.35	11.684	2.33
.254	140.02	12.700	1.00
.508	138.03	13.716	1.00
.762	134.04	14.732	1.00
1.016	130.05	17.526	-1.00
1.270	124.06		
1.524	116.74		
1.778	108.10		
2.032	99.45		
2.286	92.13		

$$X_c = 0.022 \quad Re_c = 1500 \quad x/d = 33$$

$$u_m = 128.1 \text{ mm/sec} \quad r_{m/2} = 3.37 \text{ mm} \quad \dot{m} = 0.00333 \text{ kg/sec}$$

$$u_{m0} = 210.3 \text{ mm/sec}$$

r (mm)	u (mm/sec)	r (mm)	u (mm/sec)
-13.919	-1.00	1.829	100.78
-12.649	.33	2.337	88.80
-11.379	1.66	2.845	75.50
-10.109	2.99	3.353	63.53
-8.839	5.65	3.861	48.23
-8.331	7.65	4.369	38.25
-7.823	9.65	4.877	30.27
-7.315	11.64	5.385	27.61
-6.807	15.63	5.893	21.62
-6.299	19.62	6.401	18.29
-5.791	24.28	6.909	14.97
-5.283	29.60	7.417	12.31
-4.775	38.25	7.925	10.98
-4.267	43.57	8.433	8.98
-3.759	56.87	8.941	8.31
-3.251	66.19	9.449	5.65
-2.743	80.16	9.957	4.32
-2.235	92.80	10.465	3.66
-1.727	106.76	10.973	3.66
-1.219	116.74	11.481	3.66
-.711	123.39	12.751	2.33
-.203	127.39	14.021	1.66
.305	127.39	15.291	1.00
.813	120.73	16.561	-.33
1.321	112.09	17.831	-1.00

$$X_c = 0.004 \quad Re_c = 1000 \quad x/d = 4$$

$$u_m = 141.4 \text{ mm/sec} \quad r_{m/2} = 2.24 \text{ mm} \quad \dot{m} = 0.00244 \text{ kg/sec}$$

$$u_{m0} = 154.4 \text{ mm/sec}$$

r (mm)	u (mm/sec)	r (mm)	u (mm/sec)
-8.128	.33	.254	140.02
-8.382	1.00	.508	137.36
-7.112	1.66	.762	132.71
-5.842	2.99	1.016	125.39
-5.080	5.65	1.270	115.41
-4.826	6.98	1.524	104.77
-4.572	8.98	1.778	92.80
-4.318	10.98	2.032	79.49
-4.064	13.64	2.286	66.85
-3.810	17.63	2.540	54.88
-3.556	22.28	2.794	43.57
-3.302	28.27	3.048	33.59
-3.048	36.25	3.302	26.28
-2.794	44.24	3.556	20.29
-2.540	56.21	3.810	15.63
-2.286	69.51	4.064	12.31
-2.032	82.15	4.318	8.98
-1.778	94.13	4.572	6.98
-1.524	105.43	4.826	5.65
-1.270	116.08	5.080	4.32
-1.016	125.39	5.334	3.66
-.762	132.71	5.588	2.99
-.508	137.36	6.858	1.00
-.254	140.02	8.128	.33
0.000	141.35		

$$X_c = 0.005 \quad Re_c = 1000 \quad x/d = 5$$

$$u_m = 140.0 \text{ mm/sec} \quad r_{m/2} = 2.24 \text{ mm} \quad \dot{m} = 0.00240 \text{ kg/sec}$$

$$u_{m0} = 151.4 \text{ mm/sec}$$

r (mm)	u (mm/sec)	r (mm)	u (mm/sec)
-9.652	.33	-.508	135.37
-8.382	.33	-.254	138.69
-7.112	1.00	0.000	140.02
-6.858	1.00	.254	138.69
-6.604	1.66	.508	136.03
-6.350	1.66	.762	130.71
-6.096	2.33	1.016	124.06
-5.842	2.99	1.270	115.41
-5.588	2.99	1.524	104.77
-5.334	4.32	1.778	92.80
-5.080	4.99	2.032	79.49
-4.826	6.32	2.286	67.52
-4.572	8.31	2.540	54.88
-4.318	10.31	2.794	43.57
-4.064	13.64	3.048	34.26
-3.810	16.96	3.302	26.94
-3.556	21.62	3.556	20.95
-3.302	27.61	3.810	16.96
-3.048	35.59	4.064	12.97
-2.794	44.90	4.318	9.65
-2.540	55.54	4.572	7.65
-2.286	68.18	4.826	6.32
-2.032	80.16	5.080	4.99
-1.778	93.46	5.334	3.66
-1.524	104.77	5.588	2.99
-1.270	114.75	6.858	1.00
-1.016	123.39	8.128	.33
-.762	130.71		

$$X_c = 0.010$$

$$Re_c = 1000$$

$$x/d = 10$$

$$u_m = 117.4 \text{ mm/sec}$$

$$r_{m/2} = 2.55 \text{ mm}$$

$$\dot{m} = 0.00233 \text{ kg/sec}$$

$$u_{m0} = 147.1 \text{ mm/sec}$$

r (mm)	u (mm/sec)	r (mm)	u (mm/sec)
-11.938	.33	.254	116.74
-10.668	1.00	.508	115.41
-9.398	1.00	.762	110.76
-8.128	1.66	1.016	107.43
-6.858	3.66	1.270	101.44
-6.604	3.66	1.524	93.46
-6.350	4.32	1.778	85.48
-6.096	4.99	2.032	76.83
-5.842	6.32	2.286	68.18
-5.588	8.31	2.540	59.54
-5.334	10.31	2.794	51.55
-5.080	12.31	3.048	44.90
-4.826	14.97	3.302	38.91
-4.572	16.96	3.556	32.93
-4.318	20.29	3.810	28.27
-4.064	22.95	4.064	24.28
-3.810	27.61	4.318	20.95
-3.556	32.26	4.572	17.63
-3.302	37.58	4.826	15.63
-3.048	44.24	5.080	14.30
-2.794	50.89	5.334	12.97
-2.540	58.20	5.588	10.98
-2.286	66.85	5.842	9.65
-2.032	74.83	6.096	8.31
-1.778	82.82	6.350	7.65
-1.524	90.80	6.604	6.98
-1.270	98.12	6.858	5.65
-1.016	104.77	7.112	4.99
-.762	110.09	8.382	2.99
-.508	113.42	9.652	1.66
-.254	116.74	10.922	1.00
0.000	117.41	12.192	1.00

$$x_c = 0.015$$

$$Re_c = 1000$$

$$x/d = 15$$

$$u_m = 108.8 \text{ mm/sec}$$

$$r_{m/2} = 2.83 \text{ mm}$$

$$m = 0.00235 \text{ kg/sec}$$

$$u_{m0} = 148.3 \text{ mm/sec}$$

r (mm)	u (mm/sec)	r (mm)	u (mm/sec)
-9.322	-.33	.838	100.78
-8.052	1.00	1.092	96.79
-6.782	4.99	1.346	91.46
-6.528	5.65	1.600	85.48
-6.274	6.98	1.854	79.49
-6.020	8.98	2.108	72.17
-5.766	10.98	2.362	65.52
-5.512	12.31	2.616	59.54
-5.258	14.30	2.870	52.88
-5.004	17.63	3.124	46.90
-4.750	19.62	3.378	40.91
-4.496	22.95	3.632	35.59
-4.242	26.28	3.886	30.93
-3.988	29.60	4.140	26.94
-3.734	34.26	4.394	23.61
-3.480	39.58	4.648	20.95
-3.226	44.90	4.902	18.29
-2.972	50.89	5.156	16.30
-2.718	57.54	5.410	14.30
-2.464	62.86	5.664	12.31
-2.210	69.51	5.918	8.98
-1.956	76.17	6.172	8.31
-1.702	82.82	6.426	6.98
-1.448	89.47	6.680	5.65
-1.194	95.46	6.934	4.99
-.940	100.11	7.188	4.32
-.686	103.44	7.442	3.66
-.432	106.76	7.696	2.99
-.178	108.10	7.950	2.33
.076	108.10	8.204	1.66
.330	106.76	8.458	1.00
.584	104.77	9.728	.33

$$x_c = 0.020$$

$$Re_c = 1000$$

$$x/d = 20$$

$$u_m = 95.5 \text{ mm/sec}$$

$$r_{m/2} = 3.26 \text{ mm}$$

$$\dot{m} = 0.00235 \text{ kg/sec}$$

$$u_{m0} = 148.4 \text{ mm/sec}$$

r (mm)	u (mm/sec)	r (mm)	u (mm/sec)
-16.510	.33	.762	91.46
-15.240	1.00	1.016	88.14
-13.970	1.00	1.270	84.15
-12.700	1.66	1.524	80.16
-11.430	2.33	1.778	75.50
-10.160	2.99	2.032	70.84
-8.890	4.32	2.286	65.52
-8.382	5.65	2.540	60.87
-7.874	6.98	2.794	54.88
-7.366	9.65	3.048	50.89
-6.858	11.64	3.302	46.23
-6.350	12.97	3.556	42.24
-5.842	17.63	3.810	38.25
-5.334	20.95	4.318	30.27
-4.826	24.94	4.826	25.61
-4.318	32.93	5.334	20.29
-3.810	39.58	5.842	17.63
-3.556	43.57	6.350	14.97
-3.302	48.23	6.858	12.97
-3.048	52.88	7.366	10.31
-2.794	57.54	7.874	8.31
-2.540	62.20	8.382	6.98
-2.286	66.85	8.890	6.32
-2.032	71.51	9.398	4.99
-1.778	76.83	9.906	4.32
-1.524	80.82	10.414	3.66
-1.270	85.48	10.922	2.99
-1.016	88.80	11.430	2.99
-.762	92.13	12.700	2.33
0.000	95.46	13.970	1.66
.254	94.79	16.510	1.00
.508	92.80	17.780	.33

$$X_c = 0.025$$

$$Re_c = 1000$$

$$x/d = 25$$

$$u_m = 86.81 \text{ mm/sec}$$

$$r_{m/2} = 3.58 \text{ mm}$$

$$\dot{m} = 0.00231 \text{ kg/sec}$$

$$u_{m0} = 145.7 \text{ mm/sec}$$

r (mm)	u (mm/sec)	r (mm)	u (mm/sec)
-15.723	.33	.787	83.48
-14.453	1.00	1.041	81.49
-13.183	1.66	1.295	80.16
-11.913	2.33	1.549	75.50
-10.643	2.99	1.803	72.17
-9.373	4.99	2.057	67.52
-8.865	6.32	2.311	64.19
-8.257	6.98	2.565	59.54
-7.849	8.98	2.819	55.54
-7.341	10.98	3.073	51.55
-6.833	12.97	3.327	47.56
-6.325	15.63	3.581	44.24
-6.071	17.63	3.835	40.24
-5.817	18.96	4.089	37.58
-5.563	20.95	4.343	33.59
-5.309	23.61	4.597	30.27
-5.055	25.61	4.851	26.28
-4.801	27.61	5.105	23.61
-4.547	30.93	5.359	21.62
-4.293	32.93	5.613	19.62
-4.039	36.92	5.867	17.63
-3.785	40.24	6.121	16.30
-3.531	43.57	6.375	14.97
-3.277	46.23	6.883	12.97
-3.023	51.55	7.391	10.98
-2.769	55.54	7.899	8.98
-2.515	60.20	8.407	7.65
-2.261	63.53	8.915	6.32
-2.007	66.85	9.423	5.65
-1.753	71.51	9.931	4.99
-1.499	74.83	10.439	3.66
-1.245	78.16	10.947	2.99
-.991	80.16	12.217	2.33
-.737	82.82	13.487	1.66
-.483	84.81	14.757	1.00
-.229	86.81	16.027	1.00
.025	86.81	17.297	1.00
.279	86.14	18.567	.33
.533	85.48		

$$X_c = 0.030 \quad Re_c = 1000 \quad x/d = 30$$

$$u_m = 79.5 \text{ mm/sec} \quad r_{m/2} = 3.99 \text{ mm} \quad \dot{m} = 0.00233 \text{ kg/sec}$$

$$u_{m0} = 147.14 \text{ mm/sec}$$

r (mm)	u (mm/sec)	r (mm)	u (mm/sec)
-15.697	.33	3.099	48.89
-13.157	1.00	3.607	42.24
-10.617	2.99	4.115	34.92
-9.347	5.65	4.623	30.93
-8.077	10.98	5.131	26.94
-6.807	16.30	5.639	22.28
-5.537	23.61	6.147	18.96
-5.029	28.27	6.655	16.96
-4.521	36.25	7.163	14.97
-4.013	41.57	8.433	10.98
-3.505	48.23	9.703	7.65
-2.997	53.55	10.973	5.65
-2.489	60.20	12.243	4.32
-1.981	66.19	13.513	2.99
-1.473	72.17	14.783	2.33
-.965	75.50	16.053	1.66
-.457	79.49	17.323	1.66
.051	79.49	18.593	1.00
.559	78.16	19.863	1.00
1.067	76.17	21.133	1.00
1.575	71.51	22.403	1.00
2.083	63.53	23.673	.33
2.591	56.87		

$$X_c = 0.040 \quad Re_c = 1000 \quad x/d = 40$$

$$u_m = 67.5 \text{ mm/sec} \quad r_{m/2} = 4.72 \text{ mm} \quad \dot{m} = 0.00234 \text{ kg/sec}$$

$$u_{m0} = 147.6 \text{ mm/sec}$$

r (mm)	u (mm/sec)	r (mm)	u (mm/sec)
-19.406	1.00	4.470	35.59
-16.866	1.66	4.978	30.93
-14.326	2.33	5.486	27.61
-11.786	4.32	5.994	20.29
-9.246	10.98	7.264	16.30
-7.976	13.64	8.534	12.97
-6.706	16.30	9.804	10.31
-5.436	27.61	11.074	7.65
-4.166	37.58	12.344	5.65
-2.896	50.89	13.614	4.99
-1.626	60.87	14.884	3.66
-1.118	64.19	16.154	2.99
-.610	66.19	17.424	2.33
-.102	66.85	18.694	1.66
.406	66.85	19.964	1.66
.914	64.86	21.234	1.00
1.422	62.20	22.504	1.00
1.930	58.87	23.774	1.00
2.438	54.21	25.044	1.00
2.946	50.22	26.314	1.00
3.454	44.24	27.584	.67
3.962	40.24	28.854	.33

APPENDIX DUNCERTAINTY ANALYSIS

The format shown below will be used for listing the value of a variable, A , an estimate of the uncertainty, W_A , and the units of A .

$A \pm W_A$ units of A

The data used in the following analysis is taken from the set that has

$Re_c = 2000$, $x/d = 5$ and hence $X_c = 0.01$.

The uncertainties of the following quantities are determined; u , u_m , \dot{m} , u_{m0} , Re_c , X_c , R , $R_m/2$, I , K , K_0 , K/K_0 , β and β/β_0 .

The method used is that suggested by Kline and McClintock [K2] with 20 to 1 odds.

a) Velocity (u , u_m)

This analysis applies to both u and u_m since the later is a special case of u . As an example, u_m will be considered.

$$u_m = \frac{\lambda}{2 S \sin \kappa} [E_m - E_s] \quad (D.1)$$

where

$$\lambda = 632.8 \pm 0 \text{ nm}$$

$$S = 20 \pm 0 \text{ volts/MHz}$$

$$\kappa = 13.76 \pm 0 \text{ degrees}$$

$$E_s = 1.025 \pm 0.01 \text{ Volts}$$

$$E_m = 4.56 \pm 0.01 \text{ Volts}$$

The first three values given above are set by the manufacturer and are considered to have significantly less uncertainty than the others.

Hence,

$$W_{u_m} = \left[\left(\frac{\partial u_m}{\partial E} W_{E_m} \right)^2 + \left(\frac{\partial u_m}{\partial E_s} W_{E_s} \right)^2 \right]^{1/2} \quad (D.2)$$

where

$$\frac{\partial u_m}{\partial E} = \frac{-\partial u_m}{\partial E_0} = \frac{\lambda}{2 S \sin \kappa} \quad (D.3)$$

therefore $u_m = 235 \pm 1 \text{ mm/sec } (\pm 0.4\%)$.

It should also be mentioned that the effect of the velocity gradient on the accuracy of the readings will be negligibly small due to the relative size of the jet and measuring volume.

b) Mass Flowrate (\dot{m})

The mass flowrate is calculated using the following equation

$$\dot{m} = \frac{m - m_c}{t} \quad (D.4)$$

where m = mass of fluid and container

$$= 0.785 \pm 0.01 \text{ kg}$$

m_c = mass of container

$$= 0.161 \pm 0.01 \text{ kg}$$

t = collection time

$$= 137.4 \pm 0.3 \text{ sec}$$

also

$$W_{\dot{m}} = \left[\left(\frac{\partial \dot{m}}{\partial m} W_m \right)^2 + \left(\frac{\partial \dot{m}}{\partial m_c} W_{m_c} \right)^2 + \left(\frac{\partial \dot{m}}{\partial t} W_t \right)^2 \right]^{1/2} \quad (D.5)$$

where $\frac{\partial \dot{m}}{\partial m} = -\frac{\partial \dot{m}}{\partial m_c} = \frac{1}{t}$ (D.6)

and

$$\frac{\partial \dot{m}}{\partial t} = \frac{-(m - m_c)}{t^2} \quad (D.7)$$

which gives $\dot{m} = 0.00454 \pm 0.0001 \text{ kg/sec}$ ($\pm 2.3\%$).

c) Exit Centre Line Velocity (u_{mo})

It can be shown that

$$u_{mo} = \frac{8\dot{m}}{\pi \rho d^2} \quad (D.8)$$

where $d = 6.35 \pm 0.03$ mm

$\rho = 997.3 \pm 0$ kg/sec

$\dot{m} = 0.00454 \pm 0.00010$ kg/sec

W_p is very small, based on a temperature $T = 24^\circ\text{C}$, $W_T = 0.5^\circ\text{C}$, and the physical properties of water.

$$W_{u_{mo}} = \left[\left(\frac{\partial u_{mo}}{\partial d} W_d \right)^2 + \left(\frac{\partial u_{mo}}{\partial \dot{m}} W_{\dot{m}} \right)^2 \right]^{1/2}$$

$$= \left[\left(-2 \frac{W_d}{d} \right)^2 + \left(\frac{W_{\dot{m}}}{\dot{m}} \right)^2 \right]^{1/2} u_{mo} \quad (D.9)$$

which gives $u_{mo} = 287 \pm 7$ mm/sec ($\pm 2.4\%$).

d) Reynolds Numbers (Re_c)

This value may be found as follows

$$Re_c = \frac{u_{mo} d}{\nu} \quad (D.10)$$

where $d = 6.35 \pm 0.03$ mm

$u_{mo} = 287 \pm 7$ mm/sec

$\nu = 0.915 \pm 0.003$ mm²/sec

also

$$W_{Re_c} = \left[\left(\frac{W_{u_{mo}}}{u_{mo}} \right)^2 + \left(\frac{W_d}{d} \right)^2 + \left(\frac{W_\nu}{\nu} \right)^2 \right]^{1/2} Re_c \quad (D.11)$$

which gives $Re_c = 1992 \pm 49$ ($\pm 2.5\%$).

e) Nondimensional Axial Distance (X_c, X^*)

$$X_c = \frac{x}{d Re_c} \quad (D.12)$$

where $x = 127.00 \pm 0.06$ mm

$d = 6.35 \pm 0.03$ mm

$Re_c = 1992 \pm 49$

also

$$W_{X_c} = \left[\left(\frac{W_x}{x} \right)^2 + \left(\frac{W_d}{d} \right)^2 + \left(\frac{W_{Re_c}}{Re_c} \right)^2 \right]^{\frac{1}{2}} X_c \quad (D.13)$$

which gives $X_c = 0.010 \pm 0.00025$ ($\pm 2.5\%$).

$$X^* = \frac{x}{d \sqrt{Re}} = \frac{\sqrt{2} x}{d \sqrt{Re_c}} \quad (D.14)$$

and

$$W_{X^*} = \left[\left(\frac{W_x}{x} \right)^2 + \left(\frac{W_d}{d} \right)^2 + \left(\frac{1}{2} \frac{W_{Re_c}}{Re_c} \right)^2 \right]^{\frac{1}{2}} X^* \quad (D.15)$$

which gives $X^* = 0.634 \pm 0.0084$ ($\pm 1.3\%$).

f) Nondimensional Radial Distance ($R, R_{m/2}$)

In a similar manner to u and u_m , $R_{m/2}$ is a particular value of R . It will be considered as an example.

$$R_{m/2} = \frac{r_{m/2}}{d} \quad (D.16)$$

where $r_{m/2} = 2.55 \pm 0.03$ mm

$d = 6.35 \pm 0.03$ mm

also

$$W_{R_{m/2}} = \left[\left(\frac{W_{r_{m/2}}}{r_{m/2}} \right)^2 + \left(\frac{W_d}{d} \right)^2 \right]^{1/2} R_{m/2} \quad (D.17)$$

which gives $R_{m/2} = 0.402 \pm 0.005$ ($\pm 1.3\%$).

g) Integral Value (I)

The calculation of both K and β involves the determination of the following integral:

$$I = \int_0^{\infty} u^2 d(r^2) \quad (D.18)$$

The following numerical integration scheme is used

$$I = \frac{1}{2} \sum_{i=1}^{n-1} (u_{i+1}^2 + u_i^2)(r_{i+1}^2 - r_i^2) \quad (D.19)$$

where r_i values and corresponding u_i values can be found in Appendix

C. Also,

$$W_{u_i} = W_{u_{i+1}} = W_u = 1 \text{ mm/sec}$$

$$\text{and } W_{r_i} = W_{r_{i+1}} = W_r = 0.03 \text{ mm}$$

$$I = I(u_1, u_2, \dots, u_n, r_1, r_2, \dots, r_n) \quad (D.20)$$

therefore

$$W_I = \left[\left(\frac{\partial I}{\partial u_1} W_{u_1} \right)^2 + \left(\frac{\partial I}{\partial u_2} W_{u_2} \right)^2 + \dots + \left(\frac{\partial I}{\partial u_n} W_{u_n} \right)^2 + \left(\frac{\partial I}{\partial r_1} W_{r_1} \right)^2 + \left(\frac{\partial I}{\partial r_2} W_{r_2} \right)^2 + \dots + \left(\frac{\partial I}{\partial r_n} W_{r_n} \right)^2 \right]^{\frac{1}{2}} \quad (D.21)$$

If $W_{u_1} = W_{u_2} = \dots = W_{u_n} = W_u$ and $W_{r_1} = W_{r_2} = \dots = W_{r_n} = W_r$,

after expanding the equation for I and differentiating it can be shown that

$$W_I = 2 \left[W_u^2 \{ u_1^2 (r_2^2 - r_1^2)^2 + \sum_{i=2}^{n-1} u_i^2 (r_{i+1}^2 - r_{i-1}^2)^2 + u_n^2 (r_n^2 - r_{n-1}^2)^2 \} + W_r^2 \{ r_1^2 (u_2^2 + u_1^2)^2 + \sum_{i=2}^{n-1} r_i^2 (u_{i+1}^2 - u_{i-1}^2)^2 + r_n^2 (u_n^2 + u_{n-1}^2)^2 \} \right]^{\frac{1}{2}} \quad \dots (D.22)$$

Using the data previously mentioned we get

$$I = 275,400 \pm 3930 \text{ mm}^4/\text{sec}^2 (\pm 1.4\%).$$

h) Momentum Flux ($K, K_0, K/K_0$)

$$K = \pi \int_0^{R_0} u^2 d(r^2) = \pi I \quad (D.23)$$

and hence

$$W_K = \pi W_I$$

which gives $K = 865,200 \pm 12,350 \text{ mm}^4/\text{sec}^2 (\pm 1.4\%).$

Also

$$K_0 = \frac{\pi d^2}{12} u_{m0}^2 \quad (D.25)$$

and

$$W_{K_0} = \left[\left(\frac{2W_d}{d} \right)^2 + \left(\frac{2W_{u_{m0}}}{u_{m0}} \right)^2 \right]^{1/2} K_0 \quad (D.26)$$

using the values which have previously been determined we get

$$K_0 = 869,520 \pm 42,800 \text{ mm}^4/\text{sec}^2 \quad (\pm 5.0\%).$$

Now consider K/K_0 .

and

$$W_{K/K_0} = \left[\left(\frac{W_K}{K} \right)^2 + \left(\frac{W_{K_0}}{K_0} \right)^2 \right]^{1/2} \quad (D.27)$$

which yields $K/K_0 = 0.995 \pm 0.05 \quad (\pm 5.2\%).$

i) Momentum Flux Coefficient ($\beta, \beta_0, \beta/\beta_0$)

$$\begin{aligned} \beta &= \int_0^\infty (u/u_m)^2 d(r/r_{m/2})^2 \\ &= \frac{1}{u_m^2 r_{m/2}^2} \int_0^\infty u^2 d(r^2) \\ &= \frac{I}{u_m^2 r_{m/2}^2} \end{aligned} \quad (D.28)$$

$$W_\beta = \left[\left(\frac{W_I}{I} \right)^2 + \left(\frac{-2 W_{u_m}}{u_m} \right)^2 + \left(\frac{-2 W_{r_{m/2}}}{r_{m/2}} \right)^2 \right]^{1/2} \quad (D.29)$$

which gives $\beta = 0.767 \pm 0.022 \quad (\pm 2.8\%).$ Further, $\beta_0 = 2/3$ and $W_{\beta_0} = 0.$

Finally we obtain $\beta/\beta_0 = 1.15 \pm 0.033$ ($\pm 2.9\%$).

APPENDIX EDETAILS OF UNIFORM EXIT CONDITION ANALYSIS

Evaluation of the integrals in equations 3.8 and 3.9 is accomplished as follows:

$$\frac{d}{dx_c} \int_0^{\infty} R U_0^2 dR = 0 \quad (3.8)$$

$$\frac{1}{2} \frac{d}{dx_c} \int_0^{\infty} R U_0^3 dR = - \int_0^{\infty} R \left(\frac{\partial U_0}{\partial R} \right)^2 dR \quad (3.9)$$

All of the above integrals are broken into two parts as shown below.

$$\int_0^{\infty} \text{---} dR = \int_0^B \text{---} dR + \int_B^{\infty} \text{---} dR.$$

Consider the integrals over the range $0 \leq R \leq B$ where

$$U_0 = 1 \quad (3.1)$$

and

$$\frac{\partial U_0}{\partial R} = 0$$

therefore

$$\int_0^B R U_0^2 dR = \int_0^B R dR = \frac{B^2}{2} \quad (E.1)$$

$$\int_0^B R U_0^3 dR = \int_0^B R dR = \frac{B^2}{2} \quad (E.2)$$

$$\text{and } \int_0^B R \left(\frac{\partial U_0}{\partial R} \right)^2 dR = 0. \quad (E.3)$$

Now consider the integrals over the range $B \leq R \leq \infty$ where

$$U_0 = \frac{1}{\left[1 + \frac{(R-B)^2}{16(\gamma/Re_c)^2}\right]^2} \quad (3.5)$$

by letting $\xi = \frac{(R-B)}{4(\gamma/Re_c)}$

$$R = 4(\gamma/Re_c)\xi + B \quad (A.4)$$

and

$$dR = 4(\gamma/Re_c) d\xi \quad (A.5)$$

since B is independent of R.

Substituting equation A.4 into 3.5, we get

$$U_0 = \frac{1}{[1 + \xi^2]^2} \quad (A.6)$$

We also find that

$$\left(\frac{\partial U_0}{\partial R}\right)^2 = \frac{\xi^2(\gamma/Re_c)^2}{[1 + \xi^2]^6} \quad (A.7)$$

Using equations A.4, A.5, A.6 and A.7 the integrals being considered may be found as follows making use of Table A.1 presented at the end of this appendix.

$$\begin{aligned} \int_B^{\infty} R U_0^2 dR &= \int_0^{\infty} \frac{[4(\gamma/Re_c)\xi + B] 4(\gamma/Re_c)}{[1 + \xi^2]^4} d\xi \\ &= \frac{8}{3} (\gamma/Re_c)^2 + \frac{5\pi}{8} (\gamma/Re_c) B \end{aligned} \quad (A.8)$$

$$\int_B^{\infty} R U_0^3 dR = \int_0^{\infty} \frac{[4(\gamma/Re_c)\xi + B] 4(\gamma/Re_c)}{[1 + \xi^2]^6} d\xi$$

$$= \frac{8}{5} (\gamma/Re_c)^2 + \frac{63\pi}{128} (\gamma/Re_c) B \quad (A.9)$$

$$\int_B^{\infty} R \left(\frac{\partial U_0}{\partial R} \right)^2 dR = \int_0^{\infty} \frac{[4(\gamma/Re_c)\xi + B][\xi^2/(\gamma/Re_c)^2] 4(\gamma/Re_c)}{[1 + \xi^2]^6} d\xi$$

$$= \frac{2}{5} + \frac{7\pi}{128} \frac{B}{(\gamma/Re_c)} \quad (A.10)$$

Substituting equations A.1, A.2, A.3, A.8, A.9 and A.10 into equations 3.8 and 3.9 gives

$$\frac{d}{dX_c} \left[\frac{8}{3} (\gamma/Re_c)^2 + \frac{5\pi}{8} (\gamma/Re_c) B + \frac{B^2}{2} \right] = 0 \quad (3.10)$$

and

$$\frac{d}{dX_c} \left[\frac{8}{5} (\gamma/Re_c)^2 + \frac{63\pi}{128} (\gamma/Re_c) B + \frac{B^2}{2} \right]$$

$$= - \left[\frac{4}{5} + \frac{7\pi}{64} \frac{B}{(\gamma/Re_c)} \right] \quad (3.11)$$

Integrating equation 3.10 and applying the boundary condition at $X_c=0$, $B=1/2$ and $\gamma=0$ we find that

$$\frac{8}{3} (\gamma/Re_c)^2 + \frac{5\pi}{8} (\gamma/Re_c) B + \frac{B^2}{2} = \frac{1}{8} \quad (3.12)$$

Introducing a new variable $z = B/(\gamma/Re_c)$ and rearranging equations

3.11 and 3.12 we get

$$(\gamma/Re_c)^2 = \frac{1}{8(8/3 + \frac{5\pi}{8}\zeta + \frac{\zeta^2}{2})} \quad (3.13)$$

and

$$\frac{d}{dX_c} [(\gamma/Re_c)^2 (8/5 + \frac{63\pi}{128}\zeta + \frac{\zeta^2}{2})] = - [\frac{4}{5} + \frac{7\pi}{64}\zeta] \quad (3.14)$$

Substituting equation 3.13 into equation 3.14 yields

$$\frac{d}{dX_c} \left[\frac{(8/5 + \frac{63\pi}{128}\zeta + \frac{\zeta^2}{2})}{8(8/3 + \frac{5\pi}{8}\zeta + \frac{\zeta^2}{2})} \right] = - [\frac{4}{5} + \frac{7\pi}{64}\zeta]$$

Multiplying both sides of the above equation by 1920/3 yields

$$\frac{d}{dX_c} \left[\frac{3072 + 945\pi\zeta + 960\zeta^2}{64 + 15\pi\zeta + 12\zeta^2} \right] = - [512 + 70\pi\zeta]$$

and dividing within the brackets of the left hand side gives

$$\frac{d}{dX_c} \left[80 - \frac{(255\pi\zeta + 2048)}{(12\zeta^2 + 15\pi\zeta + 64)} \right] = - [512 + 70\pi\zeta]$$

Differentiation of the left hand side and rearrangement yields

$$\frac{(3060\pi\zeta^2 + 49152\zeta + 14400\pi)}{(12\zeta^2 + 15\pi\zeta + 64)^2 (512 + 70\pi\zeta)} d\zeta = - dX_c \quad (3.15)$$

Expanding the coefficient of $d\zeta$ into partial fractions gives

$$\frac{3060\pi\zeta^2 + 49152\zeta + 14400\pi}{(12\zeta^2 + 15\pi\zeta + 64)^2 (512 + 70\pi\zeta)} = \frac{F}{(512 + 70\pi\zeta)} + \frac{G\zeta + H}{(12\zeta^2 + 15\pi\zeta + 64)} + \frac{I\zeta + J}{(12\zeta^2 + 15\pi\zeta + 64)^2} \quad (A.11)$$

Multiplying both sides of equation A.11 by $(12\zeta^2 + 15\pi\zeta + 64)^2 (512 + 70\pi\zeta)$ and grouping the coefficients of like powers of ζ yields the following set of five linear algebraic equations

$$\begin{aligned} 144 F + 840\pi G &= 0 \\ 360\pi F + (6144 + 1050\pi^2) G + 840\pi H &= 0 \\ (1536 + 225\pi^2)F + 12160\pi G + (6144 + 1050\pi^2)H + 70\pi I &= 3060\pi \\ 1920\pi F + 32768 G + 12160\pi H + 512 I + 70\pi J &= 49152 \\ 4096 F + 32768 H + 512 J &= 14400\pi \end{aligned}$$

It can be shown that the solution to the above equations yields

$$F = - 45.72106$$

$$G = 2.49488$$

$$H = 3.98876$$

$$I = 91.94632$$

$$J = 198.84458$$

Substituting equation A.11 into 3.15 and integrating yields

$$\int_{\infty}^{\zeta} \frac{F}{(512+70\pi\zeta)} d\zeta + \int_{\infty}^{\zeta} \frac{(G\zeta + H)}{(12\zeta^2+15\pi\zeta+64)} d\zeta + \int_{\infty}^{\zeta} \frac{(I\zeta + J)}{(12\zeta^2+15\pi\zeta+64)^2} d\zeta = -X_c \quad (A.12)$$

It should be noted that the boundary condition $X_c = 0, \gamma = 0$ becomes

$$X_c = 0, \zeta = \infty.$$

Considering the integrals within equation A.12 in order we get

$$\int_{-\infty}^{\infty} \frac{F}{(512+70\pi\zeta)} d\zeta = \frac{F}{70\pi} \ln |512 + 70\pi\zeta| \Big|_{-\infty}^{\infty} \quad (\text{A.13})$$

$$\int_{-\infty}^{\infty} \frac{G\zeta + H}{(12\zeta^2 + 15\pi\zeta + 64)} d\zeta = \frac{G}{24} \ln |12\zeta^2 + 15\pi\zeta + 64| \Big|_{-\infty}^{\infty} \quad (\text{A.14})$$

$$+ \frac{2H - \frac{15\pi}{12} G}{\sqrt{3072 - 225\pi^2}} \tan^{-1} \left[\frac{24\zeta + 15\pi}{\sqrt{3072 - 225\pi^2}} \right] \Big|_{-\infty}^{\infty}$$

and

$$\int_{-\infty}^{\infty} \frac{(I\zeta + J)}{(12\zeta^2 + 15\pi\zeta + 64)^2} d\zeta = \frac{(24\zeta + 15\pi) J - (15\pi\zeta + 128) \cdot I}{(3072 - 225\pi^2)(12\zeta^2 + 15\pi\zeta + 64)} \Big|_{-\infty}^{\infty} \\ + \frac{48J - 30\pi I}{(3072 - 225\pi^2)\sqrt{3072 - 225\pi^2}} \tan^{-1} \left[\frac{24\zeta + 15\pi}{\sqrt{3072 - 225\pi^2}} \right] \Big|_{-\infty}^{\infty} \quad (\text{A.15})$$

The above integrals may be found by separating them into the forms of equations 109, 111, 114 and 115 on page A-120 of The Handbook of Physics and Chemistry, 54th ed. which is published by the CRC Press.

Substituting equations A.13, A.14 and A.15 into A.12 and grouping we get

$$\frac{G}{24} \ln \left| \frac{12\zeta^2 + 15\pi\zeta + 64}{(512+70\pi\zeta)^2} \right| \Big|_{-\infty}^{\infty} \\ + \frac{1}{12\sqrt{3072-225\pi^2}} \left[24H - 15\pi G - \frac{360\pi I}{(3072-225\pi^2)} + \frac{576 J}{(3072-225\pi^2)} \right]$$

$$\begin{aligned}
 & \times \tan^{-1} \left[\frac{24\zeta + 15\pi}{\sqrt{3072 - 225\pi^2}} \right] \Big|_{\infty}^{\zeta} \\
 & + \frac{(24J - 15\pi I)\zeta + (15\pi J - 128I)}{(3072 - 225\pi^2)(12\zeta^2 + 15\pi\zeta + 64)} \Big|_{\infty}^{\zeta} = -X_c.
 \end{aligned}$$

Applying the boundary conditions yields

$$\begin{aligned}
 & - \frac{G}{24} \ln \left| \frac{12\zeta^2 + 15\pi\zeta + 64}{(512 + 70\pi\zeta)^2} \right| - \frac{1}{12\sqrt{3072 - 225\pi^2}} \left[24H - 15\pi G - \frac{360\pi I}{(3072 - 225\pi^2)} \right. \\
 & \left. + \frac{576J}{(3072 - 225\pi^2)} \right] \times \tan^{-1} \left[\frac{24\zeta + 15\pi}{\sqrt{3072 - 225\pi^2}} \right] - \frac{(24J - 15\pi I) + (15\pi J - 128I)}{(3072 - 225\pi^2)(12\zeta^2 + 15\pi\zeta + 64)} \\
 & + \frac{G}{24} \ln \left[\frac{12}{(70\pi)^2} \right] + \frac{\pi}{24\sqrt{3072 - 225\pi^2}} \left[24H - 15\pi G - \frac{360\pi I}{(3072 - 225\pi^2)} \right. \\
 & \left. + \frac{576J}{(3072 - 225\pi^2)} \right] \\
 & = + X_c.
 \end{aligned}$$

Substituting values of F, G, H, I and J yields equation 3.16.

TABLE A.1
INTEGRAL VALUES

$$\int_0^{\infty} \frac{\xi^a d\xi}{(1+\xi^2)^c} = \frac{1}{2} \left[\frac{\Gamma(\frac{a+1}{2}) \Gamma(c - \frac{a+1}{2})}{\Gamma(c)} \right]$$

when $a > -1$

and $c > \frac{a+1}{2}$

(see Handbook of Chemistry and Physics, 54th ed., 1973-74 CRC Press, p. A-161, equation 615 with $m=1$ and $b=2$)

a \ c	0	1	2	3	4	5	6
3	$\frac{3\pi}{16}$	$\frac{1}{4}$	$\frac{\pi}{16}$	$\frac{1}{4}$	$\frac{3\pi}{16}$	—	—
4	$\frac{5\pi}{32}$	$\frac{1}{6}$	$\frac{\pi}{32}$	$\frac{1}{12}$	$\frac{\pi}{32}$	$\frac{1}{6}$	—
5	$\frac{35\pi}{256}$	$\frac{1}{8}$	$\frac{5\pi}{256}$	$\frac{1}{24}$	$\frac{3\pi}{256}$	$\frac{1}{24}$	$\frac{5\pi}{256}$
6	$\frac{63\pi}{512}$	$\frac{1}{10}$	$\frac{7\pi}{512}$	$\frac{1}{40}$	$\frac{3\pi}{512}$	$\frac{1}{60}$	$\frac{3\pi}{512}$

APPENDIX FDETAILS OF PARABOLIC EXIT CONDITION ANALYSIS

The velocity profile used is that of Thomas and is repeated below

$$U_0 = (1-\psi^2)(1-\epsilon e^{\psi/\lambda})^3 + \alpha\psi + \beta\psi^2 + \gamma\psi^3 + \sigma\psi^4 \text{ for } 0 < \psi < 1$$

$$= 0 \text{ for } 1 < \psi < \phi. \quad (2.22)$$

The following boundary conditions must be satisfied:

- 1) $\psi = 0; \quad \partial U_0 / \partial \psi = 0$
- 2) $\psi = 1; \quad U_0 = 0$
- 3) $\psi = 1; \quad \partial U_0 / \partial \psi = 0$
- 4) $\psi = 1; \quad \partial^2 U_0 / \partial \psi^2 = 0$

The fourth condition is a result of the use of conditions 2 and 3 in the differential momentum equation.

Applying these conditions we get the following four equations.

$$1) \quad \alpha = \frac{3\epsilon}{\lambda} (1-\epsilon)^2 \quad (F.1)$$

$$2) \quad \alpha + \beta + \gamma + \sigma = 0 \quad (F.2)$$

$$3) \quad \alpha + 2\beta + 3\gamma + 4\sigma = 0 \quad (F.3)$$

$$4) \quad 2\beta + 6\gamma + 12\sigma = 0 \quad (F.4)$$

The solution of these equations give

$$3\alpha = -\beta = \gamma = -3\sigma = \frac{9\epsilon (1-\epsilon)^2}{\lambda} \quad (4.2)$$

Substituting these values into the velocity profile and simplifying yields:

$$U_0 = (1-\psi^2)(1-\epsilon e^{\psi/\lambda})^3 + \frac{3\epsilon\psi(1-\epsilon)^2(1-\psi)^3}{\lambda} \quad (4.3)$$

The momentum equation expressed in nondimensional terms is given below.

$$\int_0^{\frac{1}{2}} U_0^2 R dR \Big|_{x=0} = \int_0^1 U_0^2 \delta^2 \psi d\psi \Big|_x \quad (4.5)$$

This equation can be rearranged as follows since δ is a constant at any fixed axial location.

$$\delta^2 = \frac{\int_0^{\frac{1}{2}} U_0^2 R dR \Big|_{x=0}}{\int_0^1 U_0^2 \psi d\psi \Big|_x} \quad (F.5)$$

Consider first the integral in the numerator realizing that $U_0 = 1-4R^2$ at $x=0$. Therefore,

$$\int_0^{\frac{1}{2}} U_0^2 R dR \Big|_{x=0} = \int_0^{\frac{1}{2}} (1-4R^2)^2 R dR = 1/24 \quad (F.6)$$

The integral in the denominator becomes

$$\int_0^1 U_0^2 \psi d\psi \Big|_x = \int_0^1 \left[(1-\psi^2)(1-\epsilon e^{\psi/\lambda})^3 + \frac{3\epsilon\psi(1-\epsilon)^2(1-\psi)^3}{\lambda} \right]^2 \psi d\psi \quad (F.7)$$

In order to integrate this it is divided into parts as shown

$$\begin{aligned}
 \int_0^1 u_0^2 \psi d\psi \Big|_x &= \int_0^1 \left[(1-\epsilon e^{\psi/\lambda})^3 + \frac{3\epsilon\psi(1-\epsilon)^2(1-\psi)^3}{\lambda} \right]^2 \psi d\psi \\
 &\quad - 2 \int_0^1 (1-\epsilon e^{\psi/\lambda})^6 \psi^3 d\psi + \int_0^1 (1-\epsilon e^{\psi/\lambda})^6 \psi^5 d\psi \\
 &\quad - 6 \int_0^1 \frac{(1-\epsilon e^{\psi/\lambda})^3 \epsilon \psi^4 (1-\epsilon)^2 (1-\psi)^3}{\lambda} d\psi
 \end{aligned} \tag{F.8}$$

This division is made in order to utilize the result of Okabe. His velocity profile is the same as equation 4.3 with the exception of $(1-\psi^2)$ in the first term on the right hand side. As a result of this fact, Integral 1 in equation F.8 is that already reported by Okabe in reference 02 and shown below.

Integral 1

$$\int_0^1 \left[(1-\epsilon e^{\psi/\lambda})^3 + \frac{3\epsilon\psi(1-\epsilon)^2(1-\psi)^3}{\lambda} \right]^2 \psi d\psi = \sum_{n=0}^6 F_n \epsilon^n \tag{F.9}$$

where

$$F_n = \sum_{m=-2}^5 f_m \lambda^m \tag{F.10}$$

The values of f_m are given in Table 4.1. The remaining integrals are found as follows.

Integral 2

$$\begin{aligned}
-2 \int_0^1 (1-\epsilon e^{\psi/\lambda})^6 \psi^3 d\psi &= \left(-\frac{1}{2} + \frac{49}{10} \lambda - \frac{26978}{1200} \lambda^2 + \frac{336581}{6000} \lambda^3 - \frac{68165041}{1080000} \lambda^4 \right) \epsilon^0 \\
&+ \left(72\epsilon - \frac{90}{8} \epsilon^2 + \frac{80}{27} \epsilon^3 - \frac{45}{64} \epsilon^4 + \frac{72}{625} \epsilon^5 - \frac{1}{108} \epsilon^6 \right) \lambda^4 \quad (F.11)
\end{aligned}$$

Integral 3

$$\begin{aligned}
\int_0^1 (1-\epsilon e^{\psi/\lambda})^6 \psi d\psi &= \left(\frac{1}{6} - \frac{49}{20} \lambda + \frac{13489}{720} \lambda^2 - \frac{336581}{3600} \lambda^3 + \frac{68165041}{216000} \lambda^4 \right. \\
&- \left. \frac{483900263}{720000} \lambda^5 + 694 \frac{299856529}{388800000} \lambda^6 \right) \epsilon^0 \\
&+ \left(-720\epsilon + \frac{225}{8} \epsilon^2 - \frac{800}{243} \epsilon^3 + \frac{225}{512} \epsilon^4 - \frac{144}{3125} \epsilon^5 + \frac{5}{1944} \epsilon^6 \right) \lambda^6 \quad (F.12)
\end{aligned}$$

and

Integral 4

$$\begin{aligned}
-6 \int_0^1 \frac{(1-\epsilon e^{\psi/\lambda})^3 \epsilon \psi^4 (1-\epsilon)^2 (1-\psi)^3}{\lambda} d\psi \\
&= \frac{\epsilon(1-\epsilon)^2}{\lambda} \left[\left(-\frac{3}{140} + \frac{10983}{108} \lambda^4 - \frac{9052400}{54} \lambda^5 - \frac{689225}{54} \lambda^6 \right. \right. \\
&- \left. \left. \frac{4166875}{81} \lambda^7 + \frac{175679735}{1944} \lambda^8 \right) \epsilon^0 \right. \\
&- \left. (432\lambda^5 + 6480\lambda^6 + 38880\lambda^7 + 90720\lambda^8) \epsilon^1 \right. \\
&+ \left. \left(\frac{27}{2} \lambda^5 + \frac{3240}{32} \lambda^6 + \frac{1215}{4} \lambda^7 + \frac{2835}{8} \lambda^8 \right) \epsilon^2 \right. \\
&- \left. \left(\frac{16}{27} \lambda^5 + \frac{240}{81} \lambda^6 + \frac{160}{27} \lambda^7 + \frac{10080}{2187} \lambda^8 \right) \epsilon^3 \right] \quad (F.13)
\end{aligned}$$

These results are conveniently summarized as

$$\text{Integral (2 + 3 + 4)} = \sum_{n=0}^6 G_n \epsilon^n \quad (\text{F.14})$$

where

$$G_n = \sum_{m=-1}^7 g_m \lambda^m \quad (\text{F.15})$$

The values of g_m are presented in Table 4.2.

Equations F.6, F.9 and F.14 are used in equation F.5 to yield:

$$\delta^2 = \left[24 \sum_{n=0}^6 (F_n + G_n) \epsilon^n \right]^{-1} \quad (4.6)$$

Let us now consider the differential momentum equation along the jet centre line expressed in the following nondimensional manner.

$$\begin{aligned} U_m \frac{dU_m}{dx_c} &= \left(\frac{\partial^2 U_0}{\partial R^2} + \frac{1}{R} \frac{\partial U_0}{\partial R} \right)_{R=0} \quad (4.10) \\ &= 2 \left(\frac{\partial^2 U_0}{\partial R^2} \right)_{R=0} \end{aligned}$$

$$\text{since } \frac{1}{R} \frac{\partial U_0}{\partial R} \Big|_{R \rightarrow 0} = \frac{0}{0} = \frac{\partial^2 U_0}{\partial R^2} \text{ using L'Hopital's Rule.}$$

From equation 2.22 it can be seen that

$$U_m = (1-\epsilon)^3 \quad (\text{F.16})$$

and since $\epsilon = e^{-1/\lambda}$ we get

$$\frac{\partial U_m}{\partial X_c} = \frac{-3\epsilon(1-\epsilon)^2}{\lambda^2} \frac{d\lambda}{dX_c} \quad (F.17)$$

Also,

$$\left. \frac{\partial^2 U_0}{\partial R^2} \right|_{R=0} = \frac{-1}{\delta^2} \left[\frac{3\epsilon(1-\epsilon)(1-3\epsilon)}{\lambda^2} + 2(1-\epsilon)^3 + \frac{18\epsilon(1-\epsilon)^2}{\lambda} \right] \quad (F.18)$$

Using equations F.16, F.17 and F.18 in equation 4.10 it can be shown that:

$$X_c = \frac{1}{2} \int_0^\lambda \frac{\epsilon(1-\epsilon)^4 \delta^2 d\lambda}{[\epsilon(1-3\epsilon) + \frac{2\lambda^2(1-\epsilon)^2}{3} + 6\lambda\epsilon(1-\epsilon)]} \quad (4.11)$$

Simpson's method of numerical integration is used to solve this equation.

VITA AUCTORIS

- 1948 Born in Chatham, Ontario, Canada on April 23.
- 1965 Completed high school at Chatham Kent Secondary School, Chatham, Ontario, Canada in June
- 1968 Received Mechanical Technologist Diploma from St. Clair College, Windsor, Ontario, Canada in May
- 1971 Received the Degree of Bachelor of Applied Science in Mechanical Engineering from the University of Windsor, Windsor, Ontario, Canada in May
- 1974 Received the Degree of Master of Applied Science in Mechanical Engineering at the University of Windsor, Windsor, Ontario, Canada in October
- 1980 Currently a candidate for the Degree of Doctor of Philosophy in Mechanical Engineering at the University of Windsor, Windsor, Ontario, Canada.